Aus der Klinik für Neurochirurgie mit Arbeitsbereich Pädiatrische Neurochirurgie der Medizinischen Fakultät Charité – Universitätsmedizin Berlin

DISSERTATION

Ephrin-B2 – EphB4 interaction as a therapeutic target in spinal metastasis formation

zur Erlangung des akademischen Grades
Doctor medicinae (Dr. med.)

vorgelegt der Medizinischen Fakultät
Charité – Universitätsmedizin Berlin

von

András Piffkó

aus Budapest, Ungarn

Datum der Promotion: 13.12.2019

Contents

Contents

Contents

Contents

Contents

1 Abstract

1.1 Introduction

The development of spinal metastases is a common and complex problem in the management of cancer patients, with the spine being one of the main sites to where metastases will spread. If untreated, spinal metastases rapidly lead to progressive myelopathy with extensive effects on ambulatory status, quality of life and survival rates of affected patients. Although major developments in the field of surgical and oncological procedures have led to improved therapeutic options, the molecular steps of spinal metastasis formation still remain inadequately understood. EphB4 and Ephrin-B2 have repeatedly been identified as key regulators in metastatic cell dissemination, tumor cell – endothelial cell interaction and tumor growth. We investigated the effects of a therapeutic alteration of this molecular interaction on long-term metastasis formation.

1.2 Methods

Bioluminescent B16 melanoma cells were injected retrogradely into the carotid artery of Ephrin-B2-knockout (efnb2$^{i\Delta EC}$) and control (efnb2$^{lox/lox}$) mice in a pre- and post-metastatic setting ("pre-" and "post-tumor"). Potential therapeutic effects were evaluated after applying soluble Ephrin-B2-Fc, as well as NVP-BHG 712, a small molecular inhibitor of the EphB4 receptor tyrosine kinase. Tumor growth and dissemination were surveyed utilizing in-vivo bioluminescent imaging procedures and compressive spinal loci were identified using magnetic resonance imaging. Immunohistochemical evaluation of tumor cell proliferation and vasculature were performed and the organ specific tumor load was examined using a luciferase detection assay.

1.3 Results

In pre-tumor treated efnb2$^{lox/lox}$ mice the application of Ephrin-B2-Fc (median: 20.5 days, n=7, p=0.0048) and NVP-BHG 712 (median: 21 days, n=14, p=0.0002) induced significantly earlier neurologic deficits when compared to the placebo-treated group (median: 24.5 days, n=11), by increasing the number and volume of spinal metastases. In post-tumor treated efnb2$^{lox/lox}$ mice there was no significant difference in survival times or number of spinal metastases in the MRI. The earlier appearance of neurological deficits in efnb2$^{i\Delta EC}$-knockout mice (median efnb2$^{i\Delta EC}$ placebo: 18 days,

Abstract

n=7, p=<0.0001) could be significantly delayed by pre-tumor treatment with Ephrin-B2-Fc. (median: 23 days, *n*=8).

1.4 Conclusion

The molecular interaction between EphB4 and Ephrin-B2 significantly affected the formation of spinal metastases. The physiological EphrinB2-EphB4 interaction in efnb2$^{lox/lox}$ control mice showed tumor suppressive effects by increasing tumor cell repulsion from the endothelium. The therapeutic disruption of these repulsive effects decreased neurological survival through an increased number and volume of metastases. Under the effects of the prometastatic endothelial Ephrin-B2 knockout (efnb2$^{i\Delta EC}$), these physiologically inert repulsive functions could be partially reestablished through Ephrin-B2-Fc.

2 Abstrakt

2.1 Einführung

Die Entstehung spinaler Metastasen ist eine häufige und schwerwiegende Komplikation in der Behandlung von Krebspatienten. Die Wirbelsäule stellt hierbei eine der häufigsten Lokalisationen ossärer Metastasierung dar. Ohne adäquate Therapie führen spinale Metastasen binnen kürzester Zeit zu einer zunehmenden Myelopathie und Destruktion der neuralen Elemente, mit weitreichenden Auswirkungen auf das Überleben und die Lebensqualität der betroffenen Patienten. Trotz stetiger Entwicklungen in der onkologischen und neurochirurgischen Therapie dieses komplexen Krankheitsbildes bleiben die grundlegenden Entstehungsmechanismen weiterhin weitestgehend unverstanden. EphB4 und Ephrin-B2 wurden wiederholt als wichtige Regulatoren in der Metastasenentstehung, sowie in der Interaktion zwischen Tumor- und Endothelzellen identifiziert. Wir haben die Auswirkungen dieser molekularen Interaktion, sowie mögliche therapeutische Beeinflussungen der Entstehung spinaler Metastasen untersucht.

2.2 Methodik

BIolumineszierende B16-Melanomzellen wurden jeweils in einem prä- und postmetastatischen Ansatz retrograd in die A. carotis communis von Ephrin-B2-Knockout- (efnb2$^{i\Delta EC}$) und Kontrollmäusen (efnb2$^{lox/lox}$) injiziert. Potenzielle therapeutische Effekte des löslichen Antikörpers Ephrin-B2-Fc, sowie des spezifischen EphB4 Tyrosinkinaseinhibitors NVP-BHG 712 wurden evaluiert. Tumorwachstum und Verteilungsmuster wurden durch Biolumineszenz-Bildgebungsverfahren in vivo überwacht und Tumorwachstum und Myelonkompression mittels spinalem MRT dargestellt. Immunhistochemische Färbungen wurden hinsichtlich Proliferation und Angiogenese ausgewertet, sowie die Anzahl der metastatischen Tumorzellen pro Organ mittels eines Luziferase-Assays.

2.3 Ergebnisse

In prä-tumor vorbehandelten efnb2$^{lox/lox}$ Mäusen zeigten sowohl die mittels Ephrin-B2-Fc (Mittelwert: 20.5 Tage, *n*=7, p=0.0048) als auch die mit NVP-BHG 712 (Mittelwert: 21 Tage, *n*=14, p=0.0002) therapierte Gruppe signifikant frühere neurologische Defizite durch vermehrte spinale Metastasen als die Placebo-behandelten Tiere (Mittelwert: 24,5 Tage, *n*=11). In den post-tumor behandelten efnb2$^{lox/lox}$ Tieren zeigte sich kein Unterschied im Überleben oder der spinalen Tumorlast. Das signifikant frühere Auftreten neurologischer Defizite in Ephrin-B2-knockout (efnb2$^{i\Delta EC}$) Mäusen (Mittelwert efnb2$^{i\Delta EC}$ Placebo: 18 Tage, *n*=7, p=<0.0001) konnte durch die prämetastatische Gabe von Ephrin-B2-Fc deutlich verzögert werden (Mittelwert: 23 Tage, *n*=8).

2.4 Schlussfolgerung

Die molekulare Interaktion zwischen EphB4 und Ephrin-B2 beeinflusst die Entstehung spinaler Metastasen. Der physiologische Zustand inhibiert das Tumorwachstum durch vermehrte Abstoßung der zirkulierenden Tumorzellen. Die therapeutische Unterbrechung dieses protektiven Effektes führte zu einem signifikant früheren neurologischen Defizit durch vermehrtes Wachstum spinaler Metastasen. Unter dem prometastatischen endothelialen Ephrin-B2-knockout konnte durch prämetastatische Applikation des Ephrin-B2-Fc Antikörpers die physiologisch bestehende Abstoßungsreaktion partiell wiederhergestellt werden, sodass eine signifikante Verlängerung des neurologischen Überlebens erreicht wurde.

3 Introduction

3.1 Clinical relevance

Spinal metastases are a growing problem in the management of cancer patients and are thus becoming increasingly relevant in the fields of neurosurgery and oncology. Overall, around 70% of cancer patients develop distant metastases during the course of their disease. It is estimated that again around 70% of all patients with metastatic cancer will develop metastases to the spine, making it one of the most significant locations to which primary tumors will spread.[1]

A recent study estimates that in 2008, there were around 280,000 patients with metastatic bone disease in the US alone.[2] Of those patients, around 90.000 cases were accredited to cancers of the female breast, 63.000 to prostate cancer and around 35.000 to lung cancer. The spine is the most common site of bone metastasis and it is estimated that more than 10% of all cancer patients develop symptomatic metastasis of the spine.[2,3] Yet, only those patients are noted that have come to the attention of health care providers and are recorded – it is estimated that there are even more incidents of spinal metastatic disease which remain undiscovered. The thoracic spine is the most common site of metastasis formation (70%), by far surpassing the lumbar (20%) and cervical (10%) areas, however more than half of the affected patients show metastatic dissemination on multiple levels.[4,5] Nowadays, with the emergence of improved clinical imaging procedures, it is expected that even more cases will be discovered at an earlier stage of disease progression, possibly enabling further developments in the therapeutic procedures.

3.2 Different forms of spinal compression and surgical procedures

If untreated, metastases of the osseous spine can lead to rapid epidural myelon compression and progressive myelopathy, which results in the loss of sensory and motor functions, worsening of ambulatory status and autonomous deregulation. For decades, the palliative posterior laminectomy was considered to be the only expedient surgical option for patients affected by metastatic epidural spinal cord compression (MESCC).[6] The development of radiotherapy eventually enabled a combined approach,

Introduction

which included the decompressive laminectomy followed by radiotherapy. However, in 1980, a randomized, prospective trial by Young et al. found no significant advantage of the combined approach to radiotherapy alone, in regard to pain relief and improved ambulation, thus gravely undermining the necessity for a surgical approach.[7] Consequently, the role of surgical decompression was significantly diminished following this publication.

Evidently, as most spinal metastases causing MESCC are located in the vertebral body,[8] the removal of the posterior elements through laminectomy could not achieve a significant decompression of the neural elements, while at the same time posing the threat of further destabilization of the spinal column. It was only in 2005, when Patchell et al. proved in a randomized, multi-institutional, non-blinded trial the superiority of direct decompressive surgery followed by radiotherapy to radiotherapy alone that surgical procedures have again been established as the primary treatment option for this debilitating disease.[6] Nowadays, the aim of any surgical procedure has to be the immediate circumferential decompression of the spinal cord, while at the same time reconstructing and stabilizing the vertebral column.[9] Different surgical techniques, involving the use of stereotactic radiosurgery, endoscopy [minimal invasive spinal surgery (MISS)] and a vast array of internal fixation devices, have all been developed as part of the multidisciplinary approach in the treatment of these complex clinical cases.[10]

The development of spinal metastases has an enormous impact on the individual clinical prognosis, mortality and morbidity of cancer patients. Despite recent technological and scientific developments enabling the improvement in clinical detection and treatment procedures, the understanding of the basic molecular steps in metastasis formation still remains insufficient. The evolution of increasingly personalized treatment modalities, especially in clinical oncology, is of paramount significance also for patients with spinal metastatic cancer. Therefore, there is an urgent need for elucidating the biological mechanisms that underlie spinal metastasis, in order to find valid novel targets for the therapy of this devastating disease.

3.3 Metastatic cascade

3.3.1 Hallmarks of cancer

The conversion of healthy cells into malignant tumor cells that can cause metastatic disease is a long and complex process. To understand the relevant steps for this malignant procession, in 2000 Hanahan and Weinberg proposed six hallmarks of cancer, which provide an overview of the relevant biological and cellular capabilities in the multistep process leading up to human tumor pathogenesis. The hallmarks include sustaining proliferative signaling, evading growth suppressors, resisting cell death, enabling replicative immortality, inducing angiogenesis and ultimately activating invasion and metastasis.[11] However, emerging research concepts have caused them to include further steps in the process; reprogramming of energy metabolism and evading immune destruction as well as the complex concept of the "tumor microenvironment" of recruited - supposedly physiological - cells surrounding the malignant tumors, further proving the intricacy of the necessary developmental steps in the formation of malignancies.[12]

3.3.2 Steps of metastasis formation

It is the formation of metastases, rather than the primary tumor itself, which is regarded as being responsible for most cancer deaths.[13] The hypothesis that metastasis formation is based on two major factors – the properties of the cancer cell ("the seed") as well as the microenvironment of the individual organs ("the soil") – was first postulated in 1889 by Stephen Paget and has ever since molded the way malignant diseases are perceived.[14] Paget claimed that spreading of metastases does not occur by pure chance but rather by a certain affinity of tumor cells for distinctive factors of the organ-environment.[15] The main steps of metastasis formation include the proliferation and angiogenesis of the primary tumor, invasion of the circulation and embolism of circulating metastatic cells. This is followed by the adherence to vessel walls and the process of extravasation and metastasis growth in case that the surrounding microenvironment is favorable for the individual cancer cell.[14] Remarkably, each of this sequence of steps is highly inefficient, some can even be rate limiting; overall, only 0,01% of cells that intravasate into circulation will eventually form clinically detectable metastases.[16] Thus certain modifications of the metastatic cancer cells and the tumor microenvironment are crucial in order to adapt to the multitude of different environments they encounter.[17]

Introduction

Figure 1: Sequential steps of metastasis formation
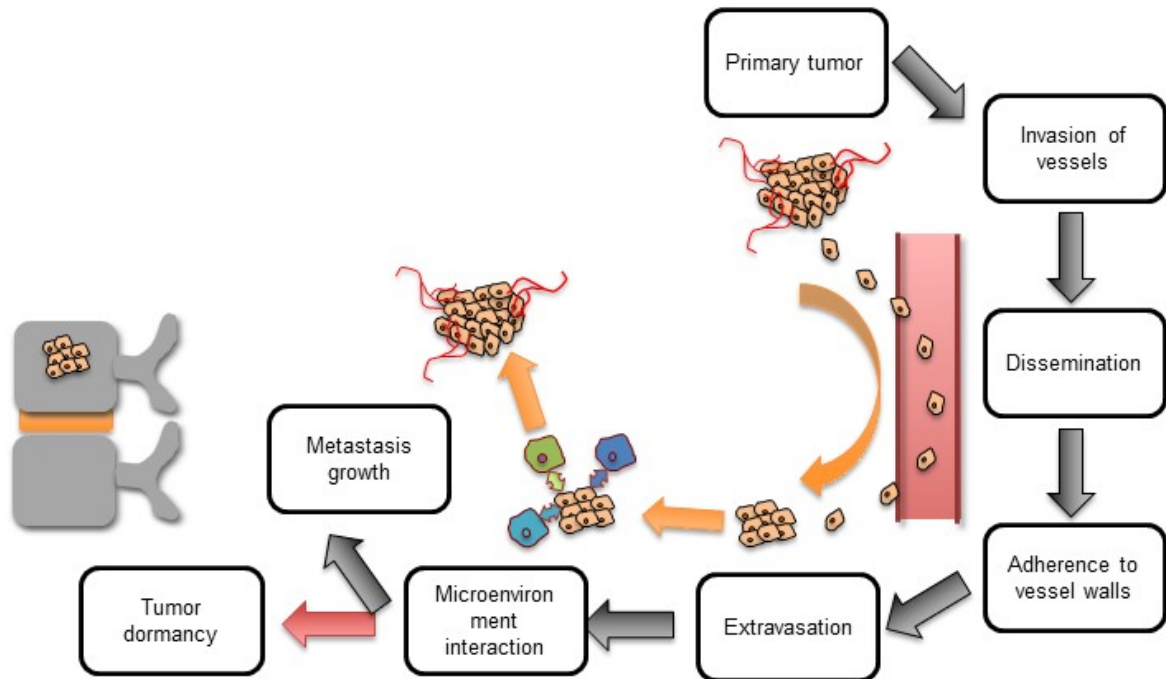
Figure 1: *Visual representation of the different steps necessary for distant metastasis formation, including the invasion of vessels, dissemination within the blood stream / lymphatic system, adherence, extravasation and interaction with a novel microenvironment. All of these steps pose novel challenges on disseminated tumor cells (DTCs) and can potentially become rate limiting.*

Currently, tumors are perceived as intricate "organs" composed of a complex interactive mixture of malignant tumor cells and their adjacent microenvironment, including surrounding stroma (fibroblasts, adipocytes, myocytes), infiltrating immune cells, and vascular cells (endothelial cells, pericytes).[18] This tumor microenvironment (TME) has diverse capacities to induce both beneficial and adverse consequences for tumorigenesis.[19] It has been shown that tumor-associated fibroblasts (TAFs)[20] or bone marrow-derived cells (BMDCs), such as tumor-associated macrophages (TAMs),[21] can sustain tumor growth by secreting cytokines and growth factors required by the growing tumor mass for replication, invasion and angiogenesis.[17] In a different experimental setting however, Mintz et al. were able to show that the microenvironment of a mouse blastocyst was not only able to suppress the tumorigenicity of teratocarcinoma cells but could also achieve stable reprogramming, thus creating normal chimeric mice, illustrating the opposing functions of the microenvironment.[22] These tumor-suppressive properties can also be reversed through states of chronic inflammation[23] or priming

mechanisms of the underlying tumor, which enable the formation of distant pre-metastatic niches via chemoattractants such as S100A8 and S100A9.[24,25]

3.3.3 Metastasis formation in bone

Upon passage through the osseous sinusoid walls, the disseminated tumor cells (DTCs) encounter a complex balance of growth promoting and apoptotic signals, which can, in certain cases, induce one of two different types of metastatic latencies. Firstly, each individual tumor cell can achieve a state of proliferative dormancy by exiting the proliferative cycle for any undetermined period of time. Secondly, any larger group of DTCs can develop indolently as micrometastatic colonies in a state termed "tumor mass dormancy", where the rate of proliferation is counterbalanced by the rate of tumor cell death.[26]

Recent observations found that in patients undergoing chemotherapy, the bone marrow inadvertently provided survival signals to support the resilience of DTCs. This form of cellular survival is enabled by the expression of CXC chemokine receptor 4 (CXCR4) on the tumor cells. CXCR4 is the receptor for stromal cell-derived factor 1 (SDF1/CXL12), which, readily produced by mesenchymal cells of the bone marrow, is an important chemokine that enables cell survival for hematopoietic stem cells as well as the dormant DTCs. Over an extended period of time, the dormant tumor cells may acquire further supporting mutations, eventually enabling successful emergence from dormancy.[27]

In the case of breast cancer metastases, the formation of the typical osteolytic lesions is facilitated by genetic mutations allowing DTCs to produce osteoclast-activating factors such as parathyroid hormone-related protein (PTHRP), tumor necrosis factor α (TNF-α) or interleukin 6 (IL-6).[28] These factors collectively activate the production of receptor activator of nuclear factor-κB ligand (RANKL) from osteoblasts and simultaneously suppress the production of bone-protective agent osteoprotegerin (OPG).[29] RANKL stimulates the development of osteoclasts from myeloid precursors by signaling through the nuclear factor-κB and c-Jun N-terminal kinase pathways, thus reinforcing the degradation of the bone matrix and contributing to the development of osteolytic metastases.[26]

3.3.4 Molecular mechanisms of tumor angiogenesis

Once growing tumors have reached the size of 400 μm, they require sufficient vasculature to maintain the influx of oxygen and essential nutrients and remove

Introduction

excessive toxins and cellular waste products.[30] The massive amount of energy required for the growing tumor makes the establishment of a suitable vascular supply one of the most crucial steps in metastasis formation.

In order to achieve either the formation of new vessels or the branching of pre-existing vessels, the tumor secretes pro-angiogenic growth factors, which act as a chemo-attractant for surrounding endothelial cells and pericytes.[18] This process is sustained by TAMs[31] and TIE2-expressing monocytes[32] of the tumor microenvironment, which have been shown, in addition to their effect on tumor growth and invasion, to contribute to the angiogenesis through the production of growth factors, cytokines and proteases such as vascular endothelial growth factor A (VEGFA)[17] and prokineticin 2 (PROK2).[33]

Two fundamental mechanisms enable the development of the tumor vasculature necessary for its rapid growth: the formation of new vessels and the branching of pre-existing vessels.[18] Both, newly formed vessels and co-opted physiological vessels share various common traits, which clearly distinguish them from normal vascular morphology. Tumor vessels tend to be unevenly distributed and usually form rather chaotic, tortuous networks compared to the evenly distributed regular vessels. Furthermore, the anatomy of the tumor blood vessel wall is also compromised, as the coating of the vessel with pericytes and smooth muscle cells is reduced. Accordingly, tumor vessels are inappropriately permeable to large macromolecules and are inefficient in clearing cellular waste products and supplying sufficient oxygen and nutrients.[18] This characteristic feature leads to a constant existence of chronically acidic and hypoxic regions within any given tumor, which increases the expression of growth factors such as platelet-derived growth factor (PDGF), Angiopoetin 2 (Ang 2) or transforming growth factor α (TGFα).[34]

3.4 Eph-Ephrin system

3.4.1 Molecular structure

The Eph (Erythropoietin-producing hepatoma) receptor tyrosine kinase (RTK) family is currently the largest known subfamily of tyrosine kinases found in mammals.[35] Including their Eph receptor family interacting proteins (Ephrin) ligands, the family consists of 23 members in total. The distinction of the individual family members is largely based on sequence homology as well as binding preferences. In total, there are two relevant binding combinations (EphA – Ephrin-A & EphB – Ephrin-B). The A-type subfamily consists of nine EphAs (EphA1-8 and EphA10) and five Ephrin-As (Ephrin-A 1-5), whereas the B-type subfamily consists of five EphBs (EphB1-4 and EphB6) and three Ephrin-Bs (Ephrin-B1-3).[36] The binding within the subclasses was for a long time believed to be strictly separated between the A and B subclasses. However, recent studies have found that receptors of the EphB subclass can also bind ligands of the Ephrin-A subclass, as indicated for example by the common binding between EphB2 and Ephrin-A5.[37] The binding within the subclasses is also highly promiscuous and certain combinations of Eph receptors and/or Ephrin ligands are present in most, if not all, cell types.[36]

The structure of the Eph receptors is closely related. Both A- and B-types consist of a globular ligand-binding domain, a cysteine rich region and two fibronectin type III repeats on their extracellular site, as well as a juxtamembrane region, a tyrosine kinase domain, a sterile α motif (SAM) domain, and ultimately a PDZ-binding motif on their intracellular site.[35] As connection to the cell membrane, the Ephrin-A subfamily utilizes a glycosylphosphatidylinositol (GPI) anchor, whereas the B-type Ephrins possess a transmembrane domain.[38]

Introduction

Figure 2: Molecular structure of Ephs and Ephrins
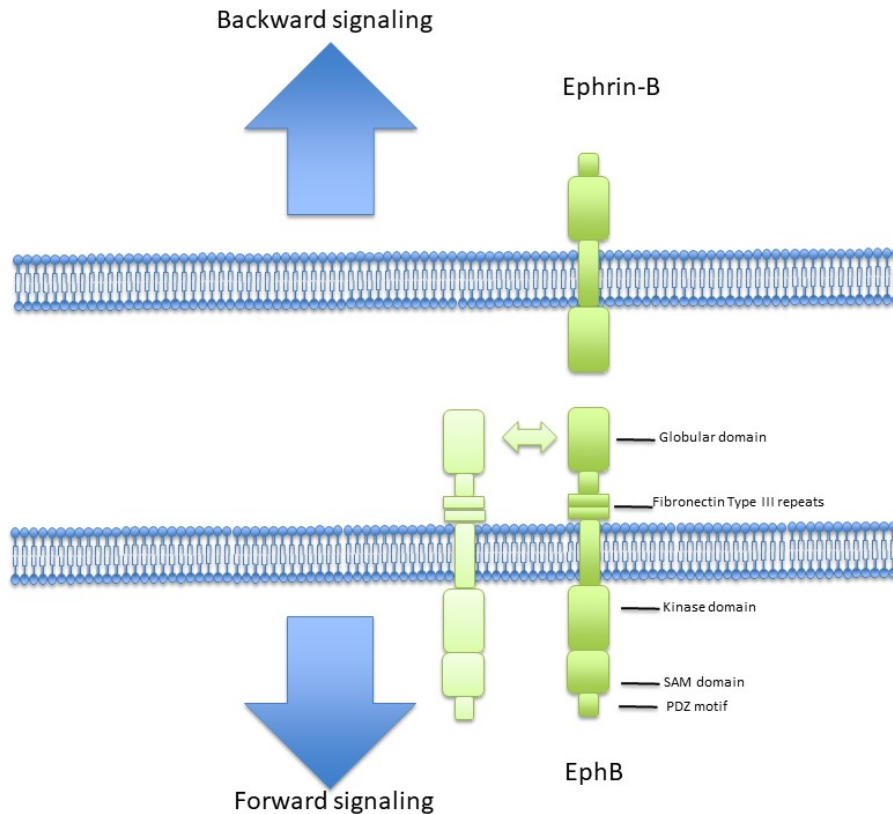
Figure 2: (based on Kandouz M, Cancer Metastasis Rev 2012) The Eph/Ephrin family is membrane-bound. The extracellular domain of Ephs is composed of a globular ligand-binding domain, a cysteine-rich region, and two fibronectin type III repeats. The intracellular cytoplasmic domain is formed by a juxtamembrane region, a tyrosine kinase domain, a sterile α motif (SAM) protein–protein interaction domain, and a C-terminal PDZ-binding motif.[35] Additionally to forward and backward "trans"-signaling, "cis"-signaling can also occur between Ephs and Ephrins within the same cell (as indicated by the small double-headed arrow).

3.4.2 Interaction mechanisms

As both receptors and ligands are membrane bound, there is generally a need for direct cell-cell interaction for binding to occur, although some evidence also suggests a possibility of soluble forms of signaling.[39] Binding of the extracellular domains has extensive effects on cell differentiation, motility, survival, shape and proliferation.[40] These effects are in fact not limited to receptor-based signaling, but can occur in both cells. The ligand-expressing cell may consequently also be affected – thus, this process is labeled bidirectional signaling.[41] "Forward" signaling occurs within the receptor-expressing cell upon binding of the Ephrin ligands, whereas the ligand-expressing cell

Introduction

undergoes "reverse" (or backward) signaling, where Eph receptors bind to a receptor-binding domain (RBD).[40] Therefore an Ephrin ligand might act as a receptor and vice versa. Yet, in contrast to the Eph receptors and Ephrin-B ligands, the Ephrin-A ligands lack the internal c-terminal PDZ domain, which is particularly important for the functions. Thus, reverse signaling in Ephrin-A ligands can only occur after the binding of co-receptors, while Ephrin-B ligands are capable of generating reverse signaling autonomously.[42] Eph receptor "forward" signaling is largely dependent on the tyrosine kinase domain, which induces autophosphorylation as well as phosphorylation of various other effector proteins.[43] The N-terminal "Ephrin-binding" domain contains the domain with the highest affinity to the Ephrin ligands, however recently two further lower-affinity Ephrin-binding sites have been identified in the Ephrin-binding domain and the cysteine-rich region, which are supposed to induce clustering of multiple receptor-ligand complexes.[40] Clustering may affect signal strength and also differentially regulate downstream pathways, thus leading to variable cellular pathways.[44]

The effect of Eph-Ephrin interaction on cellular motility is in most cases mediated through signaling effectors such as Ras/Rho family GTPases, which contribute to the proper organization of the actin cytoskeleton.[45] Upon cell-cell contact, Eph-Ephrin interaction is largely responsible for the generation of repulsive signals that lead to retraction of the two cells, although the effect can also coincidentally induce cell adhesion.[42] The effect of repulsive cellular movement is largely enabled by an unusual endocytic mechanism that involves the internalization of the receptor-ligand complex including the surrounding plasma membrane area into the respective cell, thus separating the cell surfaces.[46] An additional mechanism which enables cellular separation is based on protease-mediated cleavage of the extracellular domains, which also results in internalization and degradation of the receptor-ligand complexes.[47] The cleaved Ephrin fragments have in turn further intracellular effects that remain independent of cell-cell contact, such as the phosphorylation of the cytoplasmic domain of integral B-type Ephrins.[42,48] They could even function as monomeric inhibitors of bi-directional signaling in distant cells.[46] Another method of signal transduction applicable to the Eph-Ephrin interaction is the method of lateral "cis"-interaction, which usually takes place between Ephs and Ephrins that are co-expressed on the same cell.[49] These reactions reinforce the signals induced by contact-dependent "trans"-signaling.[50]

Introduction

3.4.3 Role in different organs

The Eph-Ephrin RTK family plays an important role in a number of different organ systems.[42] In the developing nervous system, it controls axon guidance, spatial organization and plasticity of neural cells as well as the proper formation and function of synaptic connections, mainly by generating repulsive signals.[51] Further connections have been made between Eph-Ephrin interaction and inhibition of neural repair,[52] neurodegenerative disesases[53] and chronic neuropathic pain.[54] In the cardiovascular system, the Eph-Ephrin system is crucial for the angiogenesis in the embryo, mainly segregating arterial endothelial cells from venous endothelial cells.[55] Some family members, such as EphA2 & Ephrin-A1 and EphB4 & Ephrin-B2 also retain their vital roles in adults.[56] During angiogenesis, the interaction between Ephs and Ephrins controls blood vessel sprouting, assembly and remodeling[36] by regulating the interaction between vascular endothelial cells (EC) and their supporting mural cells (pericytes, SMCs).[57] The spatial organization of ECs towards each other is also strongly affected by Eph-Ephrin interactions, with the EphB4 signaling restricting cellular intermingling and thus facilitating proper asymmetric arterio-venous EC binding of the reciprocal EphB4 and Ephrin-B2 positive cells.[58]

3.4.4 Eph-Ephrin interaction in blood vessel maturation and differentiation

The notion that the reciprocal Eph-Ephrin interaction is crucial for the segregation and boundary formation between arterial and venous cells first arose in a publication by Wang et al. in 1998. It was found, that the distribution of EphB4 and Ephrin-B2 takes place in complementary patterns.[55] Ephrin-B2 mRNA was mainly found in arteries, whereas EphB4 was expressed on all major veins, implying that, analogous to their repulsive functions in the developing nervous system, they must have an important physiological function in the vascular segregation process during embryonic angiogenesis by preventing intermixing between arterial and venous endothelial cells.[59] Adams et al. further strengthened this concept in 1999, by proving the targeted inactivation of the *Efnb2* gene, encoding the cell-surface anchored Ephrin-B2, to be lethal at E9.5 in a mouse model. This was shown to be mainly due to disruptions of the vascular morphogenesis, including severe malformations of the heart, the aortic arch and cardinal veins.[57] Furthermore, the Ephrin-B2 knockout mutants exhibited a highly primitive vascular network with homogenously sized, inadequately organized vessels

and a reduced capillary network. Additionally, they demonstrated a direct stimulatory role of Ephrin-B ligands in generating capillary networks by triggering a sprouting response of vascular endothelial cells to soluble Ephrin-B ligands, to a similar extent as other known angiogenic factors such as Ang1 and VEGF.[57] Ephrin-B2 does not merely bind EphB4, it also shows binding affinities to EphB2 and EphB3.[60]

Extensive vascular migration experiments suggest that EphB4 forward signaling inhibits migration, adhesion and sprouting angiogenesis, whereas Ephrin-B2 reverse signaling stimulates these effects.[58,61] Not only the baseline migration, but also the VEGF-induced migration of endothelial cells (ECs) is inhibited through application of soluble Ephrin-B2-Fc.[58] The subsequent EphB4 receptor activation has been shown to suppress mitogen-activated protein kinase (MAPK) activation, hence reducing VEGF and angiopoietin-1 signaling and limiting angiogenic proliferation.[62] Conversely, the application of EphB4-Fc stimulated VEGF-induced EC-sprouting, adhesion and migration by stimulating Ephrin-B2 reverse signaling.[63] Endothelial Ephrin-B2 as well as its primary functional domain, the PDZ domain, are also necessary for the internalization of the vascular endothelial growth factor receptor 2 (VEGFR2) and its angiogenic signaling.[64]

3.4.5 Interaction with pericytes and mural cells

In addition, EphB4 and Ephrin-B2 communication is not only present on the endothelial cells of the developing vascular system, but also at the junction zone of mural cells and pericytes.[65] In mural cell specific *Efnb2* mutants, pericytes showed a diminished interaction with microvessels, which is compensated for by abnormal deposits of extracellular matrix (ECM) in the gaps between pericytes and endothelial cells.[66] Likewise, the coverage of the vasculature by vascular smooth muscle cells (vSMCs) was also incomplete, indicating an inability of the mural cells to form sufficient contacts with ECs. Instead of becoming a functional integral part of the vessel wall, they remained round and merely loosely attached.[67] *Efnb2* mutant vessels rupture more frequently leading to the widespread hemorrhages seen in the skin and the intestines of the defective embryos.[68]

3.4.6 Importance of Eph-Ephrin interaction in tumor pathology

Eph receptors and Ephrins are present in almost all types of cancer cells and can directly affect the growth, angiogenesis, malignancy and metastatic potential of tumors. The most commonly overexpressed Eph receptors in tumors are EphA2 and EphB4,

where they play a pivotal role in sustaining malignancy.[69] EphB4 is overexpressed in cancers of various origins including breast,[70] colon,[71] skin[45] and ovaries[72]. The overexpression of EphB4 is detectable in 86% of ovarian cancers, where it is significantly associated with aggressive end-stage disease and poor survival.[72] Furthermore, targeting of EphB4 receptors using monoclonal antibodies or siRNA was shown to significantly hamper ovarian cancer growth, migration and invasion *in vivo.*[73] In colorectal carcinoma (CRC), both EphB2 and EphB4 are expressed in the early stages, however this expression diverges as the disease advances, as there is a progressive loss of EphB2 and a progressive increase in EphB4 levels.[74]

In murine malignant melanoma cells, EphB4 was shown to regulate migration and invasion by directly affecting the cytoskeleton reorganization through RhoA activity.[45] Furthermore it was proven that highly malignant melanoma cells express the highest levels of EphB4.[45] However, a recent study by Huang et al. found that the overexpression of EphB4 in B16 melanoma cells rather suppressed tumor growth in a subcutaneous tumor model by selectively suppressing arterial Ephrin-B2-positive endothelial cell development.[75] Recent developments point to the extent of kinase activity of EphB4 as the main regulator of these supposedly contrarious effects, as proven by analyzes of kinase-dead EphB4 mutants or blocking agents of kinase activity.[45]

3.4.7 Importance of Ephrin-B2-EphB4 interaction in tumor angiogenesis

The role of Eph-Ephrin signaling in tumor angiogenesis remains a controversially discussed topic, as opposite functions have been documented, depending on the experimental context. In human brain tumor xenografts, EphB4 was shown to act as a negative regulator of blood vessel branching and network formation. The overexpression of EphB4 initiated a switch within the vascularization program, which led to increased circumferential vessel growth and a reduction in the permeability of the tumor vasculature through activation of the angiopoetin-1/Tie2 system. The same effects were shown in a non-neoplastic setting.[76] In contrast, the overexpression of a kinase-defective EphB4 receptor on perivascular support cells stimulated proliferation and invasion of Ephrin-B2-expressing ECs, thus increasing tumor vasculature in breast cancer xenografts.[77] By blocking EphB4 – Ephrin-B2 interaction via a soluble

Introduction

extracellular domain of EphB4 (sEphB4), endothelial cell migration, adhesion and tube formation, as well as angiogenic effects of certain growth factors, such as VEGF and basic fibroblast growth factor (bFGF), were inhibited, resulting in decreased tumor growth in murine xenograft models.[78] As mentioned above, the effects on tumor vasculature of malignant melanoma have been repeatedly shown in subcutaneous tumor models, however the underlying mechanisms of the observed effects remain to be further elucidated.[45,75]

Furthermore, it has been shown that EphB4 may also interact with the Delta-like 4 (Dll4)/Notch pathway which, similar to the Eph-Ephrin interaction, plays not only a crucial role in embryonic vascular development and arterial specification, but also has far-reaching effects on murine and human tumor vasculature. Notch ligand expression and Notch activation is induced by VEGF, but shows a restricting effect on VEGF signaling, thus arresting endothelial cell proliferation and inducing vessel maturation.[79] Accordingly, inhibition of Dll4/Notch caused reduced tumor growth by increasing vessel proliferation and vessel leakiness by reducing mural cell recruitment.[80] As EphB4-Ephrin-B2 interaction is a crucial pathway downstream from the VEGF and Notch pathways, simultaneous inhibition of both pathways showed a greater efficacy in hampering tumor growth. For this, the monomeric form of the extracellular domain of EphB4 was fused to albumin at the C-terminus (sEphB4-Alb) and shown to act as an antagonist of EphB4 – Ephrin-B2 signaling by further blocking endothelial cell migration, tube formation and reducing angiogenesis.[78] The application of sEphB4-Alb alone was able to reduce the mean tumor volume by 50% in an experimental setting of insulinoma growth in RT2 mice. The synchronous suppression of the Dll4/Notch pathway through allelic deletion in combination with sEphB4-Alb inhibition resulted in a reduction of 90% of tumor volume and also resulted in an extended lifespan of +4 weeks. Histologically, a significant decrease in tumor vessel density, vessel caliber and pericytes recruitment could be observed.[78]

3.4.8 Paradoxes of EphB4 in cancer

Possibly the most striking feature of the Eph family in tumor formation is that the receptor-ligand interaction can either promote or suppress tumor-growth, depending on the cellular context and mainly on presence or absence of the respective ligand.[81] This is unlike classical RTKs, which have traditionally been shown to act as effective

Introduction

oncogenes.[35] EphB4 is widely expressed in human breast cancer cell lines, as several tumorigenic pathways can promote its expression, such as the Janus-activated kinase (JAK) or the Crk/Abl pathway.[82] EphB4 knockdown was found to reduce survival, proliferation and migration of breast cancer cells, suggesting a tumor supporting function.[83] Furthermore, the ectopic expression of EphB4 in mammary epithelial cells was shown to induce a more aggressive and invasive breast cancer phenotype in mouse mammary tumor virus (MMTV)-Neu transgenic mice by facilitating the growth of lung metastases. The increase in metastasis could be facilitated by local EphB4 activation in tumor cells adjacent to blood vessels, which enables their detachment from the tumor and entry into the circulation.[84] Intriguingly, despite the high level of EphB4 expression in breast cancer cell lines, the tyrosine phosphorylation of the receptor has been shown to be significantly lower than in non-transformed epithelial cells.[85] However, phosphorylation of the EphB4 tyrosine kinase is necessary for it to exhibit tumor-suppressing functions. The stimulation of the phosphorylation with soluble Ephrin-B2-Fc has repeatedly been shown to inhibit the viability, motility and invasion of breast cancer cells in vitro and in vivo.[85,83] Accordingly, the silencing of EphB4 signaling in breast cancer cells is consistent with their low expression of Ephrin-B2.[86]

3.4.9 Therapeutic opportunities

The widespread expression of Ephs and Ephrins in different types of cancer implicates not only the necessity to further broaden our understanding of this highly complex topic, but also the potential therapeutic possibilities that arise from these receptors. However, considering that the effects of the molecular Eph-Ephrin interaction can have such widespread and even paradoxically opposed effects, the development of effective therapeutic strategies is challenging.

In breast cancer, the most effective design to target the downstream EphB4/Abl/Crk pathway appears to be the promotion of EphB4 phosphorylation, utilizing soluble forms of Ephrin-B2 such as Ephrin-B2-Fc. Systematically administered Ephrin-B2-Fc has been shown to inhibit the growth of breast cancer xenografts.[85] Soluble monomeric EphB4 (sEphB4) has also proven to dramatically reduce tumor growth of subcutaneous A375 melanoma cells in nude mice by inhibiting forward and reverse signaling and thus reducing proliferation in vivo and reducing intratumoral microvessel density and tumor-derived angiogenesis.[78,87] In cases where the EphB4 kinase activity increases rather than reduces the malignancy of the tumor cell, kinase inhibitors, similar to those, that

are already applied in the treatment of chronic myeloid leukemia may prove effective.[88] In preliminary experiments of our research group, we found that the effectivity and site-specificity of malignant melanoma metastasis, particularly to the spine, are significantly affected by interactions between endothelial cell Ephrin-B2 and tumor cell EphB4 and not only driven by biomechanical forces and patterns of circulation.[89] Furthermore, a significant increase of spinal metastatic burden was shown under endothelial Ephrin-B2-knockout (Broggini et al., *currently under review).*

3.5 Aims of the dissertation

The main aims of this dissertation were:

1) Characterize the Ephrin-B2 – EphB4 signalling pathway in spinal metastasis formation.

2) Investigate the consequences of therapeutic intervention of the pathway on growth, development and angiogenesis of spinal metastases.

4 Materials and methods

4.1 Materials

4.1.1 Cell line and cell culture

Luciferase-expressing B16-luc mouse melanoma cells were used in the present study. B16-luc cells were generated from B16-F1 [Mus musculus (mouse) melanoma] (ATCC® CRL-6323™) cells by lentiviral infection with a firefly luciferase, green fluorescence protein and puromycin resistance construct [FFLUC-eGFP-Puro vector], as in previous experiments from our group described by Broggini et al.[90]

4.1.2 Maintenance of tumor cells

The B16-luc cells were maintained in DMEM-high glucose medium supplemented with 10% FBS, 50 units/ml penicillin, 50 µg/ml streptomycin and 5 µg/ml puromycin in a humidified incubator at 37°C and 5% CO_2. Splitting of the tumor cells was performed every two days, or whenever the cells had reached 80% confluency in the culture.

4.1.3 Freezing and thawing of tumor cells

Cryopreservation was carried out when the cells had achieved a confluency of approximately 80% in a T75 flask. Following washing three times with DPBS and discarding excess medium, the cells were trypsinized with 2 ml of Trypsin/EDTA for 5 minutes at 37°C. The enzymatic reaction was ceased by adding 10ml DMEM high glucose medium and cells were centrifuged at 1200 rpms for 5 minutes. Excess medium was again removed, and the remaining cell pellet was dissolved in 10 ml of cell freezing medium (90% FBS + 10% DMSO), aliquoted to 0.5ml cryopreservation tubes, kept at -80°C overnight and transferred to liquid nitrogen the next morning. For thawing, vials with frozen cells were placed in a 37°C water bath, then swiftly transferred to a cell culture flask and dissolved in 10 ml of DMEM high glucose medium. Cells were centrifuged, excess medium was removed, and cells were plated on a T75 flask.

4.1.4 Preparation of tumor cells for systemic inoculation

On the day of the inoculation (day 0), tumor cells were washed three times with PBS, trypsinized, dissolved in 10 ml DMEM and centrifuged. Excess medium was removed, and cells were counted using a Casy cell counter – Model TT (OMNI Life Science). If

Materials and methods

the viability was above 90%, the cells were re-suspended to obtain a final concentration of 1.000.000 cells/ml DMEM and kept on ice until injection.

4.2 Animal experiments

4.2.1 Mice strains

Adult tamoxifen inducible endothelial-cell specific Ephrin-B2-knockout (efnb2$^{i\Delta EC}$) mice and efnb2$^{lox/lox}$ C57BL/6 control mice (littermates not carrying the *CDH5*-(Pac)-CreERT^2 allele) were used for the study (C57/Bl6J.Alb.EB2.CDH5creERT2 strain).[91,92]

The mice were kept at 22°C room temperature with a 12-hour light/dark cycle and monitored daily. Animals were randomized before the first treatment and euthanized when displaying excessive discomfort during the study. Surgical tissue isolations were performed as terminal procedures after sacrificing the animals as described below, and all precautions were taken to minimize suffering.

4.2.2 Ethics statement

Animal experiments were conducted in strict accordance with German animal care guidelines. All experiments were approved by the German state office for health and social affairs (LaGeSo – Landesamt für Gesundheit und Soziales Berlin, G0260/12, Nov.26, 2012).

4.2.3 Pre-experimental procedure

Prior to the therapeutic experiments, both efnb2$^{i\Delta EC}$ knockout and control efnb2$^{lox/lox}$ animals were injected intraperitoneally with tamoxifen using approximately 75mg tamoxifen/kg body weight once every 24 hours for a total of 5 consecutive days to activate Cre-induced endothelial Ephrin-B2-knockout in efnb2$^{i\Delta EC}$ mice (according to the protocol compiled by Jackson Laboratory, Heffner, 2011)[93] and for control purposes in efnb2$^{lox/lox}$ animals. For this, tamoxifen was dissolved in corn oil solution at a concentration of 20 mg/ml by shaking overnight in a light-blocked vessel at 37°C. After dissolution, tamoxifen was routinely kept at 4°C and warmed to room temperature prior to the injections. Following the ultimate injection, all mice were submitted to a 7-day resting period in order to normalize any potential stress-related factors, before they were introduced into the experiments.

Materials and methods

4.2.4 Therapeutic study design

Before the first administration of therapeutics, both tamoxifen-pretreated efnb2$^{i\Delta EC}$ (knockout) and efnb2$^{lox/lox}$ (control) animals were randomly assigned to two different therapy groups: i) pre-tumor treatment and ii) post-tumor treatment.

The *pre-tumor treatment cohort* was designated to receive the therapeutic agents shortly before and after the intra-arterial tumor cell injection (-5 and +4 days) with the intention to affect the initial steps of metastasis formation.

The *post-tumor treatment cohort* received the therapeutics 12 – 21 days post tumor cell injection, after establishment and growth of the metastases had already begun.

4.2.5 Therapeutic agents, treatment regimens and analysis

Treatment consisted of injections either with Ephrin-B2-Fc, or NVP BHG712, a specific small molecule inhibitor of the EphB4 tyrosine kinase. Appropriate control groups of mice were treated by placebo and were administered either IgG-Fc antibody or PEG 300, according to the study protocols (Fig.3, 4, 5). In total, there were 12 experimental groups in the study.

Figure 3: Therapeutic study design
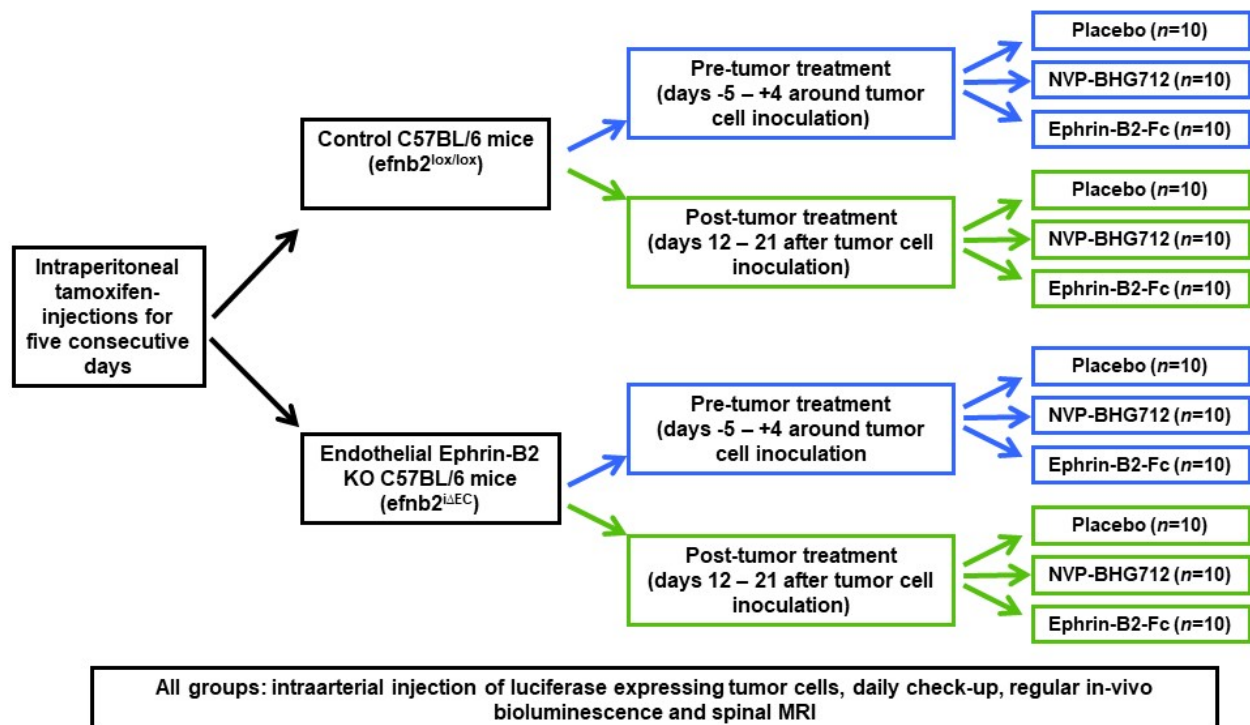
Figure 3: Schematic depicts the classification of therapy groups and controls as well as timelines and treatment regimens in the 12 different experimental groups.

Materials and methods

In the pre-tumor treatment cohort, mice received therapeutics as follows:

The Ephrin-B2-Fc treatment cohort, both with efnb2$^{i\Delta EC}$ knockout and control efnb2$^{lox/lox}$ animals, received four i.v. injections of 100 µl Ephrin-B2-Fc dissolved in sterile PBS, injected into the retro-orbital plexus once every three days, starting 5 days before to 4 days after tumor cell inoculation (Figure 4a).

Figure 4a: Timeline of injections of Ephrin-B2-Fc in pre-tumor treatment cohort:
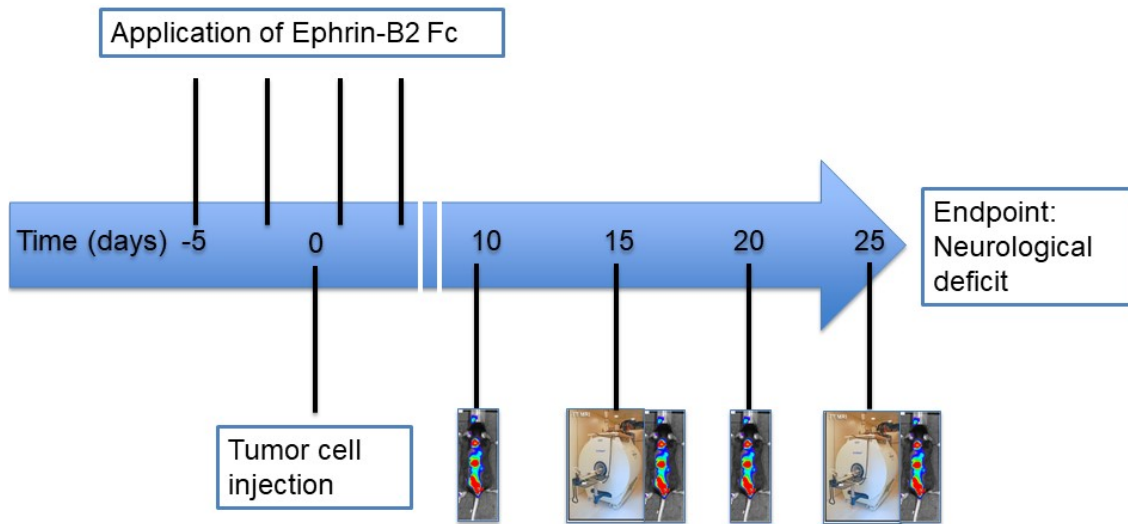
The pre-tumor treatment cohort receiving the small molecule inhibitor, both with efnb2$^{i\Delta EC}$ knockout and control efnb2$^{lox/lox}$ animals, received 100 µl of NVP-BHG 712 dissolved in PEG 300 intraperitoneally (i.p.) for 8 consecutive days, starting on day -5 (Figure 4b).

Figure 4b: Timeline of injections of NVP-BHG 712 in pre-tumor treatment cohort
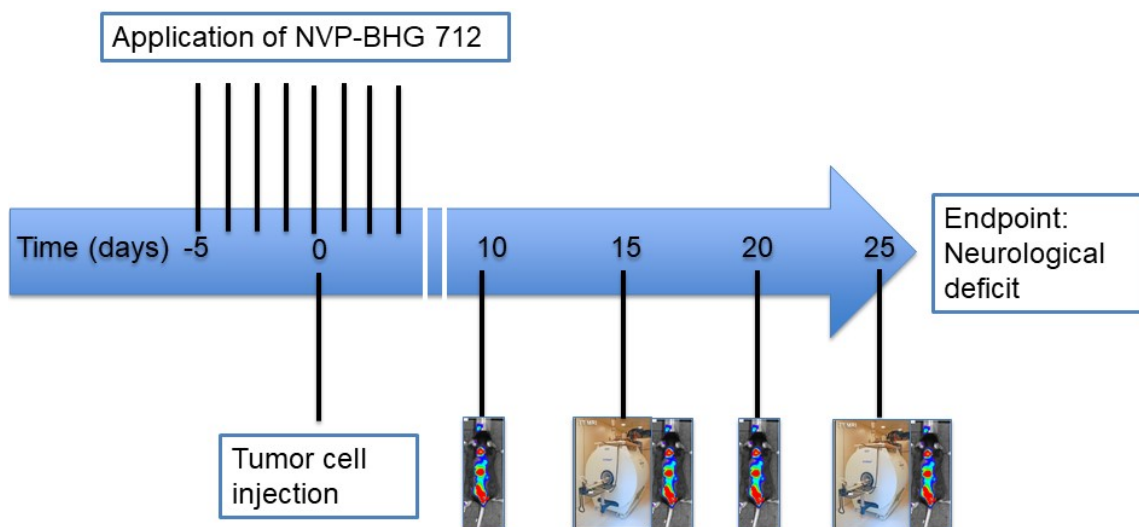
Materials and methods

Figure 4: *Pre-tumor treatment cohort received 100 µl Ephrin-B2-Fc (shown in Figure 4a) on days -5, -2, 1 and 4, or 100 µl of NVP-BHG 712 / PEG 300 (shown Figure 4b) for 8 consecutive days, starting on day -5. In-vivo bioluminescence was performed 10, 15, 20 and 25 days after tumor cell injection. Magnetic resonance imaging was performed regularly on day 15 and 25 post-injection as well as whenever neurologic deficits occurred.*

In the post-tumor treatment cohort, mice received therapeutics as follows:

Mice that were designated to receive treatment after establishment of the metastases received the therapeutics in the same regimen as previously, however the application of the therapeutics was carried out between days 12 and 21 after tumor cell injection. The first post-tumor treatment cohort, both with efnb2$^{i\Delta EC}$ knockout and control efnb2$^{lox/lox}$ animals, received 100 µl Ephrin-B2-Fc on days 12, 15, 18 and 21 after tumor cell inoculation (Figure 5a).

**Figure 5a: Timeline of injections of Ephrin-B2-Fc in post-tumor treatment cohort:**
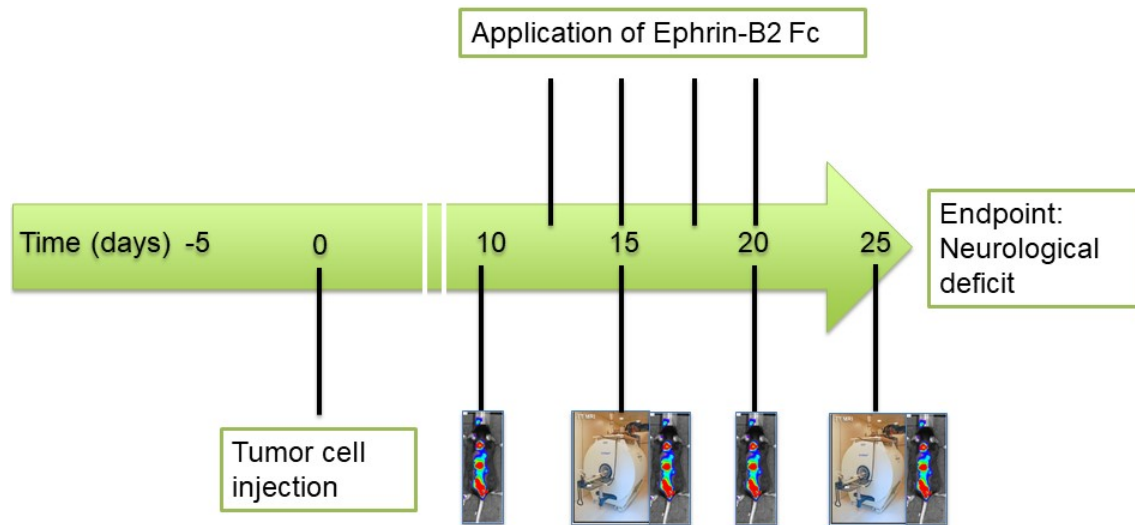
The second post-tumor treatment group, both with efnb2$^{i\Delta EC}$ knockout and control efnb2$^{lox/lox}$ animals, received 8 i.p. injections of NVP-BHG 712 / PEG 300 13 days after the tumor cell inoculation (Figure 5b).

Materials and methods

Figure 5b: Timeline of injections of NVP-BHG 712 in post-tumor treatment cohort
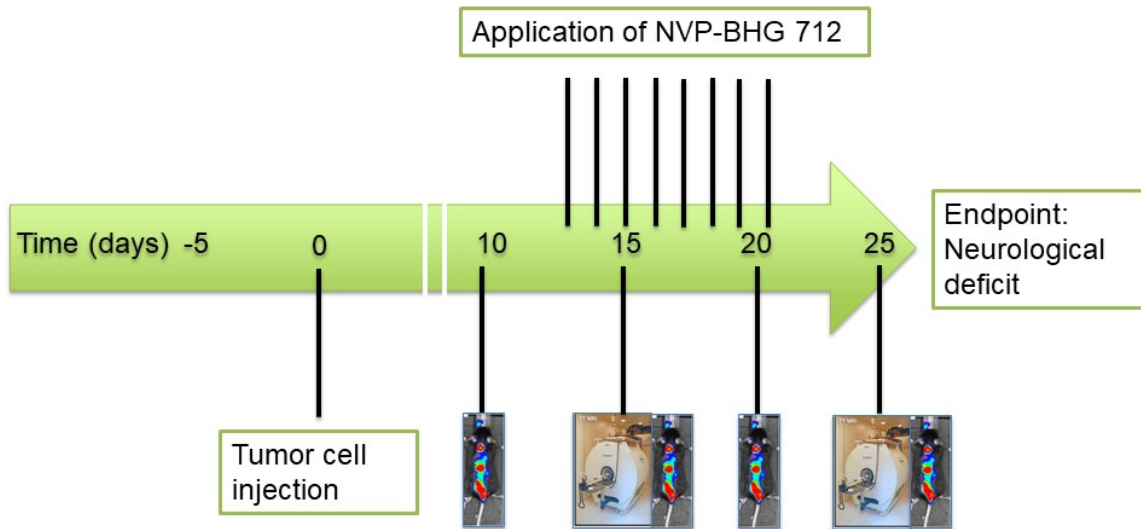
Figure 5: Post-tumor treatment cohort received 100 µl Ephrin-B2-Fc (shown in Figure 5a) on days 12, 15, 18 and 21, or 100 µl of NVP-BHG 712 / PEG 300 (shown Figure 5b) for 8 consecutive days, starting on day 13. As above, in-vivo bioluminescence was performed 10, 15, 20 and 25 days after tumor cell injection. Magnetic resonance imaging was performed regularly on day 15 and 25 post-injection as well as whenever neurologic deficits occurred.

The pre-tumor and post-tumor placebo treated groups, both with efnb2$^{i\Delta EC}$ knockout and control efnb2$^{lox/lox}$ animals, received either one injection containing 4.35 µl of IgG-Fc dissolved in 100 µl sterile PBS retro-orbitally (i.v.) every three days, or 100 µl PEG 300 (i.p.) for 8 consecutive days.

The study was terminated when mice exhibited symptoms connected with excessive tumor growth such as weight loss or behavioral changes (in accordance with German animal welfare guidelines as recommended by the Society of Laboratory Animal Science – GV-SOLAS) or whenever a paretic phenotype appeared.

4.2.6 Establishment of hematogenous spinal metastases in-vivo

After completing the 5-day tamoxifen pre-treatment and 7-day resting period, all experimental mice (bodyweight 21-35 g) were anaesthetized with a mixture of 7% ketamine and 8% xylazine hydrochloride in aqueous solution, applying 100µl/10g bodyweight. Complete unconsciousness was verified by testing foot reflexes. Under the operating microscope, the left region of the neck was shaved, the skin was opened, and the parotid gland was deviated laterally, in order to expose the left carotid artery.

Materials and methods

Connective tissue and visceral fat were removed and the vagus nerve was carefully separated from the artery. The carotid artery was temporarily ligated to prevent bleeding and a catheter (0.8 mm Ø) was retrogradely inserted into the vessel and fixed with another ligature. B16-luc mouse melanoma cells ($1x10^5$ cells suspended in 100µl DMEM) were slowly injected retrogradely into the aortic arch. The injection of the DMEM/cell suspension was followed by an injection of 100µl 0.9% NaCl to rinse any remaining cells from the catheter. Afterwards, the catheter was removed, the carotid artery was permanently ligated, and the skin was sutured. Mice were kept on heating plate (37° C) until complete consciousness was regained, before placing them back into the cages. Mice were checked upon daily to evaluate occurrence of neurological deficits and/or behavioral changes.

4.3 In-vivo imaging

4.3.1 In-vivo bioluminescence imaging

Bioluminescence imaging was performed on postoperative days 10, 15, 20 and 25 to locate the site and extent of tumor growth in vivo. 1 g of D-Luciferin was dissolved in 33.3 ml PBS to create a stock solution and kept at -20°C. 10µl/g bodyweight D-luciferin solution was thawed and injected intraperitoneally as described in the manufacturers protocol (Caliper LS). Five minutes were allowed for the solution to be absorbed and circulated in the murine organism. Subsequently, mice were anesthetized applying 1.5 – 2% (depending on weight) isoflurane in 30% O_2 and 70% NO_2 via a breathing mask, shaven along the spine and placed in the IVIS Lumina II (Caliper LS) imaging luminometer. Two pictures were obtained, one dorsal and one ventral view, each with an exposure time of 5 minutes. Representative pictures with bioluminescence images are shown in Fig. 6.

Materials and methods

Figure 6: In-vivo bioluminescence imaging
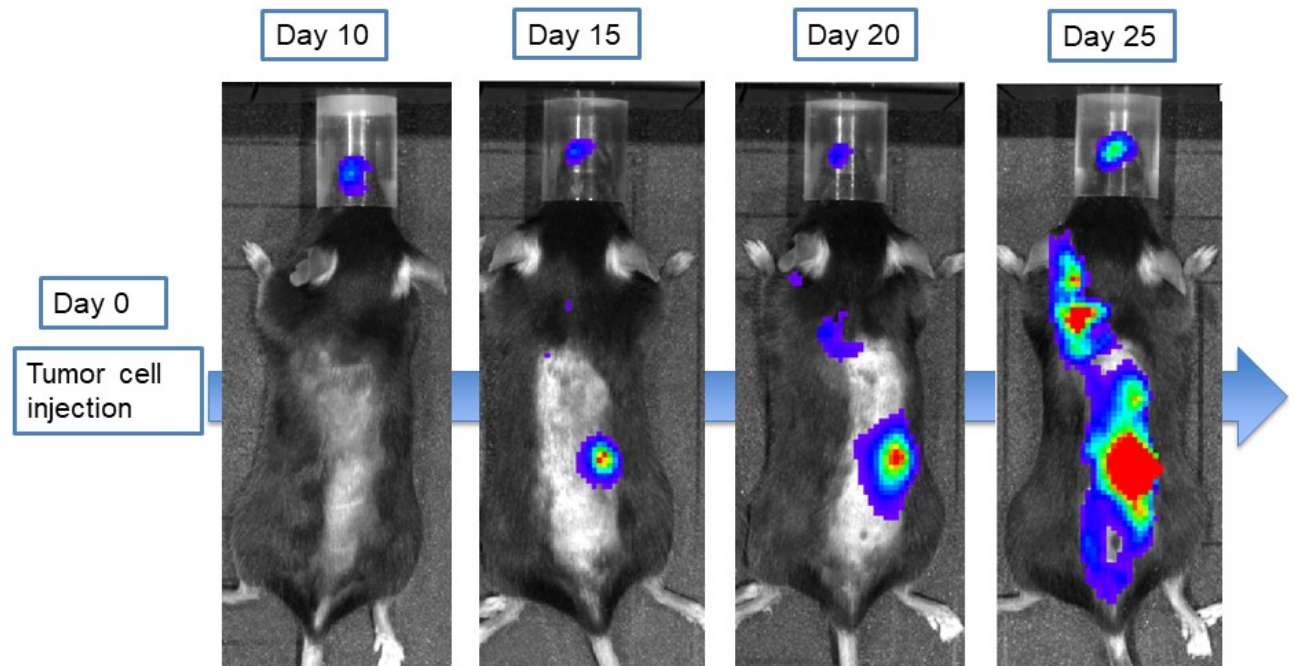
Figure 6: Bioluminescence imaging shows growth of spinal metastases over time on days 10, 15, 20 and 25 after tumor cell injection (exemplified in a placebo-treated efnb2^{lox/lox} mouse)

4.3.2 In-vivo magnetic resonance imaging

Regularly on day 15 and 25 of the experimental procedure, as well as whenever a paraparetic phenotype appeared, MRI scans were performed with a 7 Tesla rodent magnetic resonance imaging scanner (BioSpec 70/20 USR, Bruker) to evaluate a potential metastatic compression of the spinal cord. A 16cm horizontal bore magnet and a 1H-RF-Volumeresonator were used. The H-resonance frequency was 300 MHz, the maximum gradient strength was 300mT/m. Mice were placed on a heating mat and continuously anesthetized using 1.5 – 2% isoflurane in 70% NO_2 and 30% O_2. Using a pressure detector, the respiration rate, ECG and temperature were continuously analyzed during the scanning procedure to ensure sufficient depth of anesthesia [Small Animal Monitoring System (SA Instruments, Inc.)]. Paravision 6 software (Brucker) was used to generate sagittal T2 weighted images with a slice thickness of 2 mm. The images were assessed using Analyze 11.0 software (Mayo Clinic). Tumor area was marked manually in all slices. Total and mean metastatic volumes were calculated.

Figure 7: Representative series of images of metastatic epidural spinal cord compression
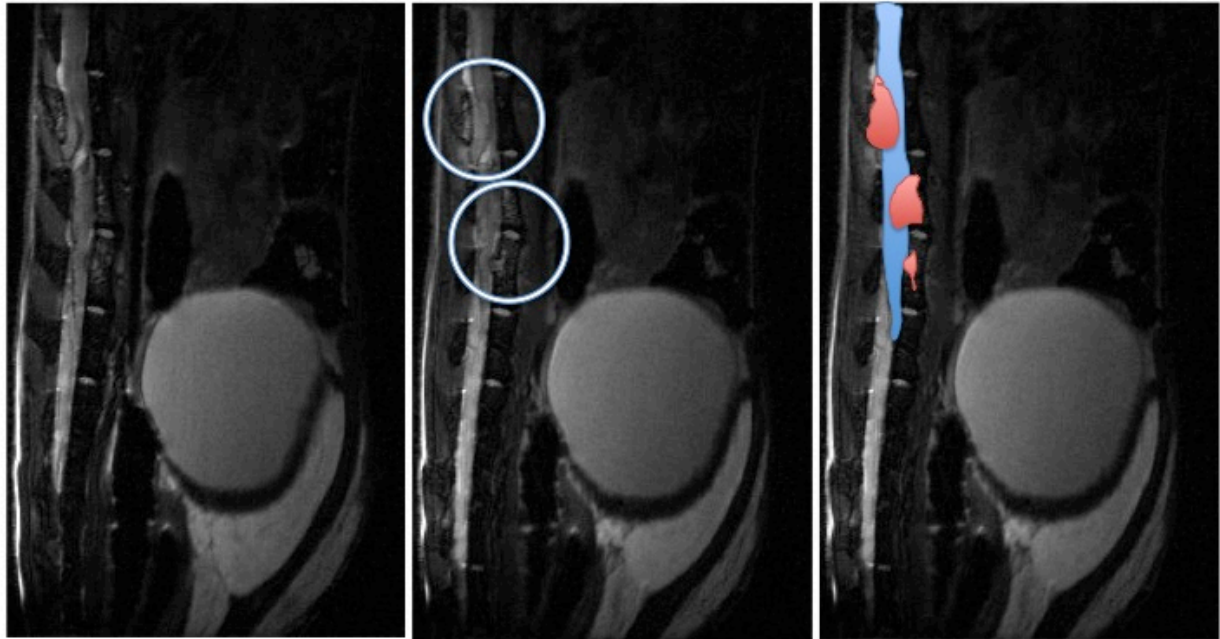
Figure 7: Representative series of sagittal, T2-weighted MR-images of spinal metastases (marked by white rings) with epidural spinal cord compression from the anterior and posterior elements of the vertebrae. (Metastatic tumors marked red, compression of the spinal cord marked blue)

4.4 In-vitro tumor imaging and tissue analysis

4.4.1 Tissue collection

At the day of termination of the study (day 35), or at occurrence of paresis, mice were anaesthetized as described above. Testing of the foot reflexes ensured complete numbness. Mice were euthanized by cervical dislocation and decapitated. Using operating scissors, the skin was longitudinally opened along the spinal column and the spine was extracted from the surrounding muscle tissue, before remaining organs were resected. All organs were immediately frozen in -50°C isopentane and transferred to -80°C for long-term storage. Murine spines were either used for the luminescence assay or further processed for immunohistochemical staining.

4.4.2 Tissue homogenization

To prepare the lysis buffer for tissue homogenization, 0.1M of TrisHCl (15.76 g) was dissolved in 1 liter of distilled water under constant stirring. After thorough stirring, 2 mM

of EDTA and 0.1% Triton-X 100 were added and the lysis buffer was kept at 4°C. All organs were constantly kept on dry ice. Pestle and mortar were used to pulverize the osseous organs under continued cooling with liquid nitrogen, until a particle size of 1-2 mm was achieved. The powder and soft tissue organs were transferred to individual gentle macs tubes. The luciferase lysis buffer was added for cell lysis. Depending on the size and weight of the individual organs, different amounts of the lysis buffer were needed. 10 ml were used for skin & hindlimbs, 5ml for cranium, forelimbs, thorax and liver and 2 ml of lysis buffer for brain, lung, heart, kidney and spleen. The spine was split into cervical, thoracic and lumbar parts and also stirred with 2 ml of lysis buffer each. The organs were further homogenized using a Xiril Dispomix tissue tearer (Miltenyi Biotec) at 4000 rpms for 15 sec (Profile 4) twice. Lysates were constantly kept on ice, and consequently centrifuged at 1300g for 5 minutes at 4°C (Heraeus Multifuge, Thermo Fisher Scientific). The supernatant was transferred and used for the in-vitro luminometry.

4.4.3 In-vitro luminometry

A standard calibration curve for the measurement of the bioluminescence of disseminated and metastatic tumor cells was generated using a Tecan 200M spectrometer (Tecan), by defining the fluorescence intensity of 100,000, 50,000, 25,000, 12,500, 6,250, 3,125 and 1,562.5 cells after the addition of 60 µl Bright-Glo luciferase substrate to 30 microliters of organ lysate supernatant in a black flat bottom 96 well plate.

The measurement and quantification of the relative number of photons (Relative Light Units = RLU) was measured for three seconds as described in the manufacturers kit (Promega). The number of tumor cells was calculated for every individual organ, applying the standard curve defining the RLUs for specific cell numbers.

4.5 Processing, freezing & sectioning of spines

4.5.1 Processing of spines for immunohistochemical staining

The murine spines were fixed in 4% (wt/vol) paraformaldehyde (PFA) for 4 hours at 4°C in a 15 ml conical tube. The spines were then added to a decalcification solution (0,5 M EDTA, pH 7,4) in order to soften the osseous tissue and improve the integrity of the tissue sections. The decalcification was carried out under constant agitation at 4°C for 96 hours to ensure homogenous effects on the entire vertebral column. For cryoprotection, a solution containing 20% (wt/vol) sucrose and 2% (wt/vol) polyvinylpyrrolidone (PVP, Sigma Aldrich) was added for another 24 hours at the end of the decalcification process. The freezing was carried out in a gelatin-based freezing solution containing 8% (wt/vol) gelatin, 20% (wt/vol) sucrose and 2% (wt/vol) PVP. Tissue samples were frozen at -80°C until sectioning. Sagittal sections of 200 μm were prepared by using a Cryotome (Microm HM 560 – Thermo Fisher Scientific).

4.5.2 Process of immunohistochemical staining

PFA-fixed and decalcified 200 μm tissue sections were permeabilized using 0,3% Triton X-100 for 10 minutes at room temperature (RT). Unspecific binding was precluded by blocking in 1% (wt/vol) casein / PBS for 30 minutes at RT. Slides were washed three times with PBS. Incubation with the primary antibodies was carried out in 1% (wt/vol) casein / PBS for 2 hours at room temperature. After primary antibody incubation, sections were washed three times with PBS and incubated with appropriate fluorescent secondary antibodies (concentration 1:400 in 1% (wt/vol) casein / PBS) in a light-blocked container for 1 hour at room temperature. Sections were again washed three times with PBS for 5 min, nuclei were counterstained with 4'-6-diamidino-2-phenylindole dihydrochloride hydrate (DAPI) for 10 mins. Sections were washed again three times with PBS. Slides were embedded in Immu-Mount (Thermo Fischer) embedding medium and mounted with glass cover slips. The slides were routinely kept in a dark place at 4°C. Reagents, primary and secondary antibodies for immunohistochemistry are detailed in the Supplemental Materials and Methods.

The intratumoral presence of Ephrin-B2 was detected by staining with anti-Ephrin-B2 primary antibody (Neuromics) at a concentration of 1:50 in PBS. Anti-endomucin antibody (Santa Cruz) was applied in a concentration of 1:100 to stain endothelial cells of the tumor vasculature and consequently analyze size, number and distribution of

tumor vessels. Double immunofluorescence-staining using anti-Ephrin-B2 and anti-endomucin antibodies verified the presence of Ephrin-B2 in tumor blood vessels. Anti-Ki-67 primary antibody (Thermo Fisher Scientific) was applied at a concentration of 1:100 to assess the proliferative fraction of tumors.

4.5.3 Evaluation of immunohistochemical staining

Confocal laser-scanning microscopy was utilized to evaluate the immunohistochemical stainings. Tile Z-stacks of 60-70 micrometers with a Z-step size of 4 micrometers were generated using an oil-immersed 63x magnification in a Leica DM 2500 microscope. The laser settings were based on emission wavelengths of the respective secondary antibodies. Four fields of view (FOV) were analyzed in at least 3 different slices per individual tumor. The number of tumor blood vessels as well as the area coverage representing the overall size of vessels (measured in % of tumor covered by vessels) was calculated.

4.6 Image analysis and quantification of tumor vascularization

ImageJ (NIH) was used to quantify staining area and coverage of tumor vessels, as well as distribution and number of marker-positive cells in immunohistochemical stainings. The percentage of tumor covered by vessels corresponds to the percentage of n=5 tumor section fields showing endomucin-positive signals. The magnetic resonance imaging data was analyzed using Image J. Tumor volume was assessed in all slices and tumor area was marked manually. The number of spinal metastasis and the individual tumor area was calculated for every animal and used to calculate the mean and total tumor volume per animal.

4.7 Data evaluation & statistical analytics

Quantitative data are given as means ± SEM. Mean values were calculated from the average values of each animal. The number of animals used is indicated in the respective figure legend. For the comparison of the survival data, the Log-rank (Mantel-Cox) test was used and the significance level was adjusted for multiple comparisons utilizing the Bonferroni method. A one-way ANOVA followed by Dunnett's multiple comparison correction was applied for differences in multiple group comparisons, and an unpaired t-test for the comparison of two groups. A result with $p \leq 0.05$ was considered significant.

Materials and methods

One star (*) indicates p ≤ 0.05, two stars (**) indicate p ≤ 0.01 and three stars (***) indicate p ≤ 0.001. The statistical analysis of all the collected data was carried out utilizing GraphPad Prism 6 (Graphpad, La Jolla, CA, USA) software and Microsoft Excel (Microsoft, Seattle, WA, USA).

5 Supplemental materials and methods

5.1 Reagents and enzymes

- Bright-Glo^{TM} Luciferase Assay System – Promega (#E2610, Fitchburg, WI, USA)
- ChromPure Mouse IgG, Fc Fragment – Jackson ImmunoResearch (#015-000-008, West Grove, PA, USA)
- Corn oil – Sigma Aldrich (#C8267, St. Louis, MO, USA)
- D-Luciferin, Firefly, potassium salt – Caliper Life Sciences (#XR-1001, Hopkinton, MA, USA)
- D-Luciferin sodium salt – Santa Cruz (#sc-207479, Santa Cruz, CA, USA)
- Dulbecco's phosphate buffered saline (DPBS) – Sigma Aldrich (#D8537, St. Louis, MO, USA)
- Ephrin-B2/Fc Chimera – R&D Systems (#496-EB, Minneapolis, MI, USA)
- Fluoromount-G – Biozol Diagnostica (#0100-01, Eching, Germany)
- Gibco^{TM} Penicillin-Streptomycin (10,000 U/mL) – Thermo Fisher Scientific (#15140122, Waltham, MA, USA)
- Ketavet (Ketamine) – Pfizer (#B2502-04, New York City, NY, USA)
- NVP-BHG 712 – Sigma Aldrich (#SML0333, St. Louis, MO, USA)
- PEG 300 – Sigma Aldrich (#90878, St. Louis, MO, USA)
- Puromycin – Thermo Fisher Scientific (#A1113802, Waltham, MA, USA)
- Rompun (Xylazine hydrochloride) – Bayer (#KP07TPA, Leverkusen, Germany)
- Tamoxifen – Cayman (#CAS 10540-29-1, Ann Arbor, MI, USA)
- Tramal (Tramadol) – Grunenthal (#PZN-7803245, Aachen, Germany)

5.2 Buffer and media

5.2.1 Cell culture media

- 90% Gibco^{TM} DMEM, 4,5 g/l D-Glucose, L-Glutamin, Pyruvate, – Thermo Fisher Scientific (#31965, Waltham, MA, USA)
- 10% Gibco^{TM} fetal bovine serum – Thermo Fisher Scientific (#10500064, Waltham, MA, USA)
- 50 µg / ml Gibco^{TM} Penicillin-Streptomycin (10,000 U/mL) – Thermo Fisher Scientific (#15140122 Waltham, MA, USA)

Supplemental materials and methods

5 µg / ml Puromycin – Thermo Fisher Scientific (#A1113802, Waltham, MA, USA)

5.2.2 Cell freezing media

- 90% Gibco^{TM} fetal bovine serum – Thermo Fisher Scientific (#10500064, Waltham, MA, USA)

- 10% DMSO – Dimethyl sulfoxide – Sigma-Aldrich (#276855, St. Louis, MO, USA)

5.2.3 Luciferase lysis buffer

- 0,1 M TrisHCl – Sigma Aldrich (RES3098T-B7, St. Louis, MO, USA)

- 0,1% Triton X-100 – Biomol GmbH (T8655.500, Hamburg, Germany)

- 2mM EDTA – Thermo Fisher Scientific (AM9260G, Waltham, MA, USA)

5.3 Immunohistochemistry antibodies

5.3.1 Primary antibodies

- 4'-6-diamidino-2-phenylindole dihydrochloride hydrate (DAPI), 1.0 mg/ml – Thermo Fisher Scientific (#D1306, Waltham, MA, USA) 1:100

- Anti-Desmin – Rabbit, Anti-Mouse Antibody, 200 µg/ml – Abcam (ab8592, Cambridge, UK) 1:100

- Anti-Endomucin – Rat, Anti-Mouse Antibody, 200 µg/ml – Santa Cruz (#sc-65495, Santa Cruz, CA, USA) 1:100

- Anti-Ephrin-B2 – Goat, Anti-Mouse Antibody, 1.0 mg/ml – Neuromics (GT15026, Edina, MN, USA) 1:50

- Anti-Ki67 – Rabbit, Anti-Mouse Antibody, 1.0 mg/ml – Thermo Fisher Scientific, (# PA5-19462 Waltham, MA, USA) 1:100

5.3.2 Secondary antibodies

- Anti-Pecam1 conjugated to Alexa Fluor488 – R&D Systems (FAB3628G, Minneapolis, MI, USA) 1:400

- Cy3 – Goat Anti-Rat IgG-Fc pre-adsorbed – Abcam (ab97035, Cambridge, UK) 1:400

- Cy5 – Goat Anti-Rabbit IgG-Fc pre-adsorbed – Abcam (ab97077, Cambridge, UK) 1:400

- FITC – Goat Anti-Rabbit IgG-Fc pre-adsorbed – Abcam (ab97199, Cambridge, UK) 1:400

5.4 Equipment

- Casy Cell Counter – Casy Modell TT – OMNI Life Science, (#5651697, Bremen, Germany)
- Centrifuge – Heraeus^{TM} Multifuge^{TM} 3SR+ – Thermo Fisher Scientific (#75004515, Waltham, MA, USA)
- Confocal microscope – Leica DM 2500 – Leica Microsystems (Wetzlar, Germany)
- Cryostat – Microm HM 560 – Thermo Fisher Scientific (Waltham, MA, USA)
- Fluorescence microscope – Zeiss Axiovision 2 – Zeiss (Jena, Germany)
- In-vivo luminometer – IVIS Lumina II – Caliper Life Sciences (Hopkinton, MA, USA)
- Microplate 96 well, PS, F-Bottom (Chimney well), Lumitrac 200, Med.Binding – Grainer Bio One (#655075, Erlangen, Germany)
- Operation microscope – Carl Zeiss OPMI CS-NC – Zeiss (Jena, Germany), Leica WILD M650 – Leica Microsystems (Wetzlar, Germany)
- Small rodent MRI – BioSpec 70/20 USR – Bruker (Billerica, MA, USA)
- Tecan Infinite 200M spectrometer – Tecan (Männedorf, Switzerland)
- Tissue homogenizator – Xiril Dispomix – Miltenyi biotec (Bergisch Gladbach, Germany)

5.5 Software

- Analyze 11.0 – Mayo Clinic (Rochester, MI, USA)
- Axiovission Microscope Software – Zeiss (Jena, Germany)
- GraphPad Prism – GraphPad (San Diego, CA, USA)
- ImageJ – NIH (Bethesda, MD, USA)
- IVIS Living Image Software 3.0 – PerkinElmer Inc. (Waltham, MA, USA)
- Magellan^{TM} – Tecan (Männedorf, Switzerland)
- Office 2011 Mac – Microsoft (Redmond, WA, USA)
- Paravision 6.0 – Bruker (Billerica, MA, USA)

6 Results

6.1 Pre-tumor treatment in efnb2$^{lox/lox}$ animals

6.1.1 The effect of therapy on survival outcomes

The primary endpoint of the experiment was defined as the appearance of partial or complete limb paresis. Mice were checked upon daily to analyze behavior and symmetrical limb movement. In efnb2$^{lox/lox}$ animals, both pre-tumor therapies with Ephrin-B2-Fc (median EB2Fc: 20.5 days, n=7, p=0.0048) and NVP-BHG 712 (median NVP-BHG 712: 21 days, n=14, p=0.0002) resulted in significantly shorter periods until the appearance of neurological deficits when compared with the placebo-treated group (median placebo: 24.5 days, n=11).

Figure 8: Survival analysis of pre-tumor treated enfb2$^{lox/lox}$ control animals

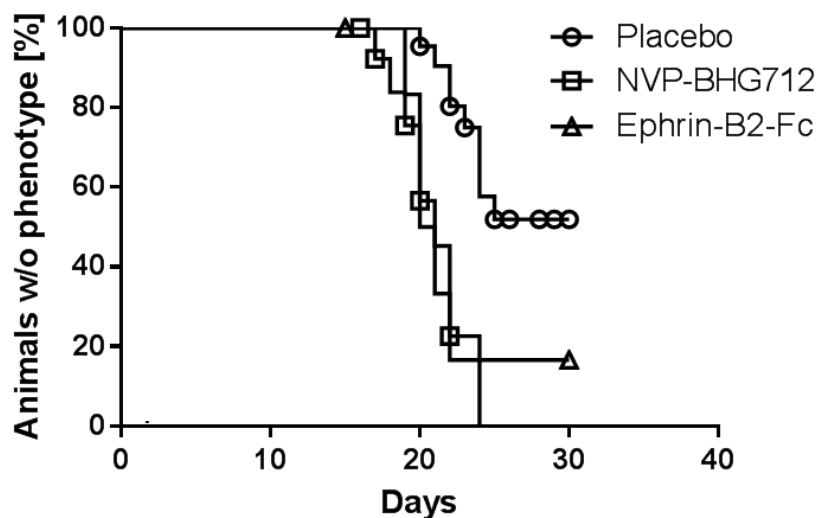*Figure 8:* *Neurological deficit occurred significantly earlier in Ephrin-B2-Fc (median: 20.5 days, n=7, p=0.0048) and NVP-BHG 712 (median: 21 days, n=14, p=0.0002) treated efnb2$^{lox/lox}$ animals compared to placebo-treated group [median: 24.5 days, n=11, Log-rank (Mantel-Cox) test]. Significance threshold was adjusted for multiple comparisons by Bonferroni correction.*

Results

6.1.2 MR imaging results in-vivo

MR imaging was performed regularly on days 15 and 25 after tumor cell inoculation and whenever animals showed a paretic phenotype. In pre-tumor placebo-treated efnb2$^{lox/lox}$ animals, the total number of metastases in the spine was significantly lower than the number found in placebo-treated enfb2$^{i\Delta EC}$ knockout mice (mean: 1.455 ± 0.1575, n=11 and 5.100 ±0.9000, n=10, respectively, p=0.0005, *data not shown).* The application of Ephrin-B2-Fc and NVP-BHG 712 in efnb2$^{lox/lox}$ animals resulted in significantly increased numbers of spinal metastases (mean placebo: 1.455 ± 0.1575, n=11, mean EB2Fc: 4.750 ± 1.750, n=4, p=0.0071; mean NVP-BHG 712: 6.500 ± 0.6455, n=4 p=0.0002, respectively).

The individual tumor volume was unaffected by application of Ephrin-B2-Fc (mean placebo: 3.169 mm^3 ± 0.5870, mean EB2Fc: 3.138 ± 0.4052 mm^3, p=0.9986) or NVP-BHG 712 (mean NVP-BHG 712: 2.640 ± 0.3623 mm^3, p=0.6428) in efnb2$^{lox/lox}$ animals. When comparing the total metastatic volume of all spinal metastases, there was a significant increase upon application of NVP-BHG 712 (mean placebo: 5.174 ± 1.036 mm^3, n=11; mean NVP-BHG 712: 16.86 ± 5.150 mm^3, n=4, p=0.0332), whereas the application of Ephrin-B2-Fc did not show any significant effect (Figure 9C).

Figure 9: Comparison of total number and size of spinal metastases in efnb2$^{lox/lox}$ pre-tumor treatment groups
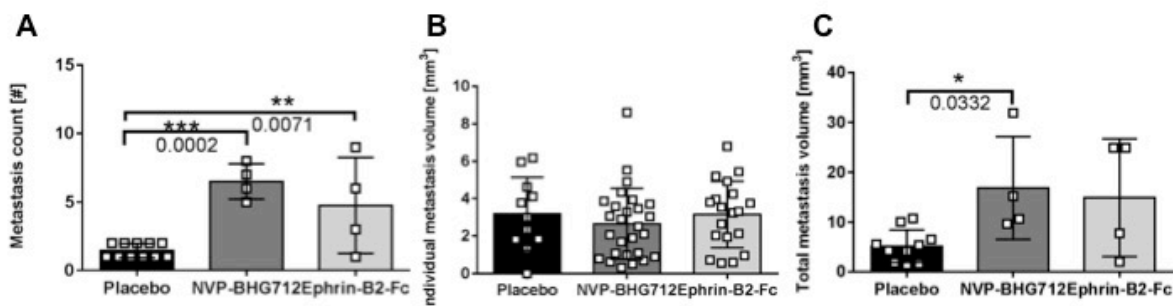
Figure 9: A) The number of spinal metastases was significantly increased both in Ephrin-B2-Fc (n=4) treated and NVP BHG-712 (n=4) treated efnb2$^{lox/lox}$ animals when compared with the placebo group (n=11, p=0.0071 and p=0.0002, respectively). B) The individual tumor volume (mm^3) was not significantly affected [mean placebo: 4.054 ± 0.6457 mm^3, mean EB2Fc: 5.356 ± 1.234 mm^3, p=0.7465 and mean NVP-BHG 712: 6.691 ± 1.708 mm^3, p=0.2720]. C) In total metastasis volume, there was a significant

Results

increase after application of NVP-BHG 712 (mean placebo: 5.174 ± 1.036 mm³, n=11, mean NVP-BHG 712: 16.86 ± 5.150 mm³, n=4, p=0.0332). The analyses were performed by one-way ANOVA with Dunnett's multiple comparison test. Mean values ± SEM for all experiments are shown.

6.1.3 In-vitro bioluminescence quantification of metastatic tumor burden in tissue homogenates

After termination of the study, all organs were resected and homogenized to identify the approximate number of metastatic tumor cells grown in individual organs. The relative light units (RLU) generated by the luminescence of organ lysates were used to calculate the number of metastatic cell equivalents in the individual organs. Beforehand, a standard calibration curve was created by using known numbers of light-emitting B16-luc tumor cells, which was then used to extrapolate the amount of relative light units generated by the tumor cell lysates. The resulting curve slope was 18.22 ± 0.7540 (95% confidence interval).

Figure 10: Standard calibration curve for the relative light units (RLU) generated by known amounts of bioluminescent B16-luc cells

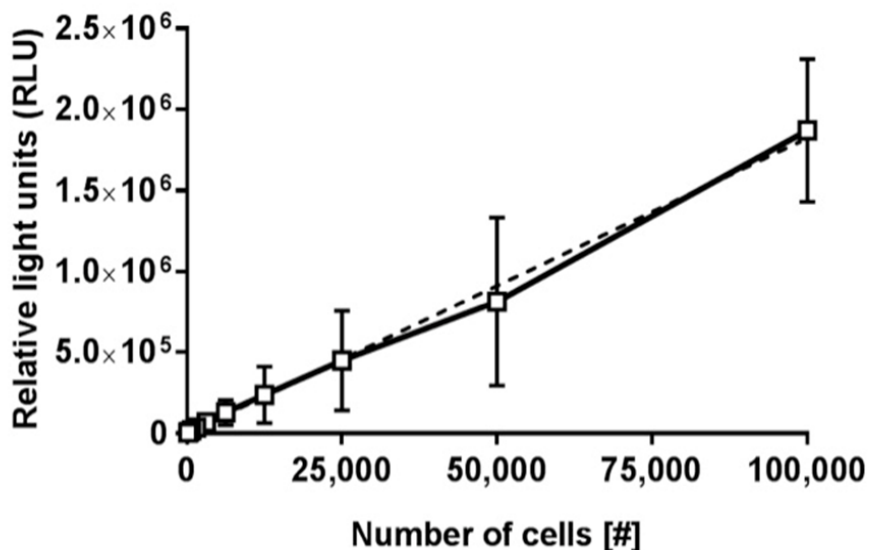*Figure 10: Bold line represents interpolations of unknowns from standard curve, dotted line represents linear regression curve with slope of 18,22 ± 0,7540 (95% confidence interval), n=3. Mean ± SEM for all experiments shown.*

Results

Multi-organ metastasis analysis by in-vitro bioluminescence demonstrated a preference of B16-luc tumor cells to form metastases in osseous organs. The cranium, thoracic bones, the spine and the fore- and hind-legs were defined as osseous organs, whereas the skin, brain, heart, liver, kidneys and spleen were defined as soft tissue organs. The metastatic tumor burden in distinct organs was differentially influenced by therapeutics (Fig.11 A-D). Accordingly, the number of metastatic cells found in the spine of efnb2$^{lox/lox}$ control mice was significantly higher in EphrinB2-Fc-treated animals compared to placebo-treated ones (mean placebo: 7.90469 ± 1.061e+006 cells, n=7, mean EphrinB2-Fc: 8.001e+006 ± 2.659e+006 cells, n=4, p=0.0002).

The organ-specific dissemination of tumor cells in placebo-treated efnb2$^{lox/lox}$ animals showed significantly higher metastatic cell numbers in osseous organs than in soft tissue organs (mean osseous: 9.281e+006 ± 2.847e+006 cells, mean soft tissue organs: 965814 ± 355439 cells, n=7, p=0.0200). The significant preference of the metastatic cells towards the osseous organs was similar in the Ephrin-B2-Fc-treated and placebo-treated animals (mean osseous: Ephrin-B2-Fc: 4.623e+007 ± 8.581e+006 cells, mean soft tissue organs: 3.315e+006 ± 1.334e+006 cells, n=4, p=0.0026)

In contrast, under treatment with NVP-BHG 712, the significant preference of the tumor cells towards osseous organs was lost (mean osseous: 3.650e+007 ± 2.330e+007 cells; mean soft tissue organs: 6.003e+006 ± 4.632e+006 cells, n=6, p=0.2281).

Results

Figure 11: Site-specific dissemination of metastatic B16-luc tumor cells to the spine, osseous and soft tissue organs under pre-tumor treatment in efnb2$^{lox/lox}$ mice
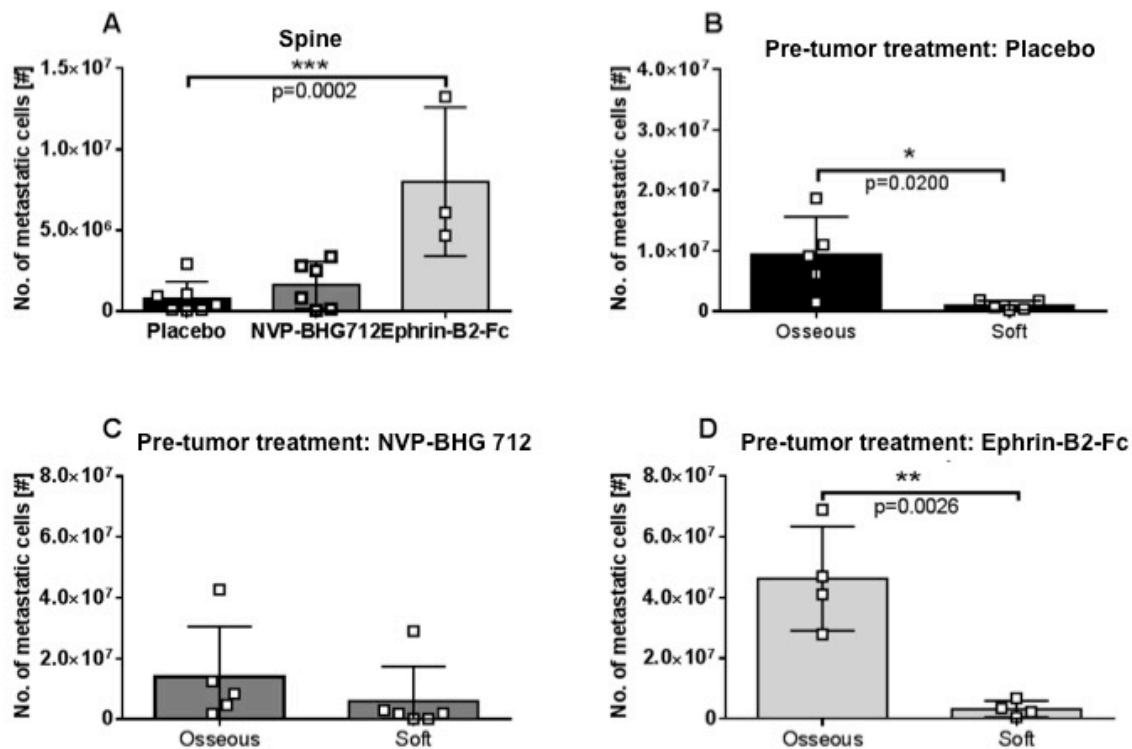
Figure 11: A) Upon pre-tumor treatment with Ephrin-B2-Fc, the number of metastatic cells found in the spine was significantly higher than in placebo-treated animals (mean placebo: 790469 ± 1.061e+006 cells, n=7, mean EphrinB2-Fc: 8.001e+006 ± 2.659e+006 cells, n=4, p=0.0002, one-way ANOVA with Dunnett's multiple comparison test). The application of NVP-BHG 712 (n=6) did not significantly affect the number of tumor cells in the spine. B) Metastatic B16-luc tumor cells showed a significantly higher tendency to metastasize into osseous tissues than to soft tissue organs in placebo-treated efnb2$^{lox/lox}$ animals (mean osseous: 9.281e+006 ± 2.847e+006 cells, n=5; mean soft: 965814 ± 355439 cells, n=5, p=0.0200, unpaired t-test). C) Under NVP-BHG 712 treatment, the significant osseous metastasis preference was lost (mean osseous: 3.650e+007 ± 2.330e+007 cells, mean soft: 6.003e+006 ± 4.632e+006 cells, n=6, p=0.2881; unpaired t-test). D) Under the application of Ephrin-B2-Fc, the tendency of metastasizing into osseous organs was similar to placebo-treated animals (mean osseous: 4.623e+007 ± 8.581e+006 cells, mean soft: 3.315e+006 ± 1.334e+006 cells, n=4, p=0.0026, unpaired t-test). Mean values ± SEM for all experiments are shown.

Results

6.1.4 Immunohistochemical assessment of proliferation activity and tumor vasculature in spinal metastases

The number of proliferating tumor cells per field of view (FOV), as well as tumor vascularization – in terms of size and number of tumor blood vessels – were evaluated by confocal laser microscopy. Proliferating tumor cells were detected by using anti-Ki-67 antibody, whereas endothelial cells were stained by anti-endomucin antibody in a double-fluorescence immunohistochemistry.

The placebo treated efnb2$^{lox/lox}$ control animals exhibited a mean number of 40.13 ± 5.355 proliferating cells per FOV (n=6). Upon application of NVP-BHG 712, there was no significant change in proliferation rate (mean: 59.29 ± 16.13 proliferating cells/FOV, n=7, p=0.4567). Similar results were noted upon pre-tumor application of Ephrin-B2-Fc (mean: 61.23 ± 12.44 proliferating cells/FOV, n=4, p=0.4897).

The application of NVP-BHG 712 did not have any statistically significant effect on the number of tumor blood vessels compared to placebo (mean placebo: 8.600 ± 1.673 vessels/FOV, mean NVP-BHG 712: 10.67 ± 0.8819 vessels/FOV, p=0.3219). Ephrin-B2-Fc also did not significantly affect the number of blood vessels (mean: 11.50 ± 0.500, p=0.1394).

When comparing the size of tumor blood vessels, the percentage of tumor area covered by vessels was analyzed. In placebo treated efnb2$^{lox/lox}$ animals, the mean percentage of tumors covered by endomucin positive blood vessels was 5.492 ± 1.154% (n=6). The pre-tumor application of NVP-BHG 712 did not significantly alter this ratio (mean: 7.444 ± 0.8313%, n=7, p=0.9432). Upon application of Ephrin-B2-Fc, the size of vessels covering the tumor increased significantly (mean: 11.67 ± 1.184%, n=4, p=0.0034).

Results

Figure 12: Number of Ki-67+ tumor cells, vessel size and number in spinal metastases under pre-tumor treatment of efnb2$^{lox/lox}$ mice
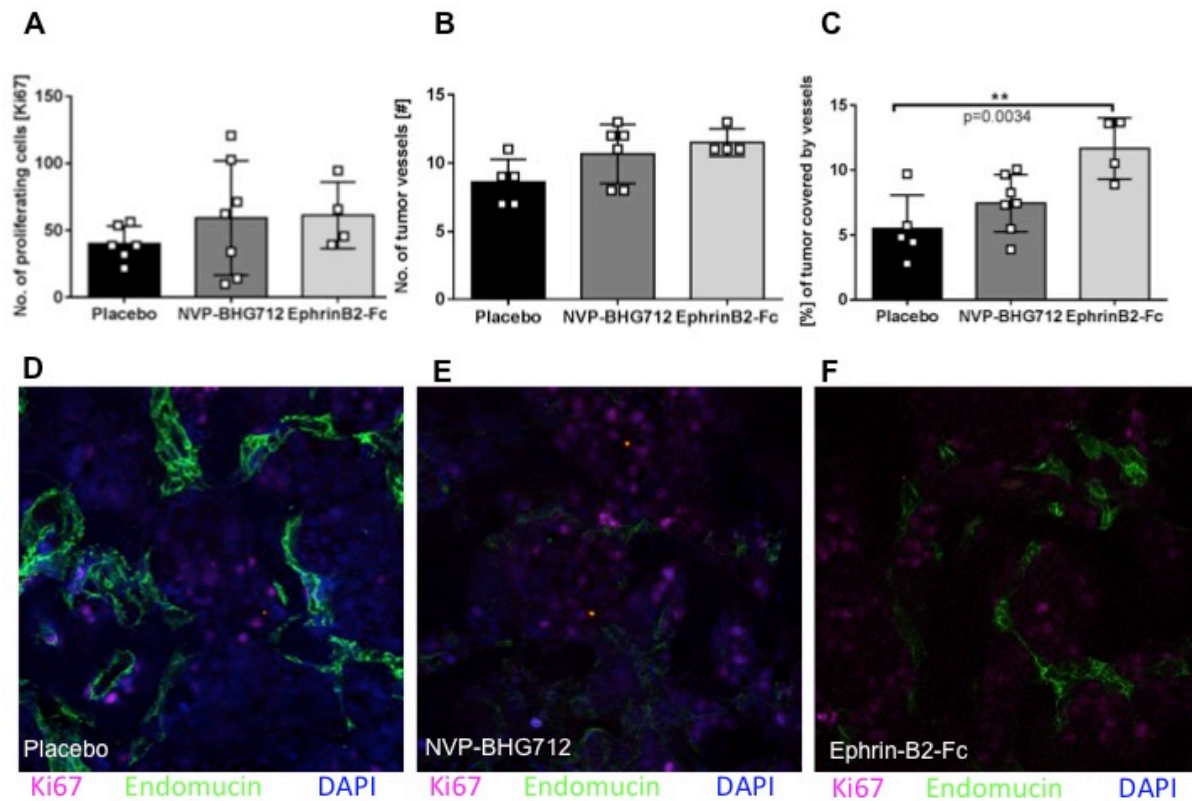
Figure 12: A) The number of proliferating cells did not show significant differences upon application of NVP-BHG 712 or Ephrin-B2-Fc compared to placebo (mean placebo: 40.13 ± 5.355 proliferating cells/FOV, n=6, mean NVP-BHG 712: 59.29 ± 16.13 proliferating cells/FOV, n=6, mean EB2Fc: 61.23±12.44 proliferating cells/FOV, n=4). B) The number of tumor vessels per FOV was not altered significantly by therapeutic use of NVP-BHG 712 and Ephrin-B2-Fc compared to placebo-treatment. C) The size of tumor vessels (measured in % of tumor covered by vessels) increased significantly upon administration of Ephrin-B2-Fc (mean: 11.67 ± 1.184%, n=4) compared to the placebo-treated group (mean: 5.492 ± 1.154%, n=6, p=0.0034, one-way ANOVA followed by Dunnett's multiple comparison test). Mean values ± SEM for all experiments shown. D-F) Confocal microscopic images of spinal metastatic tumors showing endothelial cells marked by green-fluorescent Endomucin-Ab and proliferating tumor cells marked by violet-fluorescent Ki67-Ab. Pre-tumor treatments as indicated.

6.2 Post-tumor treatment in efnb2$^{lox/lox}$ animals

6.2.1 The effect of therapy on survival outcomes

In post-tumor treated efnb2$^{lox/lox}$ animals, the median time until the appearance of neurologic deficits was 28 days under placebo therapy (*n*=17). The application of Ephrin-B2-Fc did not have any significant effect on this (median EB2Fc: 27 days, *n*=11). However, there was a statistically significant decrease of symptom-free survival time in the group of mice receiving the EphB4 RTK inhibitor NVP-BHG 712, compared to the placebo-treated group. They showed a significantly earlier appearance of hind leg paresis [median NVP-BHG 712: 23 days, *n*=7, median placebo: 28 days, p=0.0355, Log-rank (Mantel-Cox) test].

Figure 13: Survival analysis of post-tumor treatment in enfb2$^{lox/lox}$ control animals
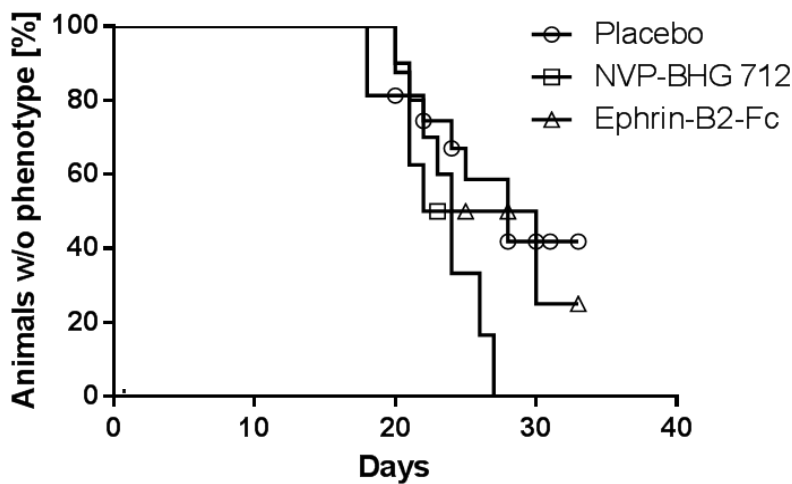
Figure 13: *There was no significant difference in survival times until the appearance of neurological deficits in the placebo treated group (median: 28 days, n=17) when compared with Ephrin-B2-Fc treated animals (median: 27 days, n=11). Animals treated with NVP-BHG 712 showed significantly earlier signs of neurological symptoms, when compared with the placebo group [median NVP-BHG 712: 23 days, n=7, p=0.0355, Log-rank (Mantel-Cox) test]. Significance threshold adjusted for multiple comparisons by Bonferroni method.*

6.2.2 MR imaging results in-vivo

Under post-tumor placebo treatment in efnb2$^{lox/lox}$ animals, the mean number of spinal metastases observed in the focused spinal MRI was 3.077 ± 0.788 (n=13). The application of NVP-BHG 712 (mean: 2.375 ± 0.844, n=7) or Ephrin-B2-Fc (mean: 2.625 ± 0.565, n=6) did not significantly alter the number of metastases. The mean individual tumor volume (in mm^3) was also unaffected by the therapeutic regimen (mean placebo: 2.296 ± 0,343 mm^3, mean NVP-BHG 712: 2.508 ± 0.413 mm^3, mean Ephrin-B2-Fc: 2.097 ± 0.387 mm^3). Similar results were observed in total tumor volume (in mm^3) (mean placebo: 8.360 ± 2.101 mm^3, mean NVP-BHG 712: 5.957 ± 1.948 mm^3, mean Ephrin-B2-Fc: 5.506 ± 2.183 mm^3).

Figure 14: Comparison of total number and size of spinal metastases in efnb2$^{lox/lox}$ therapeutic treatment groups
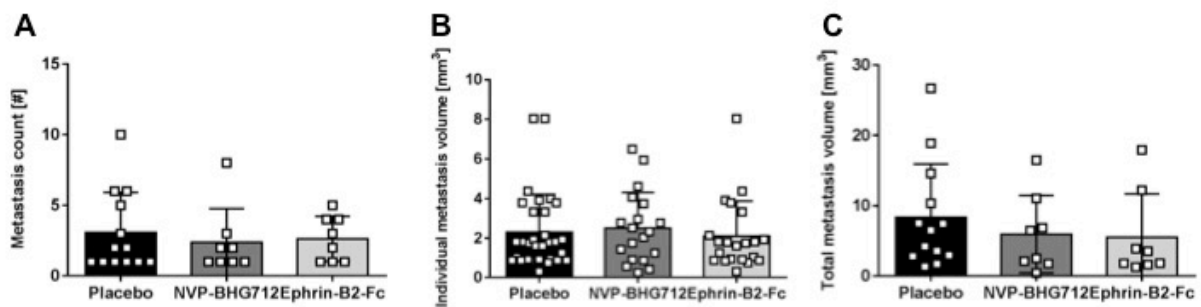
Figure 14: A) Number of spinal metastases was not significantly affected by application of therapeutics (mean placebo: 3.077 ± 0.788 mm^3, n=13, mean NVP-BHG 712: 2.375 ± 0.844 mm^3, n=7, mean Ephrin-B2-Fc: 2.625 ± 0.565 mm^3, n=6). B) Mean individual tumor volume in mm^3 was also unaffected by therapy (mean placebo: 2.296 ± 0,343 mm^3, mean NVP-BHG 712: 2.508 ± 0.413 mm^3, mean Ephrin-B2-Fc: 2.097 ± 0.387 mm^3). C) Similar results were observed in total tumor volume (mean placebo: 8.360 ± 2.101 mm^3, mean NVP-BHG 712: 5.957 ± 1.948 mm^3, mean Ephrin-B2-Fc: 5.506 ± 2.183 mm^3). One-way ANOVA with Dunnett's multiple comparisons test. Mean ±SEM for all experiments shown.

6.2.3 In-vitro bioluminescence quantification of metastatic tumor burden in tissue homogenates

The dissemination of metastatic cells in the spine showed no significant difference upon post-tumor treatment with Ephrin-B2-Fc (5.086e+006 ± 2.155e+006 cells, *n*=5) or NVP-BHG 712 (3.661e+006 ± 2.399e+006 cells, *n*=5) when compared with the placebo-treated group (7.329e+006 ± 2.351e+006 cells, *n=5*). In-vitro bioluminescence analysis of tumor cell dissemination between osseous und soft tissue organs showed a similar effect in the placebo-treated cohort as already observed under pre-tumor placebo-treatment: a significant tendency of metastatic B16-luc tumor cells to colonize osseous organs (mean osseous: 1.662e+007 ± 2.207e+006 cells; mean soft: 1.463e+006 ±639333 cells, p=0.0002). Under application of NVP-BHG 712, the tendency to metastasize primarily into osseous organs is reduced and the statistical significance is lost (mean osseous: 2.742e+007 ± 1.371e+007 cells, mean soft: 1.567e+007 ± 1.301e+007 cells, p=0.5516). After application of Ephrin-B2-Fc, no statistically significant difference was found in metastatic burden (mean osseous: 4.283e+007 ± 1.271e+007 cells, mean soft: 1.253e+007 ± 5.304e+006 cells, p=0.0590).

Figure 15: Site-specific dissemination of metastatic B16-luc tumor cells to osseous and soft tissue organs under post-tumor treatment in efnb2$^{lox/lox}$ mice
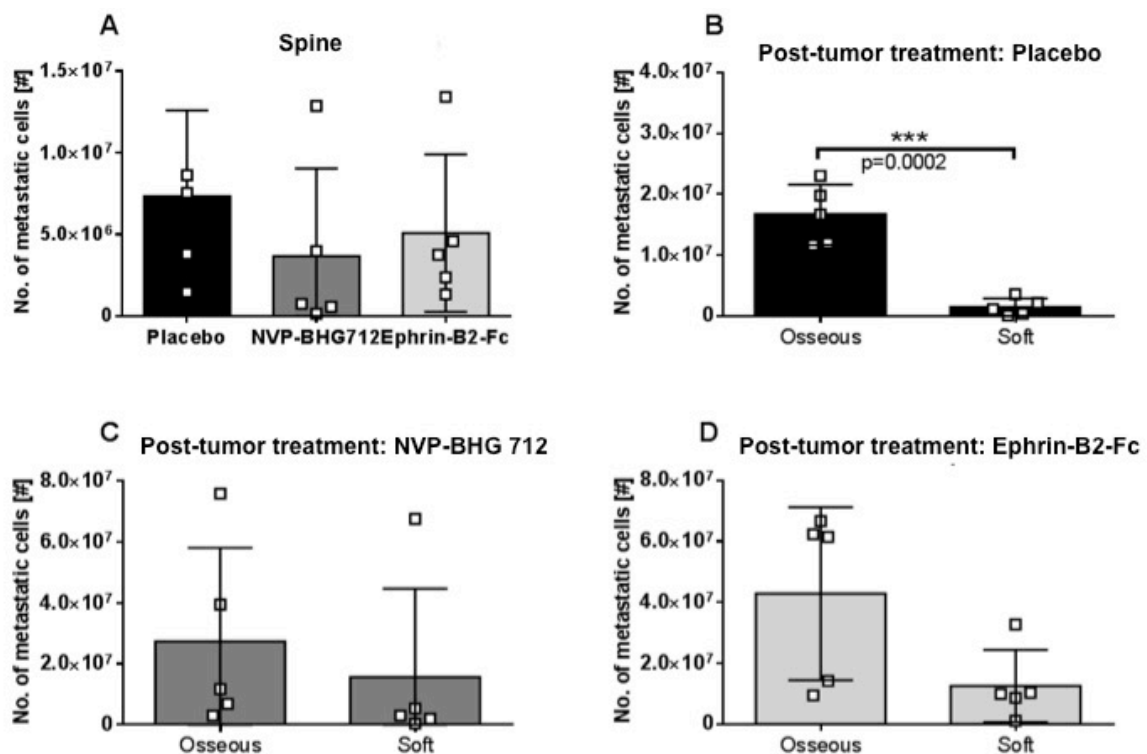
Results

Figure 15: A) No significant difference is noted after post-tumor treatment application of Ephrin-B2-Fc and NVP-BHG 712 in the number of tumor cells found in the spine. B) Placebo treated animals showed significantly higher numbers of metastatic tumor cells in osseous organs than soft tissue organs (mean osseous: 1.662e+007 ± 2.207e+006 cells, mean soft: 1.463e+006 ±639333 cells, n=5, p=0.0002, unpaired t-test) C) Under NVP-BHG 712 post-tumor therapy, the statistically significant preference for osseous metastasis formation is lost (mean osseous: 2.742e+007 ± 1.371e+007 cells, mean soft: 1.567e+007 ± 1.301e+007 cells, n=5, p=0.5516, unpaired t-test). D) Similar results were observed under Ephrin-B2-Fc post-tumor therapy (mean osseous: 4.283e+007 ± 1.271e+007 cells, mean soft: 1.253e+007 ± 5.304e+006 cells, n=5, p=0.0590, unpaired t-test). Mean ± SEM for all experiments shown.

6.2.4 Immunohistochemical assessment of proliferative activity and tumor vasculature in spinal metastases

The number of Ki-67 positive proliferating tumor cells under placebo-treatment of efnb2$^{lox/lox}$ mice was 40.13 ± 5,355 cells per FOV (*n*=7). The therapeutic application of NVP-BHG 712 and the consecutive blockade of the EphB4 tyrosine kinase did not have a significant effect on the amount of proliferating tumor cells (mean: 39.92 ± 10.55 proliferating cells/FOV, *n*=3). Neither did the treatment with Ephrin-B2-Fc (mean: 52.65 ± 15.45 proliferating cells/FOV, *n*=5).

The number of tumor vessels in placebo-treated efnb2$^{lox/lox}$ mice was 8.286 ± 1.128 vessels per FOV. The application of NVP-BHG 712 did not significantly alter the number of vessels (mean: 6.000 ± 0.5774 vessels/FOV). However, under application of Ephrin-B2-Fc, the number of endomucin-positive blood vessels was significantly increased to 12.80 ± 1.068 vessels per FOV (p=0.0196).

The size of tumor vasculature was significantly increased in the treatment group that received Ephrin-B2-Fc as a post-tumor treatment regimen compared to the placebo-treated cohort (mean placebo: 5.077 ± 1.030%, mean Ephrin-B2-Fc: 10.60 ± 1.379%, p=0.0078). In the NVP-BHG 712 treated group, no statistically significant difference in size of vessels could be noted.

Results

Figure 16: *Number of Ki-67+ tumor cells, vessel size and number in spinal metastases under post-tumor treatment of efnb2$^{lox/lox}$ mice*
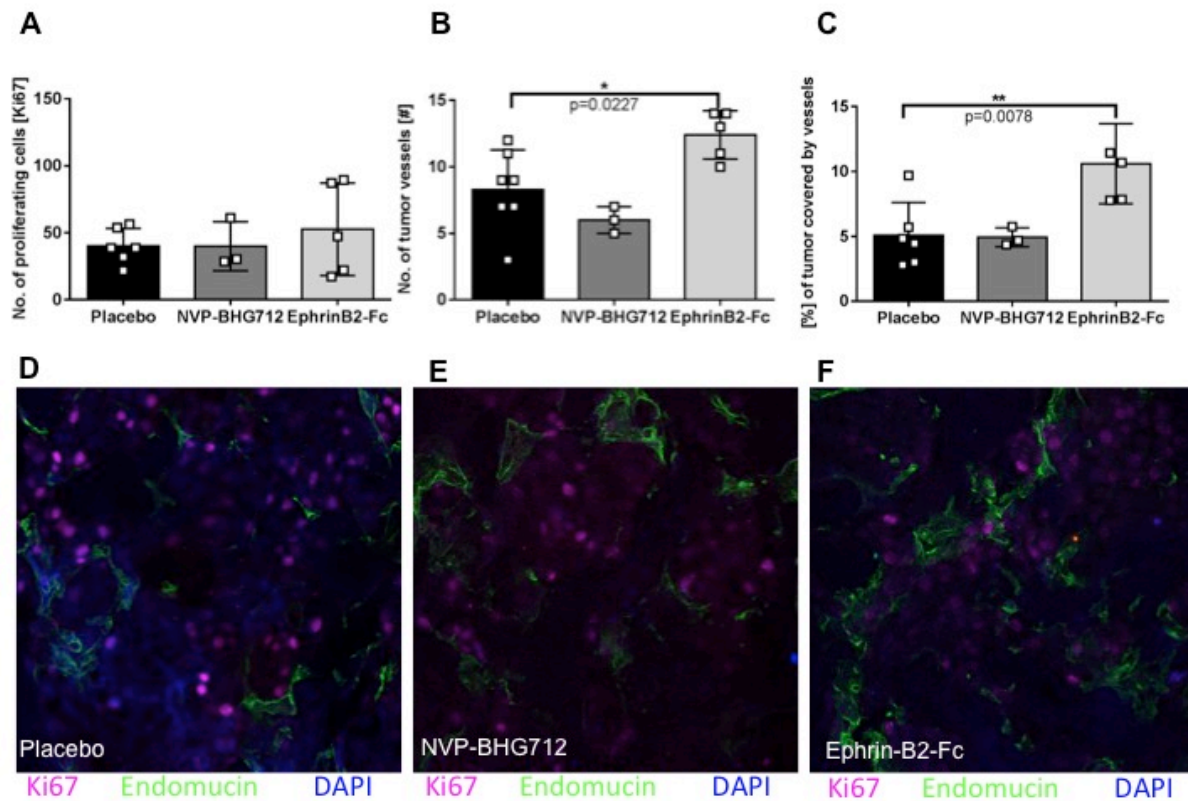
Figure 16: A) No significant differences were observed under therapeutic treatment in efnb2$^{lox/lox}$ mice. The number of Ki-67 positive proliferating cells was similar in all three groups [mean placebo: 40.13 ± 5.355 proliferating cells/FOV, n=7, mean NVP-BHG 712: 39.92 ± 10.55 proliferating cells/FOV, n=3, mean EB2Fc: 52.65 ± 15.45 proliferating cells/FOV, n=5, p=0.472 (one-way ANOVA with Dunnett's multiple comparison test)]. B) Statistically significant increase in the number of tumor blood vessels of Ephrin-B2-Fc treated group [mean placebo: 8.286 ± 1.128 vessels/FOV, n=7, mean EB2Fc: 12.80 ± 1.068 vessels/FOV, n=5, p=0.0196 (one-way ANOVA with Dunnett's multiple comparisons test)]. C) The application of Ephrin-B2-Fc also significantly increased the size of tumor blood vessels [mean placebo: 5.077 ± 1.030%, (n=6), mean EB2Fc: 10.60 ± 1.379%, n=5, p=0.0078 (one-way ANOVA with Dunnett's multiple comparison test)]. Mean ± SEM for all experiments shown. D-F) Confocal microscopic images of spinal metastatic tumors showing endothelial cells marked by green-fluorescent Endomucin-Ab and proliferating tumor cells marked by violet-fluorescent Ki67-Ab, post-tumor treatment as indicated.

6.3 Pre-tumor treatment in efnb2$^{i\Delta EC}$ animals

6.3.1 The effect of therapy on survival outcomes

In efnb2$^{i\Delta EC}$ knockout mice, the appearance of neurological symptoms occurred at a significantly earlier date when comparde to efnb2$^{lox/lox}$ control littermates [mean efnb2lox/lox placebo: 24.5 days n=22, mean efnb2iΔEC placebo: 18 days, n=7, p=<0.0001, Log-rank (Mantel-Cox) test, data not shown]. Application of Ephrin-B2-Fc prolonged neurological survival of efnb2$^{i\Delta EC}$ mice when compared to the placebo-treated group (median placebo: 18 days, *n*=7, median EB2Fc: 23 days, *n*=8, p=0.0018). By applying NVP-BHG 712, neurological survival was not altered in a statistically significant way (median placebo: 18 days, median NVP-BHG 712: 21 days, *n*=9, p= 0.2313).

Figure 17: Survival analysis of pre-tumor treatment in enfb2$^{i\Delta EC}$ animals
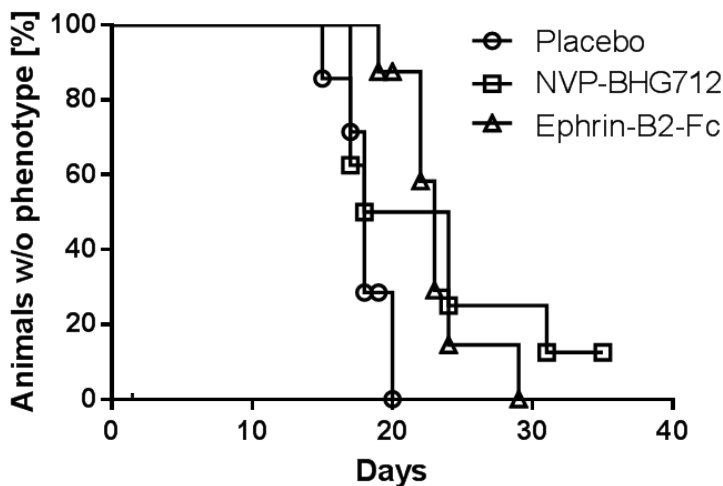
Figure 17: Neurological deficit occurred significantly later in Ephrin-B2-Fc treated efnb2$^{i\Delta EC}$ animals (median 23 days, n=8) compared to the placebo treated group [median placebo: 18 days, n=7, p=0.0452, Log-rank (Mantel-Cox) test]. By application of NVP-BHG 712, the time of neurological survival was not affected (n=9). Significance threshold adjusted for multiple comparisons by Bonferroni method.

6.3.2 MR imaging results in-vivo

The number of spinal metastases in pre-tumor treated efnb2$^{i\Delta EC}$ mice was significantly lower in the Ephrin-B2-Fc treated group when compared with the placebo-treated

Results

animals (mean EB2Fc: 1.250 ± 0.250; *n*=4, mean placebo: 5.100 ± 0.900, *n*=10, p=0.0371). The application of NVP-BHG 712 did not show a significant effect on the metastasis count (mean NVP-BHG 712: 6.750 ±1.315, *n*=4). The mean individual tumor volume in placebo-treated efnb2$^{i\Delta EC}$ animals was 2.331 ± 0.2767 mm^3. This was unaffected by the application of Ephrin-B2-Fc (mean EB2Fc: 2.434 ± 0.866 mm^3, p=0.991) or NVP-BHG 712 (mean: 3.149 ± 0.437 mm^3, p=0.1812). The mean total tumor volume decreased significantly after application of Ephrin-B2-Fc (mean placebo: 14,240 ± 2.310 mm^3, mean Ephrin-B2-Fc 3.042 ± 0,807 mm^3, p=0.0455). The application of NVP-BHG 712 did not show any significant effect on the total tumor volume in pre-tumor treated efnb2$^{i\Delta EC}$ mice (mean NVP-BHG 712: 21.260 ± 5.637 mm^3).

Figure 18: Comparison of total number and size of spinal metastases in pre-tumor efnb2$^{i\Delta EC}$ treatment groups
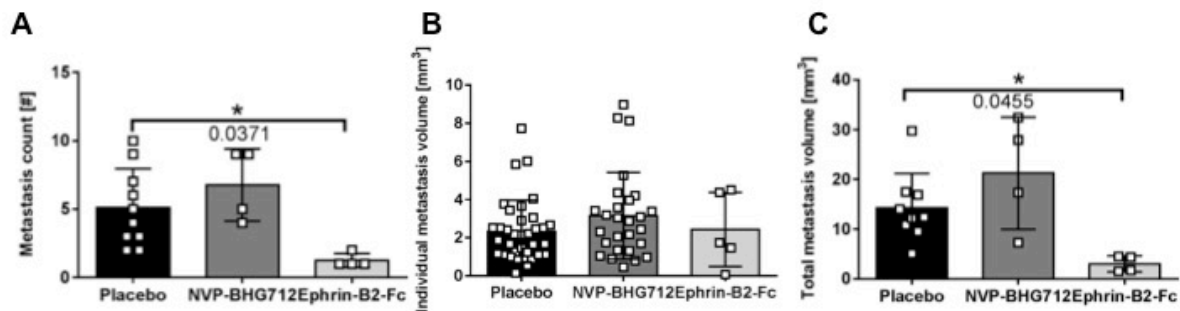
Figure 18: A) The number of spinal metastases was significantly lower in Ephrin-B2-Fc treated efnb2$^{i\Delta EC}$ animals when compared with the placebo treated group [mean EB2Fc: 1.250 ± 0.250, n=4, mean placebo: 5.100 ± 0.900, n=10, p=0.0371 (one-way ANOVA with Dunnett's multiple comparison test)]. Application of NVP-BHG 712 showed no significant effect on the number of spinal metastases. B) The individual metastasis volume was not significantly changed in both treatment groups. C) The total tumor volume (mm^3) was significantly decreased after application of Ephrin-B2-Fc (mean placebo: 14,240 ± 2.310 mm^3, mean Ephrin-B2-Fc: 3.042 ± 0,807 mm^3. It was unaffected by the application of NVP-BHG 712 (21.260 ± 5.637 mm^3, n=4). Mean ±SEM for all experiments shown

6.3.3 In-vitro bioluminescence quantification of metastatic tumor burden in tissue homogenates

In placebo-treated efnb2$^{i\Delta EC}$ knockout animals, the pre-tumor treatment did not significantly alter the number of metastatic tumor cells found in the spine. The placebo-

Results

treated group displayed 3.604e+006 ± 1.075e+006 cells in the spine (*n*=5). Neither the treatment with NVP-BHG 712 (mean: 2.461e+006 ± 980023 cells, *n*=4) nor with Ephrin-B2-Fc (mean: 4.046e+006 ± 1.325e+006 cells, *n*=6) showed any significant effects.

Multi-organ metastasis analysis demonstrated a significant preference of B16-luc tumor cells to metastasize into osseous organs upon pre-tumor Ephrin-B2-Fc treatment (mean osseous: 1.727e+007 ± 4.798e+006 cells, mean soft tissue organs: 1.101e+006 ± 466509 cells, p=0.01534).

Under pre-tumor treatment with NVP-BHG 712, the number of metastatic cells found in osseous tissues was significantly higher than in soft tissue organs (mean osseous: 1.040e+007 ± 2.354e+006 cells, mean soft tissue organs: 2.113e+006 ± 887723 cells, p=0.0087). In Ephrin-B2-Fc treated efnb2$^{i\Delta EC}$ animals in the pre-tumor treatment protocol, there was no statistically significant site preference of B16-luc tumor cells to form metastases (mean osseous: 1.894e+007 ± 7.590e+006 cells, mean soft tissue organs: 1.710e+006 ± 614597 cells, p=0.0643).

Figure 19: Site-specific dissemination of metastatic B16-luc tumor cells to the spine, osseous and soft tissue organs under pre-tumor treatment in efnb2$^{i\Delta EC}$ mice
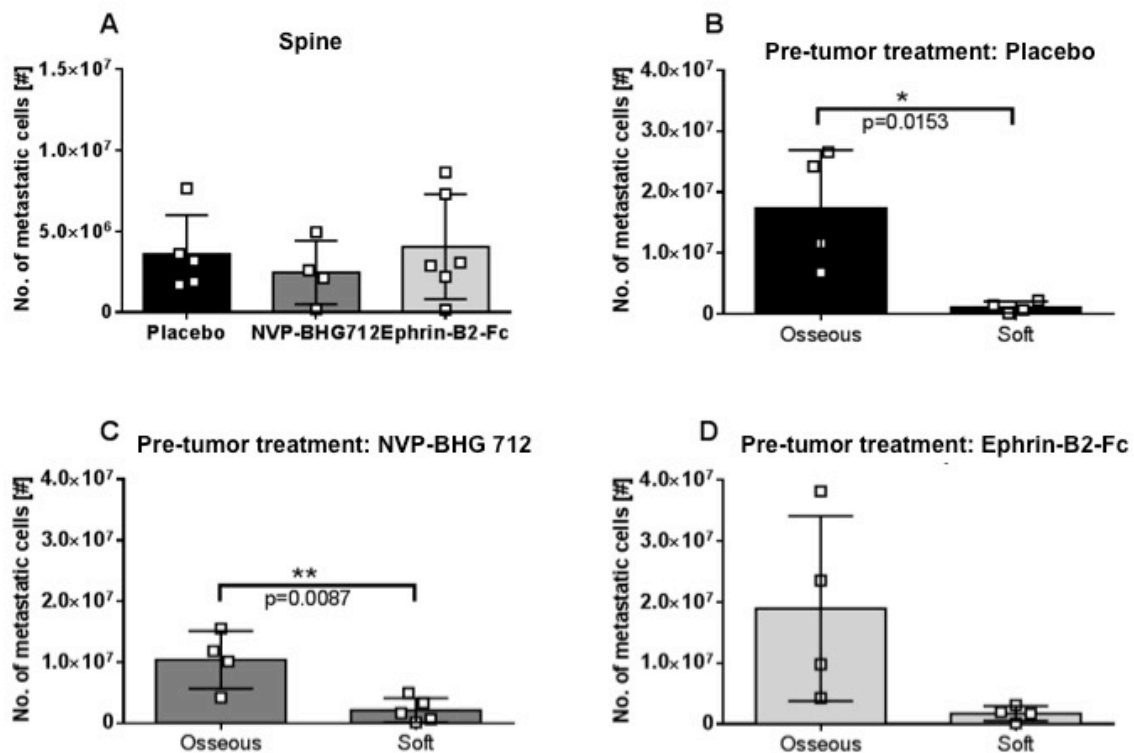
Results

Figure 19: A) *There was no significant difference in metastasis formation to the spine in placebo-, NVP-BHG 712- and Ephrin-B2-Fc-treated animals (mean: 3.604e+006 ± 1.075e+006 cells, n=5, mean: 2.461e+006 ± 980023 cells, n=4, mean: 4.046e+006 ± 1.325e+006 cells, n=6, respectively).* ***B)*** *B16-luc tumor cells showed a significantly higher preference to metastasize into osseous tissues than soft tissue organs in placebo-treated efnb2$^{i\Delta EC}$ mice [mean osseous: 1.727e+007 ± 4.798e+006 cells, mean soft: 1.101e+006 ± 466509 cells, n=5, p=0.01534 (unpaired t-test)].* ***C)*** *The preference for osseous metastasis remained significant in NVP-BHG 712-treated efnb2$^{i\Delta EC}$ mice [mean osseous: 1.040e+007 ± 2.354e+006 cells, mean soft: 2.113e+006 ± 887723 cells, n=4, p=0.0087 (unpaired t-test)].* ***D)*** *Under application of Ephrin-B2-Fc, there was no significant difference in the site-specific metastasis formation between osseous and soft tissue organs [mean osseous: 1.894e+007 ± 7.590e+006 cells, mean soft tissue organs: 1.710e+006 ± 614597 cells, n=6, p=0.0643 (unpaired t-test)]. Mean values ±SEM for all experiments shown.*

6.3.4 Immunohistochemical assessment of proliferation activity and tumor vasculature in spinal metastases

Under pre-tumor application of placebo in efnb2$^{i\Delta EC}$ animals, the mean fraction of Ki67 positive tumor cells per FOV was 53.27 ± 5.844 (*n*=11). Under pre-tumor treatment with NVP-BHG 712, the fraction of proliferating cells per FOV within the tumor increased significantly (mean NVP-BHG 712: 87.13 ± 13.26 proliferating cells/FOV, *n*=4, p= 0.0121). The application of Ephrin-B2-Fc did not significantly alter the amount of Ki67 positive tumor cells compared to placebo (mean Ephrin-B2-Fc: 75.38 ± 4.459 proliferating cells/FOV, *n*=6, p=0.0610).

Regarding tumor vasculature, the application of NVP-BHG 712 did not affect the number of tumor vessels significantly when compared to the placebo-treated cohort (mean placebo: 8.333 ± 0.333 vessels/FOV, mean NVP-BHG 712: 9.000 ± 1.000 vessels/FOV, p=0.7409). Similar results were observed under pre-tumor treatment with Ephrin-B2-Fc (mean 8.167 ± 0.4014 vessels/FOV, p=0.9770). The mean percentage of tumors covered by blood vessels in the pre-tumor placebo-treatment group of efnb2$^{i\Delta EC}$ knockout animals was 4.954 ± 0.2410%. The size of vessels significantly increased upon application of Ephrin-B2-Fc (mean: 7.910 ± 0.3535%, p=0.0010). The pre-tumor application of NVP-BHG 712 did not significantly alter the size of vessels (mean: 5.704 ±0.4869%, p=0.4226).

Results

Figure 20: *Number of Ki-67+ tumor cells, vessel size and number in spinal metastases under pre-tumor treatment of efnb2$^{i\Delta EC}$ mice*
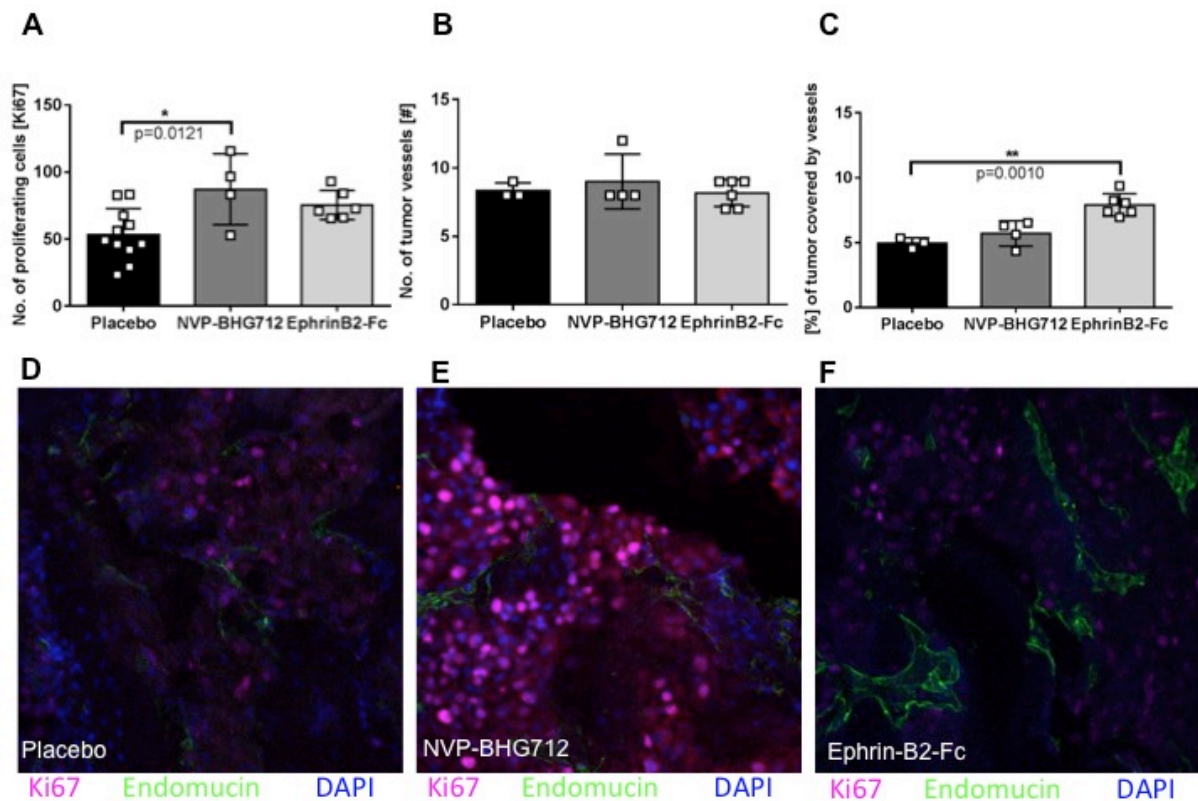
Figure 20: A) The fraction of Ki67 positive tumor cells in the placebo-treated group (mean 53.27 ± 5.844 proliferating cells/FOV, n=11) was significantly increased through application of NVP-BHG 712 (mean NVP-BHG 712: 87.13 ± 13.26 proliferating cells/FOV, n=4, p=0.0121) and revealed no statistically significant difference upon treatment with Ephrin-B2-Fc [mean Ephrin-B2-Fc: 75.38 ± 4.459 proliferating cells/FOV n=6, p=0.0610 (one-way ANOVA with Dunnett's multiple comparison test)]. B) The number of tumor vessels was not significantly altered in efnb2$^{i\Delta EC}$ animals by therapeutic use of Ephrin-B2-Fc and NVP-BHG 712 compared to placebo. C) The percentage of tumor covered by vasculature in the placebo treatment group was 4.954 ± 0.2410%. This was not significantly affected by the application of NVP-BHG 712. The application of Ephrin-B2-Fc significantly increased the size of tumor blood vessels [mean Ephrin-B2-Fc: 7.910 ± 0.3535%, p=0.0010 (one-way ANOVA with Dunnett's multiple comparisons test)]. Mean values ± SEM for all experiments shown. D-F) Confocal microscopic images of spinal metastatic tumors in efnb2$^{i\Delta EC}$ mice, pre-tumor treatment as indicated.

6.4 Post-tumor treatment in efnb2$^{i\Delta EC}$ animals

6.4.1 The effect of therapy on survival outcomes

There was no statistically significant difference between the median times until appearance of neurological symptoms in the treatment groups (median Ephrin-B2-Fc: 24 days, n=11 median NVP-BHG 712: 23 days, n=9) when compared to the placebo-treated group (median placebo: 19 days, n=9).

Figure 21: Survival analysis of post-tumor treated enfb2$^{i\Delta EC}$ animals
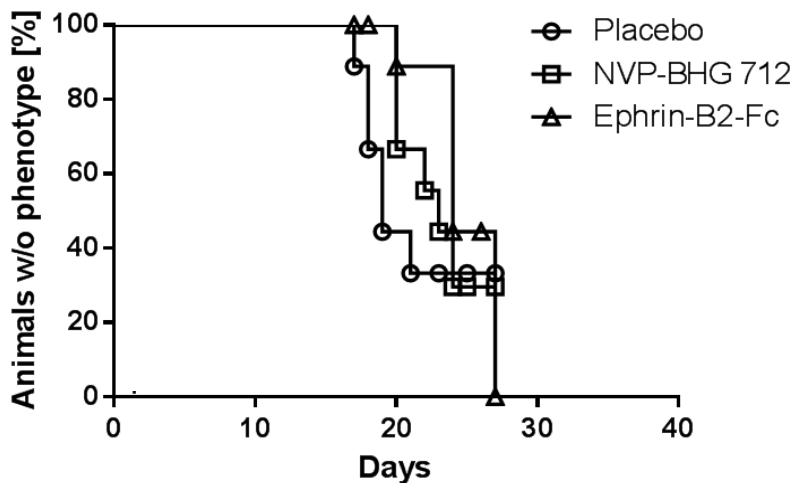
Figure 21: The median time until neurological deficit was 19 days in the placebo treated group (n=9). Neither the application of Ephrin-B2-Fc nor NVP-BHG 712 showed a significant effect on symptom-free survival [median EB2Fc: 24 days, n=11, median NVP-BHG 712: 23 days, n=9, Log-rank (Mantel-Cox) test]. Significance threshold adjusted for multiple comparisons by Bonferroni method.

6.4.2 MR imaging results in-vivo

The mean number of spinal metastases identified by focused spinal MRI imaging in the placebo-treated efnb2$^{i\Delta EC}$ animals was 4.778 ± 0.863 (n=9). The application of NVP-BHG 712 did not show a significant effect on the number of spinal metastases (mean NVP-BHG 712: 3.182 ± 0.483, n=11). The therapeutic application of Ephrin-B2-Fc also did not alter the mean number of spinal tumors (mean EB2-Fc: 3.111 ± 0.5232, n=9).

The mean individual tumor volume in mm^3 in the placebo-treated cohort was 3.110 ± 0.255 mm^3. The application of NVP-BHG 712 did not show any significant effect on the size of spinal metastases (mean NVP-BHG 712: 2.636 ± 0.225 mm^3). The mean size of

metastases also remained unaffected by the therapeutic application of Ephrin-B2-Fc (mean EB2-Fc: 3.516 ± 0.297 mm^3).

The total tumor volume in mm^3 also remained unaffected by the application of Ephrin-B2-Fc and NVP-BHG 712 (mean placebo: $14,860 \pm 3.624$ mm^3, mean NVP-BHG 712: 8.387 ± 1.621 mm^3, mean Ephrin-B2-Fc: 10.740 ± 2.313 mm^3).

Figure 22: MRI Comparison of total number and size of spinal metastases in efnb2$^{i\Delta EC}$ therapeutic treatment groups
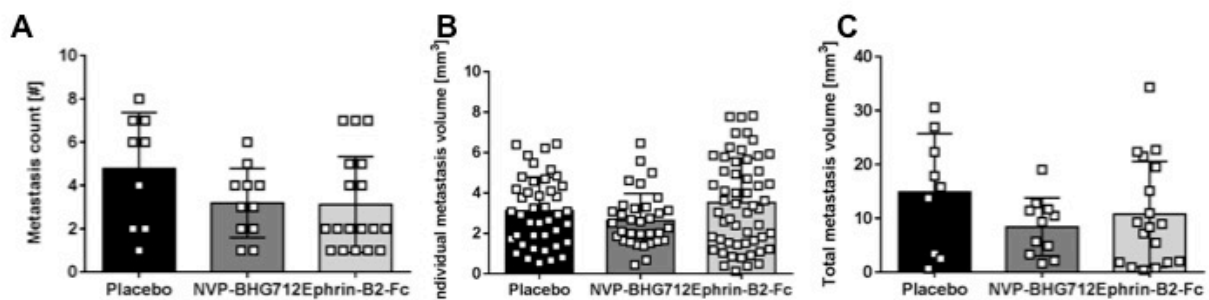
Figure 22: A) No statistical significance could be noted in the mean metastasis count upon application of post-tumor treatment regimens in efnb2$^{i\Delta EC}$ knockout groups. Mean number of spinal metastases remained unchanged (mean placebo: 4.778 ± 0.863, n=9, mean NVP-BHG 712: 3.182 ± 0.483, n=11, mean EB2-Fc: 3.111 ± 0.5232, n=9). B) No significant changes were shown in the mean individual tumor volume under therapeutic treatment of efnb2$^{i\Delta EC}$ mice (mean placebo: 3.110 ± 0.255 mm^3, mean NVP-BHG 712: 2.636 ± 0.225 mm^3, mean EB2-Fc: 3.516 ± 0.297 mm^3) C) The total tumor volume in mm^3 also remained unaffected by the application of Ephrin-B2-Fc and NVP-BHG 712 (mean placebo: 14,860 ± 3.624 mm^3, mean NVP-BHG 712: 8.387 ± 1.621 mm^3, mean Ephrin-B2-Fc: 10.740 ± 2.313 mm^3). One-way ANOVA with Dunnett's multiple comparisons test, mean ±SEM for all experiments shown.

6.4.3 In-vitro bioluminescence quantification of metastatic tumor cell burden in tissue homogenates

The number of metastatic tumor cells in the spine of the post-tumor treatment group showed no significant difference after treatment with Ephrin-B2-Fc (mean 814505 ± 341095 cells, *n*=4) or NVP-BHG 712 (mean: 3.849e+006 ± 1.944e+006 cells, *n*=4) when compared to the placebo-treated group (mean: 1.475e+006 ± 421123 cells, *n*=4).

Regarding site-specific metastasis, there were a significantly higher number of B16-luc tumor cells in osseous tissues compared to soft tissue organs in the placebo-treated

group (mean osseous: 7.160e+006 ± 1.149e+006 cells, mean soft: 1.082e+006 ± 604322 cells, p=0.0034). The significant preference towards osseous metastasis formation was also observed upon treatment with NVP-BHG 712 (mean osseous: 2.772e+007 ± 6.467e+006 cells, mean soft: 3.919e+006 ± 1.227e+006 cells, p=0.112). Under post-tumor treatment with Ephrin-B2-Fc, the significant preference for metastasizing into osseous organs was lost (mean osseous: 1.005e+007 ± 2.374e+006 cells, mean soft: 4.177e+006 ± 1.522e+006 cells, p=0.0826).

Figure 23: Site-specific dissemination of metastatic tumor cells to osseous and soft organs under post-tumor treatment in efnb2$^{i\Delta EC}$ mice
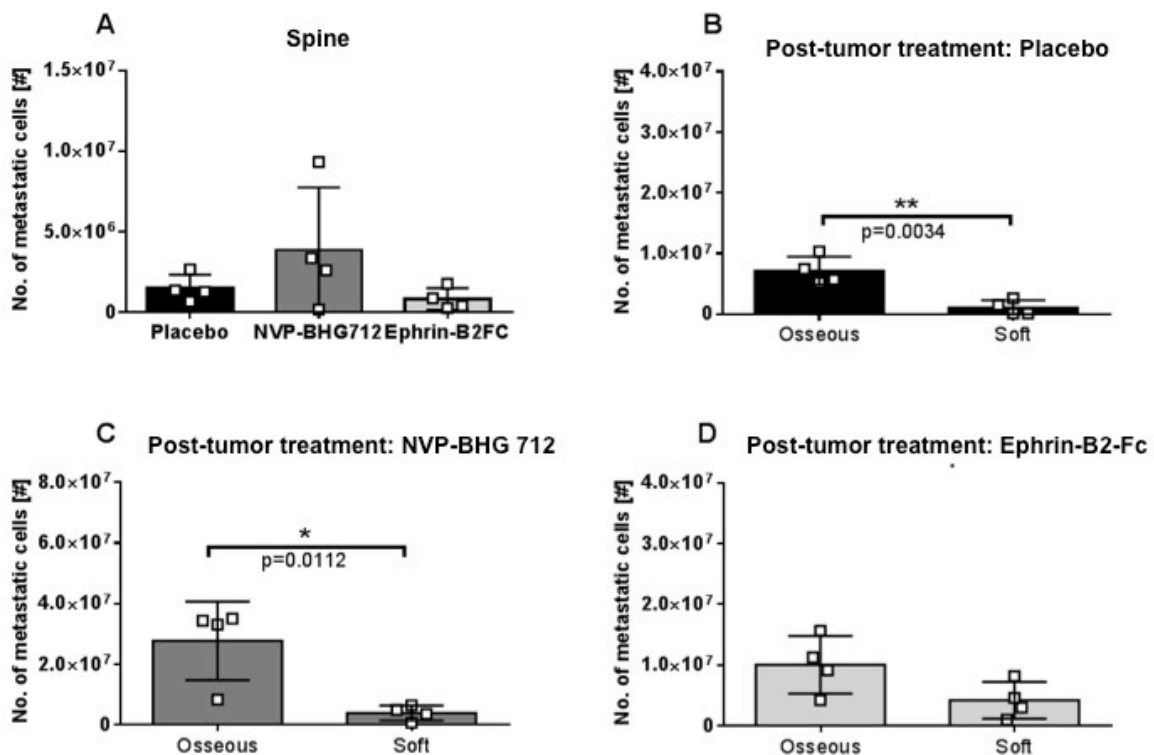
Figure 23: A) The number of spinal metastatic cells in the placebo-treated group (mean: 1.475e+006 ± 421123 cells, n=4) was not significantly affected by Ephrin-B2-Fc (mean: 814505 cells ± 341095, n=4) or NVP-BHG 712 (mean: 3.849e+006 ± 1.944e+006 cells, n=4). B) Significant tendency to metastasize into osseous organs under placebo treatment [mean osseous: 7.160e+006 ± 1.149e+006 cells, mean soft: 1.082e+006 ± 604322 cells n=4, p=0.0034 (unpaired t-test)]. C) Significant tendency for osseous metastasis formation under NVP-BHG 712 treatment [mean osseous: 2.772e+007 ± 6.467e+006 cells, mean soft: 3.919e+006 ± 1.227e+006 cells, n=4, p=0.112 (unpaired t-test)]. D) The significant preference for osseous organs is lost under Ephrin-B2-Fc treatment [mean osseous: 1.005e+007 ± 2.374e+006 cells, mean

Results

soft tissue organs: 4.177e+006 ± 1.522e+006 cells n=4, p=0.0826 (unpaired t-test)].
Mean values ± SEM for all experiments shown.

6.4.4 Immunohistochemical assessment of proliferation activity and tumor vasculature in spinal metastases

A trend of increase in the number of proliferating Ki-67+ B16-luc tumor cells was observed under treatment with NVP-BHG 712 (mean: 117.9 ± 23.88 proliferating cells/FOV, *n*=2) when compared to placebo treated groups (mean: 53.27 ± 5.844 proliferating cells/FOV, *n*=11, p=0.0042), although the number of examined tumors in the NVP-BHG 712 group was not sufficient to provide statistical significance in this case. The application of Ephrin-B2-Fc did not alter the number of proliferating tumor cells significantly (mean EB2-Fc: 43.75 ± 12.18 proliferating cells/FOV, p=0.6654, *n*=5). The number of tumor vessels was not significantly affected by the application of therapeutics in the post-tumor treatment group of efnb2$^{i\Delta EC}$ knockout mice. The mean number of tumor vessels/FOV under placebo treatment was 7.667 ± 0.4714, under the application of NVP-BHG 712 10.67 ± 0.333 and under Ephrin-B2-Fc therapy 9.40 ± 1.364. The size of the tumor vessels (in % of tumor covered) significantly decreased upon post-tumor application of Ephrin-B2-Fc (mean placebo: 8.315 ± 0.3822%, mean EB2Fc: 6.004 ± 1.840%, p=0.0130) Moreover, the application of NVP-BHG 712 also negatively influenced the size of the tumor vasculature, thus the percentage of tumor covered by endomucin-positive vessels was lower than in the placebo-treated group (mean NVP-BHG 712: 5.850 ± 0.0788%, *n*=3), without reaching statistical significance.

Results

Figure 24: *Number of Ki-67+ tumor cells, vessel size and number in spinal metastases under post-tumor treatment of efnb2$^{i\Delta EC}$ mice*
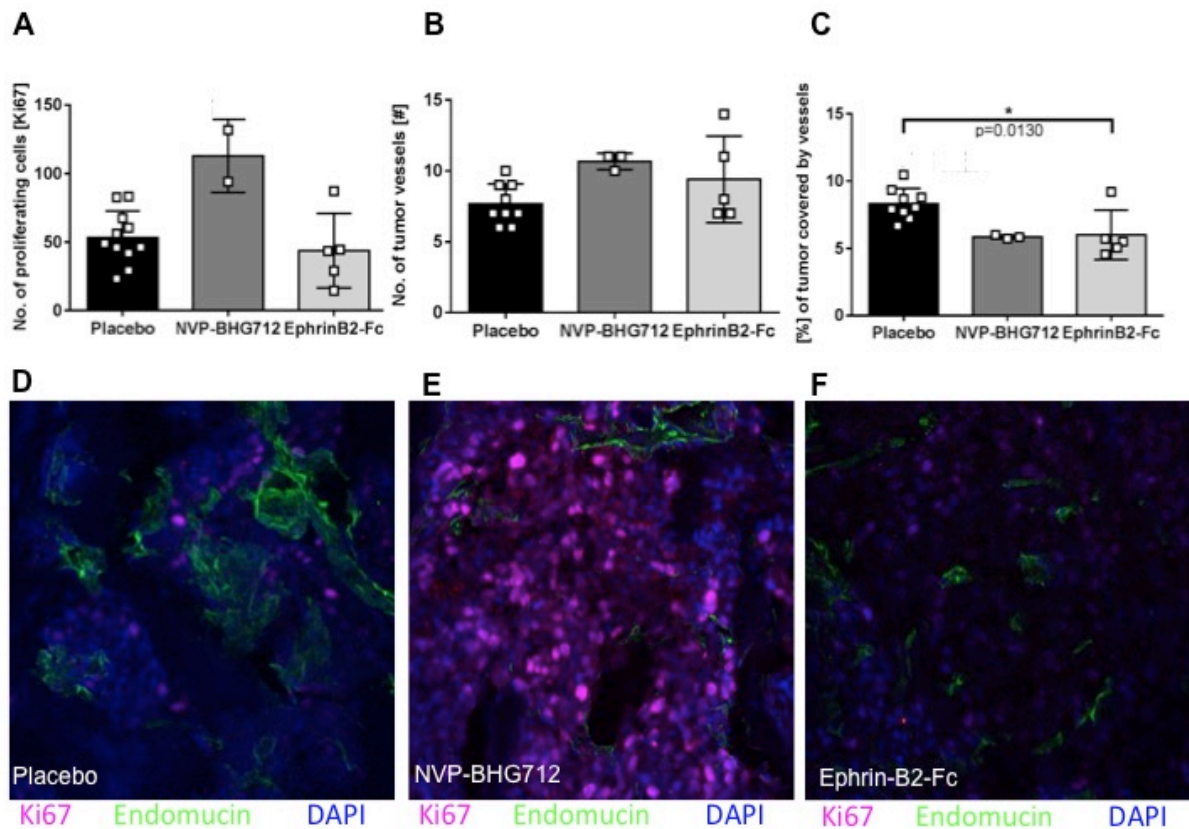
Figure 24: A) *The mean number of proliferating cells under placebo treatment was 53.27 ± 5.844 proliferating cells/FOV (n=11). The amount of proliferation seemed to increase through NVP-BHG 712 administration (mean: 117.9 ± 23.88 proliferating cells/FOV, n=2). The proliferation remained unaffected by Ephrin-B2-Fc administration (mean: 53.27 ± 5.844 proliferating cells/FOV, n=5, p=0.6654).* ***B)*** *The numbers of tumor vessels were not significantly changed by the two therapeutic regimens.* **C)** *Treatment with Ephrin-B2-Fc significantly reduced the percentage of tumor area covered by vessels (mean: 6.004 ± 1.840%) when compared to the placebo-treated group (mean placebo: 8.315 ± 0.3822%, p=0.0130). Similar effects are observed under EphB4 blockade through NVP-BHG 712 (mean: 5.850 ± 0.0788%, p=0.0251). One-way ANOVA with Dunnett's multiple comparison test was used, mean ± SEM for all experiments are shown.* ***D-F)*** *Confocal images show staining patterns of spinal metastatic tumors in efnb2$^{\Delta EC}$ mice. Post-tumor treatment as indicated.*

7 Discussion

The two main aims of this dissertation were:

1) Characterization of the Ephrin-B2-EphB4 signalling pathway in spinal metastasis formation.

2) Investigation of the consequences of therapeutic intervention of the pathway on development of spinal metastases.

The historical concept of the "seed and soil" theory of metastasis formation originally published by the English surgeon Stephen Paget in 1889 was based on a review of autopsy records from 735 women with fatal breast cancer. Paget proposed that the distribution of metastases produced by different human neoplasms was not due to chance, but rather that certain tumor cells (the seed) have a specific affinity for the milieu of certain organs (the soil), and that metastases occur only when the seed and soil are compatible.[15] Paget's observations contradicted the prevailing theory of the time proposed in 1858 by Rudolf Virchow that metastasis can be explained simply by the arrest of tumor cells in the vasculature.[94] In 1928, James Ewing challenged the "seed and soil" hypothesis. He proposed that purely mechanical forces and circulatory patterns between the primary tumor and the secondary site accounted for organ specificity.[95] This viewpoint was considered as standard for many decades. In the late 1970s and early 1980s, the seminal studies by Isaiah Fidler and co-workers provided the definitive proof of Paget's hypothesis by demonstrating that metastasis is not random, but site-selective, and that metastatic patterns are injection-site dependent in vivo.[96–98]

The Eph-Ephrin system is viewed as a key regulator in these highly complex processes and preliminary experiments of our research group have underlined the crucial role of Ephrin-B2-EphB4 interaction for spinal metastasis formation.[89] Regarding the activities of the Eph-Ephrin system in cancer, recent findings reveal complex interactions and paradoxical effects on tumor growth, invasiveness, angiogenesis and metastasis.[46] Accordingly, also the effect of EphB4 on tumor growth is contradictory and appears to be highly dependent on the cellular context, especially on co-expression of its preferred ligand Ephrin-B2. In particular, EphB4 was shown to promote tumor growth only when

Discussion

co-expressed with Ephrin-B2 in melanoma cells.[81,99,100] In previous in-vitro experiments, we found that EphB4 overexpressing B16-luc cells, generated by retroviral infection, showed decreased cell viability at high cellular densities and increased 2D cell migration compared to controls.[76] We could also show in parallel investigations that endothelial Ephrin-B2 depletion in efnb2$^{i\Delta EC}$ knockout mice led to increased metastatic dissemination in the spinal column and thus reduced the time until occurrence of neurological deficits in-vivo.[89]

In the present study, we investigated responses in extent, timing, site-specificity and aggressiveness of allogeneic melanoma metastasis upon pharmacological modification of the EphB4-Ephrin-B2 signal pathway in inducible endothelial Ephrin-B2 knockout mice compared to efnb2$^{lox/lox}$ control animals, in-vivo.

7.1 Discussion of Materials and Methods

7.1.1 Tumor cells: generation and application of B16-luc tumor cells

In the present study, genetically modified murine melanoma cells (B16-F1-luc) were utilized because of their known tendency to readily form metastases to the osseous spine. In previous experiments of our group, tumor cells were infected with a lentiviral vector carrying a firefly-luciferase-eGFP-puromycin (*FFLUC-GFP-Puro)* resistance gene, harboring two 2A self-cleavage sites.[90] Stable infected B-16-luc cells could be selected by adding 5µg/ml Puromycin to the cell medium, and the expression of luciferase enabled visualization of tumor cell dissemination and assessment of spinal metastases both in-vivo and in-vitro. Furthermore, the innate production of melatonin in the melanoma cells results in darkly pigmented colonies, making tumors easily distinguishable from normal organ parenchyma. One of the main advantages of using allogeneic cancer cells in experimental metastasis models is the possibility of investigating tumor growth in immunocompetent mice, as immunodeficiency can have a major effect on metastatic behavior and angiogenesis.[101]

7.1.2 Endothelial Ephrin-B2 knockout mice (efnb2$^{i\Delta EC}$) and controls (efnb2$^{lox/lox}$)

The tamoxifen-inducible depletion of Ephrin-B2 on endothelial cells was accomplished by crossing CDH5-(Pac)-CreERT^2 mice with Ephrin-B2-floxed animals. This model has been well established in previous studies.[91,102] Our present findings of increased

Discussion

metastatic dissemination of melanoma cells to the spine and most other organs under endothelial Ephrin-B2-knockout are in accordance with our earlier results.[89] The increase in spinal tumor burden observed in Ephrin-B2-knockout animals could be partially explained by two different mechanisms. First, an increased rate of extravasation of tumor cells during the metastatic colonization in the bone marrow could lead to a higher number of spinal metastases in total. Secondly, the interaction between the disseminated tumor cells and the microenvironment could lead to an increase in the size and aggressiveness of the bone-metastatic tumor outgrowths. There are, however, other possible explanations related to multiple and complex signaling pathways in an interrelated molecular network of metastasis generation, of which the Eph-Ephrin interactions represent only one, but significant part.

7.1.3 Establishment of an experimental spinal metastasis model in-vivo

The research methods for investigating metastasis formation are based on two main pillars: spontaneous and experimental metastasis generation. Spontaneous metastasis generation models apply orthotopic implantation of tumor tissues, which then form metastases in distant organs spontaneously. This process involves all steps of the metastatic cascade, as described previously, from dissemination of circulating tumor cells, infiltration of distant tissues, evasion of immune defenses, survival and eventually growth of overt metastases.[14] Thus, this approach is comparable to clinically observed metastasis formation in humans. However, there are also several objections to the spontaneous metastasis models, the main one being that solely based on oncogenic transformation, many tumor models are not able to establish distant metastases, as the transformed cancer cells do not automatically have sufficient abilities to overcome the natural barriers against metastasis.[103,104] Furthermore, the steps of vascular infiltration, extravasation and metastatic colonization are all separated by variable periods of latency, which makes the planning of such experimental settings highly difficult and time consuming.[105]

In our experimental approach, we developed a modified experimental model, based on previous work by Arguello et al., who demonstrated that after intra-cardiac injection of 10^5 B16 melanoma cells 100% of mice developed metastases of the spinal region (cervical 0/10, thoracic 10/10, lumbar 9/10, sacral 5/10).[106] In the intra-cardiac injection

setting, the bone marrow has been described as the organ that seemingly best supported metastatic colonization.[106] This is mainly due to a unique combination of morphological and mechanical factors, such as the fenestrated basement membrane in the osseous sinusoids, as well as the alternate and stagnant blood flow within the bone marrow cavities, both of which might more readily facilitate the extravasation of circulating tumor cells.[107]

In previous experiments, we also observed a remarkably common and widespread appearance of osseous metastases, with the main focus on thoracic and lumbar parts of the spine.[103] A drawback of this experimental metastasis model is that the direct injection of tumor cells into arterial circulation only recreates certain aspects of the metastatic cascade, disregarding the necessary steps of primary tumor growth, vessel invasion and preparation of the metastatic niche. Keeping in mind this limitation, we chose the route of intra-arterial injection instead of intra-venous injection for our present study, as it was shown that the vast majority of i.v. injected tumor cells are rapidly arrested and destroyed in the lung capillaries, making metastases of the remaining organs less likely to occur.[108] In contrast, injection of the tumor cells directly into the aortic arch enables a systemic distribution pattern. The risk of the intra-cardiac injection is higher through direct affection of the thoracic cavities, which can lead to lung collapse or cardiac arrest. Because of the improved accessibility and fewer operating complications, as well as the circumvention of cranial circulation and subsequent brain metastasis, the cervical intra-arterial injection of tumor cells into the left carotid artery was the preferable method for our experiments. As it has been demonstrated before, the loss of one carotid artery is generally well tolerated and we did not observe any neurological effects within the first days after operation.[109] Thus, it is highly unlikely for the symmetric plegia of the hind-legs to be caused by a delayed onset of cerebral malperfusion or stroke events.

7.1.4 Pharmacological compounds and experimental therapeutic strategies for targeting EphB4-Ephrin-B2 signaling

Two different pharmacological interventions were applied to evaluate their effects on EphB4 – Ephrin-B2 interaction with potential therapeutic implications. First, for systemic inhibition of the EphB4 receptor tyrosine kinase (RTK), the small molecule inhibitor NVP-BHG 712 was utilized. This molecule was identified by computer design, applying

Discussion

a model of the EphB4 kinase domain and has been shown to have a high selectivity for EphB4 and potently inhibit autophosphorylation, as well as VEGF-driven angiogenesis in vivo.[110] However, although NVP-BHG 712 has been evaluated in-vitro and in-vivo to be essentially directed towards the inhibition of EphB4 kinase activity, a partial inhibition of other similar kinases could not be ruled out entirely as the activities of EphB2, EphA2, EphB3 and EphA3 were also partly affected in cell-based Eph receptor autophosphorylation assays.[110] In addition, all of the aforementioned receptors have been reported to be co-expressed with EphB4, either on endothelial cells or adjacent pericytes.[111] The effect of the partial blockade of these receptors as well as the effects on the inhibition of VEGF-driven angiogenesis cannot be entirely accounted for.

Secondly, for the evaluation of the specific functional role of endothelial Ephrin-B2 in the molecular interactions with EphB4, the dimeric Ephrin-B2-Fc, a soluble extracellular domain (ECD) of Ephrin-B2, was injected to specifically induce EphB4-phosphorylation and substitute the knocked out endothelial Ephrin-B2 in efnb2$^{i\Delta EC}$ animals. Recombinant ECDs are frequently used to activate and/or inhibit Eph-Ephrin signaling and have been shown to have a high affinity towards their respective counterparts.[112] However, similar to NVP-BHG 712, these ECDs may also affect other members of the Eph family, which could enhance their efficacy but could also increase the risk of unwanted side effects as well as making the distinction between the effects of certain Eph family members difficult.[36] Furthermore, Fc-fused Ephrin ECDs have been described to both enhance and decrease Eph forward signaling, in certain cases by promoting Eph downregulation or competing with their endogenous counterparts, making the distinction between the effects more complicated.[113] It was also shown, that Ephrin-Fc proteins may function as inhibitors of Eph activity if they are not oligomerized, as the monomeric molecules appear to be weaker activators than their endogenous counterparts they displace. However, the exact mechanisms still remain unclear.[114,115]

It has been shown that Ephrin-B2-Fc can induce phosphorylation of the EphB4 RTK and thus increase forward signaling.[77] However, looking at the efnb2$^{lox/lox}$ experiments, one has to keep in mind that the binding of Ephrin-B2-Fc would also cause the displacement of the physiological endothelial-bound Ephrin-B2 ligand, thus recreating only certain aspects of the signaling pathway such as the forward signaling of EphB4, while at the same time blocking the backward signaling towards the endothelial cells. Multiple,

seemingly contradictory reports of EphB4 expression in cancers emphasize the duality of EphB4 action depending on cellular context, phosphorylation status and availability of Ephrin-B2.[116,117,71] This dual role as tumor promoter and suppressor may be regulated via ligand-dependent and –independent signaling pathways, respectively.[70] However, few studies have addressed this topic with specific focus on Eph-Ephrin interaction.[81]

Overall, therapies targeting Eph-receptors could potentially be strongly associated with side effects or toxicities in vivo, as numerous physiological processes, such as glucose tolerance, bone homeostasis or immune functions are regulated through Eph-Ephrin interaction.[36] However, the complex diversity of the Eph-Ephrin system may in these cases even provide an advantage through compensatory mechanisms of other family members. Furthermore, other feedback mechanisms involving different signaling systems may compensate for the loss of one specific molecular interaction.[36]

7.2 Results discussion

In the present study, we applied two different pharmacological treatment strategies for firstly targeting the metastatic dissemination and EC-DTC interaction and secondly affecting the growth of established spinal metastases. Accordingly, we defined two different time points for the systemic administration of therapeutics. The first approach was aiming at preventing the onset of metastatic colonization. In this study arm (pre-tumor), therapeutics were administered around the same time as the intra-arterial tumor cell inoculation (-5 to +4 days). The second approach was intended as a therapy of overt spinal metastases. In this latter (post-tumor) study arm, therapeutics were administered 12 to 21 days after tumor cell inoculation, when spinal metastases had already manifested.

7.2.1 Pre-tumor treatment in efnb2$^{lox/lox}$ mice

In pre-tumor treatment of efnb2$^{lox/lox}$ mice, our results showed that the application of Ephrin-B2-Fc as well as the application of NVP-BHG 712 both significantly reduced the period until the appearance of hind leg paresis (Figure 8). This implies that the physiological EphB4 – Ephrin-B2 interaction may act as a natural repulsive barrier. This would hinder the attachment of circulating tumor cells to the endothelial lining of the vertebral sinusoids in a similar repulsive manner as it does in the organization of arterial and venous endothelial cells[55] and axon cell guidance.[42,50] Altering this physiological interaction either through blocking of the EphB4 tyrosine kinase via NVP-BHG 712, or potentially occupying the Ephrin-binding site of the EphB4 receptor by the application of soluble Ephrin-B2-Fc, would reduce these repulsive forces, thus leading to increased spinal metastasis formation. Although EphB4-mediated forward signaling is not altered by the binding of Ephrin-B2-Fc, the efficacy of Ephrin-B2 backward signaling, which also forms a vital part of the interaction, is severely impeded, if the soluble agent occupies binding sites of EphB4.[118] Especially for the reverse signaling taking place in the endothelial cells, the proper binding of Ephrin-B2 to its receptor seems to be of crucial importance in order to affect the transmigration of circulating tumor cells.

The theory of the disrupted natural barrier is further underlined by the fact that both NVP-BHG 712 and Ephrin-B2-Fc pre-tumor treated efnb2$^{lox/lox}$ animals showed a significantly higher metastasis count in the spinal MRI (Figure 9). Although the number of spinal metastases increased in both groups, the individual metastasis volume remained unaffected, implying that primarily seeding mechanisms are affected by the pre-tumor therapeutic application of the two agents. It seems that the effect of the pre-tumor therapy on the initial steps of the metastatic process is greater than the effect on the growth of the established tumor. Thus, we conclude that altering this repulsive/protective system in any way increases the ability of the metastatic tumor cells to attach to the endothelial lining of the organ vessels, eventually leading to an increased metastatic count and earlier neurological deficits.

Discussion

Figure 25: Proposed model of the effects of pre-tumor therapeutic alteration of EphB4 – Ephrin-B2 interaction on the tumor load of spinal metastasis in efnb2$^{lox/lox}$ mice
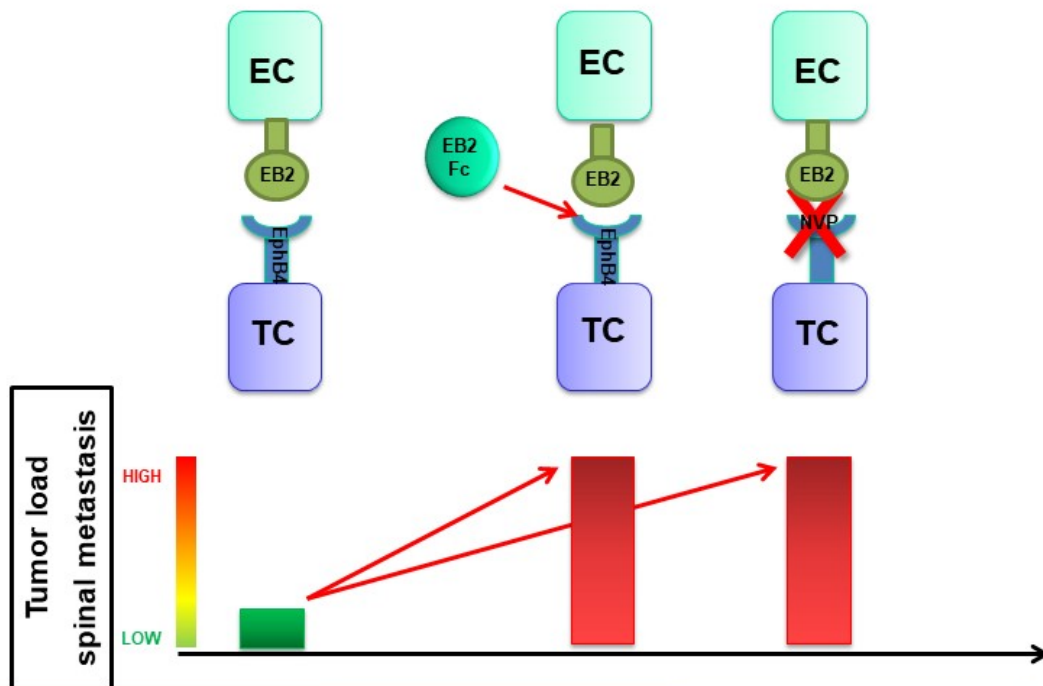
Figure 25: The model is based on functional data summarized in this dissertation and takes into account published data on Eph-Ephrin interaction and its effect on malignancy. Similar to the effects observed in arterial and venous endothelial cells[55] and axon cell guidance[42,50] physiological Eph-Ephrin interaction in efnb2$^{lox/lox}$ mice may promote a repulsive environment, where circulating tumor cells are less likely to attach to the endothelium of the osseous sinusoid walls of the vertebrae, consequently reducing the tumor load of spinal metastasis. Altering this interaction in any way decreases the time until neurological deficit and increases metastasis count in the spine, possibly by disturbing this natural barrier and increasing the attachment of DTCs to the endothelial lining. Colored bars represent the relative extent of spinal metastasis (green = relatively low tumor load, red = relatively high tumor load, EC = endothelial cell, TC = tumor cell, EB2 = Ephrin-B2, EB2 Fc = Ephrin-B2-Fc, NVP = NVP BHG712)

In Ephrin-B2-Fc treated animals, there was a significant preference of the tumor cells to metastasize into osseous organs, which could account for the decrease in neurological survival and also the significant increase in the number of spinal metastases (Figure 8, 9A and 11D). Our results further imply that the preference of the metastatic cells to colonize osseous organs, such as the spine or limbs, was lost under the treatment with

Discussion

NVP-BHG 712, possibly because the dissemination pattern is of a more general nature, and a greater variety of organs are colonized by DTCs. As mentioned above, the inhibition of the EC-based backward signaling through application of Ephrin-B2-Fc increases the number of metastatic tumor cells in the luminometric experiments, while maintaining the preference for osseous organs. Thus, we conclude that blocking of the backward signaling of the endothelial cells (through application of Ephrin-B2-Fc) seems more relevant for the dissemination process in bones, whereas targeting the EphB4 receptor, which is universally expressed on all tumor cells irrespective of their localization, leads to a more generalized modification of tumorigenicity. Heroult et al. have already demonstrated that the interference with tumor-cell expressed EphB4 is capable of significantly altering tumor cell trafficking in certain soft-tissue organs such as the lungs, the liver and kidneys.[100] Similar to this effect, the application of Ephrin-B2-Fc significantly affects the size of tumor vessels by involving endothelial cells, while the blocking of EphB4 on the tumor cell surface is unlikely to directly affect the growth of spinal endothelial cells and does not affect tumor vessel size.

However, an unsolved question remains how the effect of the pre-tumor treatment changes over the course of the disease and why its effects are still perceivable weeks after the end of therapy.This difference in time between tumor cell injection and explantation of the spine also has to be taken account for in the number of bioluminescent tumor cells found in the site-specific dissemination experiments. It is expected that an increase in survival time would also increase the time of tumor cell proliferation and cellular division, supposedly generating more tumor cells per organ. In the case of the pre-tumor-treated efnb2$^{lox/lox}$ animals, both therapeutics even increased the number of metastatic tumor cells found in the luminometric experiments, while at the same time significantly decreasing the survival time. (Figure 11) However, in other cases, this argument may even counter-act certain effects of tumor growth by significantly decreasing the survival times, thus allowing less time for the tumor cells to proliferate.

Discussion

7.2.2 Post-tumor treatment in efnb2$^{lox/lox}$ mice

By applying the therapeutics between days 12 and 21 after tumor cell injection, the common clinical setting was mimicked, when patients present to health care professionals after the initial steps of the metastatic cascade have already taken place. In this setting, a potentially therapeutic intervention could be favorable for the patients' quality of life and prolong survival if the growth of spinal metastases could be reduced. However, at this point in time, it is unlikely for any therapeutic effect on the tumor cell dissemination to occur. Under the post-tumor treatment of efnb2$^{lox/lox}$ mice, the application of Ephrin-B2-Fc did not have any effect on the appearance of the neurological deficit, whereas the NVP-BHG 712 treatment group showed a significantly earlier appearance of hind leg paresis, i.e. a decreased neurological survival. (Figure 13)

The mean number of spinal metastases remained unaffected by both therapeutic regimens (Figure 14). However, this was expected, as by the time of the first application, 12 days after tumor cell injection, spinal metastases would have already been established, as seen in bioluminescent in-vivo images. When compared to the placebo group in the luminometric experiments, both treatment cohorts showed a loss of significant affinity for osseous organs. There were no representative changes in the rate of tumor cell proliferation or tumor vasculature under NVP-BHG 712 treatment either (Figure 16), which could account for the significant decrease of neurological survival. Therefore, the driving force behind the significant negative effect of the systemic blockade of EphB4 by NVP-BHG 712 on survival remains to be elucidated in further studies, as it appears not to be related to tumor angiogenesis. In contrast, under application of Ephrin-B2-Fc, both the number and the size of the tumor blood vessels increased significantly, implying that Ephrin-B2 exerts significant pro-angiogenic effects in the developing tumors, however without effectively influencing neurological survival. These significant Ephrin-B2-dependend effects observed on the tumor vasculature are similar to those seen in the pre-tumor treatment and are most likely to be caused by the involvement of backward signaling performed in endothelial cells.

Discussion

7.2.3 Pre-tumor treatment in efnb2$^{i\Delta EC}$ mice

In efnb2$^{i\Delta EC}$ knockout mice, the load of metastases was significantly increased compared to efnb2$^{lox/lox}$ animals and thus the appearance of neurological symptoms occurred at a significantly earlier date [mean efnb2$^{lox/lox}$ placebo: 24.5 days n=22, mean efnb2$^{i\Delta EC}$ placebo: 18 days, n=7, p=<0.0001, Log-rank (Mantel-Cox) test, *data not shown*]. These findings are in line with out earlier results,[89] and further strengthen the notion that the physiological interaction between EphB4 and Ephrin-B2 reduces metastasis formation by creating a repulsive environment. In the setting of endothelial Ephrin-B2 knockout, the EphB4 receptor expressed on circulating tumor cells lacks its respective ligand on the vascular endothelium, thus phosphorylation and activation of the receptor are decreased.[119] This lack of stimulation induces ligand-independent tumor-promoting properties of EphB4. In the dephosphorylated state, the EphB4 receptor has repeatedly been shown to exhibit tumor promoting properties by increasing tumor growth, angiogenesis and tumor cell migration.[81] Moreover, the repulsion of circulating tumor cells appears to be less effective, hence an increased number of metastases are able to form. Thus, the primary setting in efnb2$^{i\Delta EC}$ knockout mice is contrarious to the setting in enfb2$^{lox/lox}$ mice.

The substitution of knocked out endothelial Ephrin-B2 in efnb2$^{i\Delta EC}$ mice, by applying Ephrin-B2-Fc, partially re-establishes the physiological repulsive pathway, as it leads to an activation of the forward signaling of the EphB4-RTK, when there are no physiological endothelial ligands available. By increasing the phosphorylated state of EphB4 receptors, it was shown to reduce the tumor-growth promoting activities of the dephosphorylated receptor.[86] Thus it seems possible to mimic the tumor-inhibitory profile of activated EphB4-receptors by applying Ephrin-B2-Fc. The backward signaling pathway however, which proved to be crucial for role of the endothelial cells in the interaction is entirely lost under the knockout setting. Consequently, in the knockout model, mainly the characteristics of the circulating tumor cells are affected by application of the therapeutics. Therefore, the therapeutic substitution of Ephrin-B2-Fc is only able to partially reactivate the pathway in regard to the forward signaling of the EphB4 receptor on DTCs, however does not seem to be as effective as the physiological setting with its bilateral EC-DTC signaling effects.

Discussion

Though this may seem inapprehensible at first sight, especially since the initial experiments have proven the importance of Ephrin-B2 in spinal metastasis formation, one has to bear in mind that under the endothelial Ephrin-B2 knockout, the biological context is utterly different. The function of EphB4 has proven to be different, if not contrarious, depending on the presence or absence of its ligand[81] and the effects are mainly taking place on the disseminated tumor cells, altering the phenotype of the tumor cells, rather than functions of the endothelial cells. Furthermore, as the signaling effects in this ligand-depleted setting are mainly Ephrin-B2-independent, other molecules such as P selectin glycoprotein ligand – 1 (PSGL-1), which has been shown to mutually interact with EphB4,[120] or ICAM-1, which can directly affect spinal metastasis formation,[90] may prove to be the surrogate regulators of metastasis formation.

The proposed mode of action of the EphB4 kinase-blocking agent NVP-BHG 712 in this setting is also an entirely different one, yet possibly resulting in similar effects in Ephrin-B2-knockout mice, i.e. blocking the tumor-promoting activities of the dephosphorylated EphB4 receptor. However, the application in pre-tumor treated efnb2$^{i\Delta EC}$ mice did not show a significant effect on the time until appearance of neurological deficits despite the trend of increasing the survival time. (Figure 17) It seems that a minor step towards a tumor-inhibitory function can be achieved by blocking the tyrosine kinase, yet this does not prove to be as effective as the phosphorylation by its natural ligand as part of the natural Ephrin-B2-EphB4 barrier. The "partial reestablishment" of the pathway through activation of forward signaling through Ephrin-B2-Fc however seems to be more efficient in this case, since the pre-tumor treatment using Ephrin-B2-Fc was able to not only significantly reduce the survival time but also reduce the total metastatic volume and metastasis count in the spine of efnb2$^{i\Delta EC}$ mice (Figures 17, 18 A, C).

In contrast, under pre-tumor application of NVP-BHG 712 treatment, there were no significant effects on the size or number of metastases found in the focused spinal MRI. The application of NVP-BHG 712 did not show the same anti-tumoral effects as Ephrin-B2-Fc in the setting of the endothelial Ephrin-B2-knockout. In the bioluminescent assays, in all therapeutic groups a preference of the tumor cells for homing in osseous organs was perceivable. In the setting of the pre-tumor Ephrin-B2-Fc treatment this did not prove to be statistically significant, although the effect might be counteracted by the considerable variance of the results in this experiment. In the context of tumor cell

Discussion

proliferation, it even led to an increase in the number of Ki 67-positive proliferating tumor cells, however one cannot entirely rule out the possibility of the decreased specimen number simulating an effect in this case.

This implies that 1) primarily post-seeding effects are effective when blocking the EphB4 receptor, and 2) that physiological Ephrin-B2 binding shows a stronger effect on the tumor-reducing properties of the EphB4 receptor as the blockade of the tumor-promoting dephosphorylated receptor could achieve. Therefore, the effects of blocking the tumor-promoting dephosphorylated EphB4 using a small molecule inhibitor seem to be less effective in hampering tumor growth as partially re-establishing the physiological signaling pathway through the application of Ephrin-B2-Fc.

Figure 26: Proposed model of the effects of pre-tumor therapeutic alteration of EphB4 – Ephrin-B2 interaction on the tumor load of spinal metastasis in efnb2$^{i\Delta EC}$ mice
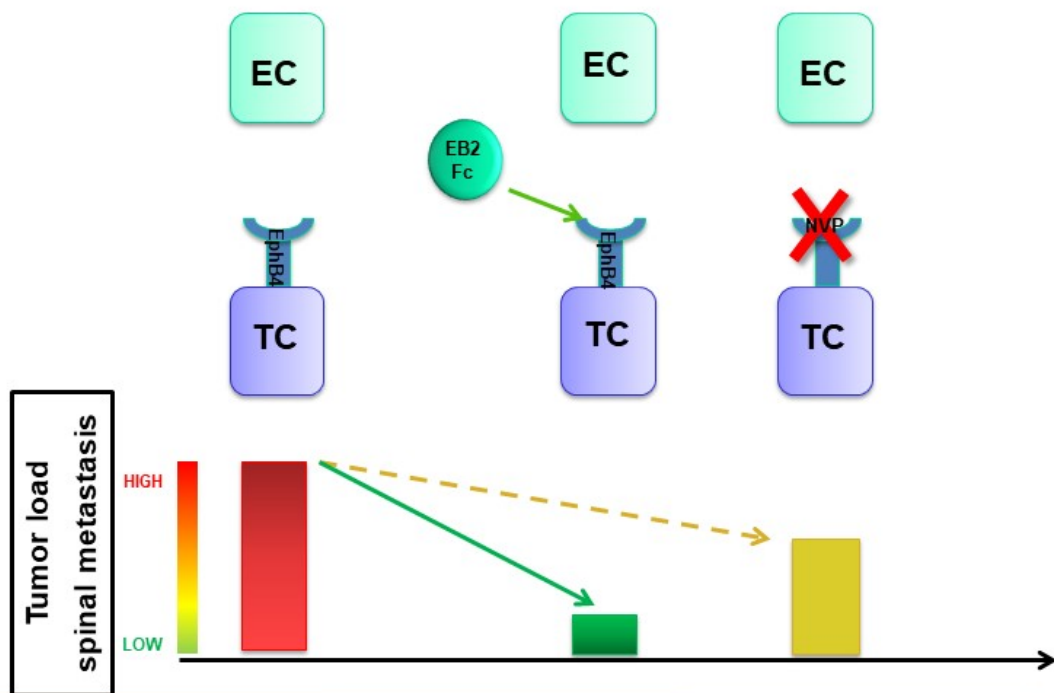
Figure 26: *In efnb2$^{i\Delta EC}$, the initial setting is tumor-growth promoting as visualized by the relatively high spinal tumor load. Application of Ephrin-B2-Fc effectively reduces tumor growth by mimicking sub-steps of the physiological interaction. The application of NVP-BHG 712 is not as effective in blocking the tumor-promoting properties of the dephosphorylated EphB4 receptor. Colored bars represent the relative extent of spinal*

Discussion

metastasis (green = relatively low tumor load, red = relatively high tumor load), EC = endothelial cell, TC = tumor cell, EB2 Fc = Ephrin-B2-Fc, NVP = NVP BHG712).

7.2.4 Post-tumor treatment in efnb2$^{i\Delta EC}$ mice

In the post-tumor treated efnb2$^{i\Delta EC}$ knockout animals, there was no significant change in the symptom-free survival. Furthermore, there was no effect on size or number of spinal metastases as observed in the rodent MRI (Figures 21 & 22). In the bioluminescence assay in all therapeutic settings there was a preference of osseous tissues, yet again the variance in results after Ephrin-B2-Fc application did not allow for statistical significance.

The application of NVP-BHG 712 led to a trend of increase in the number of Ki-67 positive proliferating tumor cells, as it did in the pre-tumor treatment cohort too, however the change in proliferation did not significantly affect tumor size and the number of examined tumors was not sufficient to provide statistical significance of the increased proliferation, thus further experiments would be necessary to examine this particular effect. Ephrin-B2-Fc significantly decreased the size of the tumor vasculature, although the number of tumor vessels remained unaffected, suggesting that the partial re-establishment of the signaling pathway decreases tumor angiogenesis in the post-tumor-treated Ephrin-B2-knockout setting. (Figure 24) These results may implicate that possibly contrarious effects of the EphB4 interaction on certain aspects of malignancy as the increase in proliferation of tumor cells and decrease of size of tumor vasculature could theoretically cancel each other out when it comes to neurological survival. However, the angiogenic functions of Eph RTKs in disease make these molecules an attractive target for the development of new anti-angiogenic cancer therapies. Targeting this interaction may simultaneously affect the endothelial cells of the growing tumor vasculature and the stromal cells of the tumor microenvironment.[121]

8 Conclusions

The most significant findings of this study are the following:

1) Under the presence of physiological Ephrin-B2, any therapeutic alteration of EphB4–Ephrin-B2 signaling disturbs the protective barrier against tumor cell dissemination, manifesting in a more aggressive metastatic phenotype and earlier neurological deficits. As this effect was also perceivable under endothelial Ephrin-B2 knockout, we hypothesize that the physiological molecular interaction generates repulsive signals. Hence, hampering this protective mechanism leads to an increased attachment and subsequent extravasation of circulating metastatic cells and a greater metastatic burden of the spine.

2) The backward-signaling pathway contained within the Ephrin-B2-expressing endothelial cells crucially regulates adhesion and repulsion of circulating tumor cells. Furthermore, it is an important regulator in the angiogenesis of spinal metastases under physiological settings.

3) The RTK EphB4 that is mainly expressed on the DTCs is not involved in mediating organ specificity of metastasis formation, as it leads to a more generalized modification of tumorigenicity.

4) The protective antitumoral properties of the physiological pathway can be partially re-established under the prometastatic endothelial Ephrin-B2-knockout. The addition of Ephrin-B2-Fc and the consequent activation of EphB4 forward signaling is in this case more efficient than blocking the dephosphorylated EphB4 RTK through NVP-BHG 712.

9 References

1. Paul Klimo, Jr., M. H. S. Surgical Management of Spinal Metastases. *Oncologist* **9**, 188–196 (2004).

2. Arneson, T. J., Shuling Li, Y., Yi Peng, E. D., Weinhandl, E. D., Blaes, A., Cetin, K., Chia, V. M., Stryker, S., Pinzone, J. J. and Acquavella, J. Estimated number of prevalent cases of metastatic bone disease in the US adult population. *Clin. Epidemiol.* **4**, 87 (2012).

3. Maccauro, G., Spinelli, M. S., Mauro, S., Perisano, C., Graci, C. and Rosa, M. A. Physiopathology of spine metastasis. *Int. J. Surg. Oncol.* **2011**, 107969 (2011).

4. Gerszten, P. C. and Welch, W. C. Current surgical management of metastatic spinal disease. *Oncology (Williston Park).* **14**, 1013–1024; discussion 1024, 1029–1030, (2000).

5. Gilbert, R. W., Kim, J.-H. and Posner, J. B. Epidural spinal cord compression from metastatic tumor: Diagnosis and treatment. *Ann. Neurol.* **3**, 40–51 (1978).

6. Patchell, R. A., Tibbs, P. A., Regine, W. F., Payne, R., Saris, S., Kryscio, R. J., Mohiuddin, M. and Young, B. Direct decompressive surgical resection in the treatment of spinal cord compression caused by metastatic cancer: A randomised trial. *Lancet* **366**, 643–648 (2005).

7. Young, R. F., Mo, S. and King, G. A. *Treatment of spinal epidural metastases Randomized prospective comparison of laminectomy and radiotherapy. J Neurosurg* **53**, (1980).

8. Algra, P. R., Heimans, J. J., Valk, J., Nauta, J. J., Lachniet, M. and Van Kooten, B. Do metastases in vertebrae begin in the body or the pedicles? Imaging study in 45 patients. *Am. J. Roentgenol.* **158**, 1275–1279 (1992).

9. Siegel, G. W., Biermann, J. S., Calinescu, A.-A., Spratt, D. E. and Szerlip, N. J. Surgical Approach to Bone Metastases. *Curr. Osteoporos. Rep.* **16**, 512–518 (2018).

10. Reeves, R. A., DeWolf, M. C., Shaughnessy, P. J., Ames, J. B. and Henderson, E. R. Use of minimally invasive spine surgical instruments for the treatment of bone tumors. *Expert Rev. Med. Devices* **14**, 881–890 (2017).

11. Hanahan, D. and Weinberg, R. A. The hallmarks of cancer. *Cell* **100**, 57–70 (2000).

References

12. Hanahan, D. and Weinberg, R. A. Hallmarks of Cancer: The Next Generation. *Cell* **144**, 646–674 (2011).

13. Chambers, A. F., Groom, A. C. and MacDonald, I. C. Dissemination and growth of cancer cells in metastatic sites. *Nat. Rev. Cancer* **2**, 563–572 (2002).

14. Fidler, I. J. The pathogenesis of cancer metastasis: the 'seed and soil' hypothesis revisited. *Nat. Rev. Cancer* **3**, 1–6 (2003).

15. Paget, S. The distribution of secondary growths in cancer of the breast. *Lancet* **133**, 571–573 (1889).

16. Chambers, A. F., Naumov, G. N., Varghese, H. J., Nadkarni, K. V, MacDonald, I. C. and Groom, A. C. Critical steps in hematogenous metastasis: an overview. *Surg. Oncol. Clin. N. Am.* **10**, 243–55, vii (2001).

17. Joyce, J. A. and Pollard, J. W. Microenvironmental regulation of metastasis. *Nat Rev Cancer* **9,** 239-252 (2009).

18. Ziyad, S. and Iruela-Arispe, M. L. Molecular mechanisms of tumor angiogenesis. *Genes Cancer* **2**, 1085–96 (2011).

19. Quail, D. F. amd Joyce, J. A. Microenvironmental regulation of tumor progression and metastasis. *Nat Med* **19**, 1423–1437 (2013).

20. Baglole, C. J., Ray, D. M., Bernstein, S. H., Feldon, S. E., Smith, T. J., Sime, P. J., and Phipps, R. P. More Than Structural Cells, Fibroblasts Create and Orchestrate the Tumor Microenvironment. *Immunol. Invest.* **0139**, 297–325 (2009).

21. Egeblad, M., Nakasone, E. S. and Werb, Z. Tumors as organs: complex tissues that interface with the entire organism. *Dev. Cell* **18**, 884–901 (2010).

22. Mintz, B. and Illmensee, K. Normal genetically mosaic mice produced from malignant teratocarcinoma cells. *Cell Biology* **72**, (1975).

23. Mantovani, A., Allavena, P., Sica, A. and Balkwill, F. Cancer-related inflammation. *Nature* **454**, 436–44 (2008).

24. Kaplan, R. N., Riba, R. D., Zacharoulis, S., Bramley, A. H., Loic Vincent, L., Costa, C., Macdonald, D. D., Jin, D. K., Shido, K., Kerns, S. A., Zhu, Z., Hicklin, D., Wu, Y., Port, J. L., Altorki, N., Port, E. R., Ruggero, D., Shmelkov, S. V, Jensen, K. K., Rafii, S. and Lyden, D. VEGFR1-positive haematopoietic bone marrow progenitors initiate the pre-metastatic niche. *Nature* **438**, 820–827 (2005).

25. Hiratsuka, S., Watanabe, A., Aburatani, H. and Maru, Y. Tumour-mediated

upregulation of chemoattractants and recruitment of myeloid cells predetermines lung metastasis. *Nat. Cell Biol.* **8**, 1369–1375 (2006).

26. Nguyen, D. X., Bos, P. D. and Massague, J. Metastasis: from dissemination to organ-specific colonization. *Nat Rev Cancer* **9**, 274–84 (2009).

27. Becker, S., Becker-Pergola, G., Wallwiener, D., Solomayer, E.-F. and Fehm, T. Detection of cytokeratin-positive cells in the bone marrow of breast cancer patients undergoing adjuvant therapy. *Breast Cancer Res. Treat.* **97**, 91–96 (2006).

28. David Roodman, G. *Mechanisms of Bone Metastasis. N Engl J Med* **350**, (2004).

29. Lacey, D. L., Timms, E., Tan, H. L., Kelley, M. J., Dunstan, C. R., Burgess, T., Elliott, R., Colombero, A., Elliott, G., Scully, S., Hsu, H., Sullivan, J., Hawkins, N., Davy, E., Capparelli, C., Eli, A., Qian, Y. X., Kaufman, S., Sarosi, I., Shalhoub, V., Senaldi, G., Guo, J., Delaney, J. and Boyle, W. J. Osteoprotegerin ligand is a cytokine that regulates osteoclast differentiation and activation. *Cell* **93**, 165–76 (1998).

30. Hanahan, D., Folkman, J., Flax, J., Blumenfeld, W., Folkman, J., Moore, D. ., Meli, S., Gasparini, G., Sage, E., Folkman, J., Ward, L., Hayward, N. and Weber, G. Patterns and emerging mechanisms of the angiogenic switch during tumorigenesis. *Cell* **86**, 353–64 (1996).

31. Lin, E. Y., Li, J.-F., Gnatovskiy, L., Deng, Y., Zhu, L., Grzesik, D. A., Qian, H., Xue, X. and Pollard, J. W. Macrophages Regulate the Angiogenic Switch in a Mouse Model of Breast Cancer. *Cancer Res.* **66**, 11238–11246 (2006).

32. De Palma, M., Venneri, M. A., Galli, R., Sergi, L. S., Politi, L. S., Sampaolesi, M. and Naldini, L. Tie2 identifies a hematopoietic lineage of proangiogenic monocytes required for tumor vessel formation and a mesenchymal population of pericyte progenitors. *Cancer Cell* **8**, 211–226 (2005).

33. Kurebayashi, H., Goi, T., Shimada, M., Tagai, N., Naruse, T., Nakazawa, T., Kimura, Y., Hirono, Y. and Yamaguchi, A. Prokineticin 2 (PROK2) is an important factor for angiogenesis in colorectal cancer. *Oncotarget* **6**, 26242–51 (2015).

34. Harris, A. L. Hypoxia- a key regulatory factor in tumour growth. *Nat. Rev.* **2**, 38–47 (2002).

35. Kandouz, M. The Eph/Ephrin family in cancer metastasis: Communication at the service of invasion. *Cancer and Metastasis Reviews* **31**, 353–373 (2012).

References

36. Barquilla, A. and Pasquale, E. B. Eph receptors and ephrins: therapeutic opportunities. *Annu. Rev. Pharmacol. Toxicol.* **55**, 465–87 (2015).

37. Pasquale E. Eph-ephrin promiscuity is now crystal clear. *Nat. Neurosci.* **7**, 417–418 (2004).

38. Nievergall, E., Lackmann, M. and Janes, P. W. Eph-dependent cell-cell adhesion and segregation in development and cancer. *Cell. Mol. Life Sci.* **69**, 1813–1842 (2012).

39. Oricchio, E., Nanjangud, G., Wolfe, A. L., Schatz, J. H., Mavrakis, K. J., Jiang, M., Liu, X., Bruno, J., Heguy, A., Olshen, A. B., Socci, N. D., Teruya-Feldstein, J., Weis-Garcia, F., Tam, W., Shaknovich, R., Melnick, A., Himanen, J. P., Chaganti, R. S. K. and Wendel, H.-G. The Eph-receptor A7 is a soluble tumor suppressor for follicular lymphoma. *Cell* **147**, 554–64 (2011).

40. Pasquale, E. B., Hunter, S., Hwang, Y., Chen, J., Bouvier, D., Doucet, G., Corera, A. T., Fon, E. A., Zisch, A. H., Murai, K. K. Eph-Ephrin Bidirectional Signaling in Physiology and Disease. *Cell* **133**, 38–52 (2008).

41. Salvucci, O., Maric, D., Economopoulou, M., Sakakibara, S., Merlin, S., Follenzi, A. and Tosato, G. EphrinB reverse signaling contributes to endothelial and mural cell assembly into vascular structures. *Blood* **114**, 1707–1716 (2009).

42. Egea, J. and Klein, R. Bidirectional Eph-ephrin signaling during axon guidance. *Trends Cell Biol.* **17**, 230–8 (2007).

43. Matsuoka, H., Obama, H., Kelly, M. L., Matsui, T. and Nakamoto, M. Biphasic functions of the kinase-defective Ephb6 receptor in cell adhesion and migration. *J. Biol. Chem.* **280**, 29355–63 (2005).

44. Pasquale, E. B. Developmental Cell Biology: Eph receptor signalling casts a wide net on cell behaviour. *Nat. Rev. Mol. Cell Biol.* **6**, 462–475 (2005).

45. Yang, N. Y., Pasquale, E. B., Owen, L. B. and Ethell, I. M. The EphB4 receptor-tyrosine kinase promotes the migration of melanoma cells through Rho-mediated actin cytoskeleton reorganization. *J. Biol. Chem.* **281**, 32574–32586 (2006).

46. Pasquale, E. B. Eph receptors and ephrins in cancer: bidirectional signaling and beyond. *Nat Rev Cancer* **10**, 165–180 (2010).

47. Lin, K.-T., Sloniowski, S., Ethell, D. W. and Ethell, I. M. Ephrin-B2-induced Cleavage of EphB2 Receptor Is Mediated by Matrix Metalloproteinases to Trigger Cell Repulsion S. *J. Biol. Chem.* **283**, 28969–28979 (2008).

References

48. Beauchamp, A., Lively, M. O., Mintz, A., Gibo, D., Wykosky, J. and Debinski, W. EphrinA1 Is Released in Three Forms from Cancer Cells by Matrix Metalloproteases. *Mol. Cell. Biol.* **32**, 3253–3264 (2012).

49. Marquardt, T., Shirasaki, R., Ghosh, S., Andrews, S. E., Carter, N., Hunter, T. and Pfaff, S. L. Coexpressed EphA receptors and ephrin-A ligands mediate opposing actions on growth cone navigation from distinct membrane domains. *Cell* **121**, 127–39 (2005).

50. Kao, T.-J. and Kania, A. Ephrin-Mediated cis-Attenuation of Eph Receptor Signaling Is Essential for Spinal Motor Axon Guidance. *Neuron* **71**, 76–91 (2011).

51. Hruska, M. and Dalva, M. B. Ephrin regulation of synapse formation, function and plasticity. *Mol. Cell. Neurosci.* **50**, 35–44 (2012).

52. Du, J., Fu, C. and Sretavan, D. W. Eph/ephrin Signaling as a Potential Therapeutic Target After Central Nervous System Injury. *Curr. Pharm. Des.* **13**, 2507–2518 (2007).

53. Cissé, M., Halabisky, B., Harris, J., Devidze, N., Dubal, D. B., Sun, B., Orr, A., Lotz, G., Kim, D. H., Hamto, P., Ho, K., Yu, G.-Q. and Mucke, L. Reversing EphB2 depletion rescues cognitive functions in Alzheimer model. *Nature* **469**, 47–52 (2011).

54. Cibert-Goton, V., Yuan, G., Battaglia, A., Fredriksson, S., Henkemeyer, M., Sears, T. and Gavazzi, I. Involvement of EphB1 Receptors Signalling in Models of Inflammatory and Neuropathic Pain. *PLoS One* **8**, (2013).

55. Wang, H. U., Chen, Z.-F. and Anderson, D. J. Molecular Distinction and Angiogenic Interaction between Embryonic Arteries and Veins Revealed by ephrin-B2 and Its Receptor Eph-B4. *Cell* **93**, 741–753 (1998).

56. Zhang, J. and Hughes, S. Role of the ephrin and Eph receptor tyrosine kinase families in angiogenesis and development of the cardiovascular system. *J. Pathol.* **208**, 453–461 (2006).

57. Adams, R. H., Wilkinson, G. A., Weiss, C., Diella, F., Gale, N. W., Deutsch, U., Risau, W. and Klein, R. Roles of ephrinB ligands and EphB receptors in cardiovascular development: demarcation of arterial/venous domains, vascular morphogenesis, and sprouting angiogenesis. *Genes Dev.* **13**, 295–306 (1999).

58. Füller T, Korff T, Kilian A, Dandekar G and Augustin H. Forward EphB4 signaling in endothelial cells controls cellular repulsion and segregation from ephrinB2

positive cells. *J. Cell Sci.* **116**, 2461–2470 (2003).

59. Klein, R. Eph/ephrin signalling during development. *Development* **139**, 4105–4109 (2012).

60. Qin, H., Noberini, R., Huan, X., Shi, J., Pasquale, E. B. and Song, J. Structural characterization of the EphA4-Ephrin-B2 complex reveals new features enabling Eph-ephrin binding promiscuity. *J. Biol. Chem.* **285**, 644–54 (2010).

61. Hamada, K., Oike, Y., Ito, Y. amd Suda, T. Distinct Roles of Ephrin-B2 Forward and EphB4 Reverse Signaling in Endothelial Cells. *Arterioscler. Thromb. Vasc. Biol.* **23**, 190–197 (2003).

62. Kim, I., Shin Ryu, Y., Jin Kwak, H., Young Ahn, S., Oh, J.-L., Yancopoulos, G. D., Gale, N. W. and Young Koh, G. EphB ligand, ephrinB2, suppresses the VEGF- and angiopoietin-1-induced Ras/mitogen-activated protein kinase pathway in venous endothelial cells. *FASEB J.* **16**, 1126–8 (2002).

63. Groppa, E., Brkic, S., Uccelli, A., Wirth, G., Korpisalo-Pirinen, P., Filippova, M., Dasen, B., Sacchi, V., Muraro, M. G., Trani, M., Reginato, S., Gianni-Barrera, R., Ylä-Herttuala, S. and Banfi, A. EphrinB2/EphB4 signaling regulates non-sprouting angiogenesis by VEGF. *EMBO Rep.* **19**, (2018).

64. Sawamiphak, S., Seidel, S., Essmann, C. L., Wilkinson, G. a, Pitulescu, M. E., Acker, T. and Acker-Palmer, A. Ephrin-B2 regulates VEGFR2 function in developmental and tumour angiogenesis. *Nature* **465**, 487–491 (2010).

65. Nakayama, A., Nakayama, M., Turner, C. J., Höing, S., Lepore, J. J. and Adams, R. H. Ephrin-B2 controls PDGFRβ internalization and signaling. *Genes Dev.* **27**, 2576–89 (2013).

66. Kida, Y., Ieronimakis, N., Schrimpf, C., Reyes, M. and Duffield, J. S. EphrinB2 reverse signaling protects against capillary rarefaction and fibrosis after kidney injury. *J. Am. Soc. Nephrol.* **24**, 559–72 (2013).

67. Kuijper, S., Turner, C. J. and Adams, R. H. Regulation of Angiogenesis by Eph-Ephrin Interactions. *Trends in Cardiovascular Medicine* **17**, 145–151 (2007).

68. Foo, S. S., Turner, C. J., Adams, S., Compagni, A., Aubyn, D., Kogata, N., Lindblom, P., Shani, M., Zicha, D. and Adams, R. H. Ephrin-B2 Controls Cell Motility and Adhesion during Blood-Vessel-Wall Assembly. *Cell* **124**, 161–173 (2006).

69. Ireton, R. and Chen, J. EphA2 Receptor Tyrosine Kinase as a Promising Target

References

for Cancer Therapeutics. *Curr. Cancer Drug Targets* **5**, 149–157 (2005).

70. Vaught, D., Brantley-Sieders D and Chen J. Eph receptors im breast cancer: roles in tumor promotion and tumor suppression. *Breast Cancer Res.* **10**, (2008).

71. Liu, W., Ahmad, S. A., Jung, Y. D., Reinmuth, N., Fan B.S., F., Bucana, C. D. and Ellis, L. M. Coexpression of ephrin-Bs and their receptors in colon carcinoma. *Cancer* **94**, 934–939 (2002).

72. Kumar, S., Masood, R., Spannuth, W., Singh, J., Scehnet, J., Kleiber, G., Jennings, N., Deavers, M., Krasnoperov, V., Dubeau, L., Weaver, F., Sood, A. and Gill, P. The receptor tyrosine kinase EphB4 is overexpressed in ovarian cancer, provides survival signals and predicts poor outcome. *Br. J. Cancer* **96**, 1083–1091 (2007).

73. Spannuth, W. A., Mangala, L. S., Stone, R. L., Carroll, A. R., Nishimura, M., Shahzad, M. M. K., Lee, S.-J., Moreno-Smith, M., Nick, A. M., Liu, R., Jennings, N. B., Lin, Y. G., Merritt, W. M., Coleman, R. L., Vivas-Mejia, P. E., Zhou, Y., Krasnoperov, V., Lopez-Berestein, G., Gill, P. S. and Sood, A. K. Converging evidence for efficacy from parallel EphB4-targeted approaches in ovarian carcinoma. *Mol. Cancer Ther.* **9**, 2377–2388 (2010).

74. Kumar, S. R., Scehnet, J. S., Ley, E. J., Singh, J., Krasnoperov, V., Liu, R., Manchanda, P. K., Ladner, R. D., Hawes, D., Weaver, F. A., Beart, R. W., Singh, G., Nguyen, C., Kahn, M. and Gill, P. S. Preferential Induction of EphB4 over EphB2 and Its Implication in Colorectal Cancer Progression. *Cancer Res* **69**, 3736–45 (2009).

75. Huang, X., Yamada, Y., Kidoya, H., Naito, H., Nagahama, Y., Kong, L., Katoh, S.-Y., Li, W.-L., Ueno, M. and Takakura, N. EphB4 Overexpression in B16 Melanoma Cells Affects Arterial-Venous Patterning in Tumor Angiogenesis. *Cancer Res* **67**, 9800–9808 (2007).

76. Erber, R., Eichelsbacher, U., Powajbo, V., Korn, T., Djonov, V., Lin, J., Hammes, H.-P., Grobholz, R., Ullrich, A. and Vajkoczy, P. EphB4 controls blood vascular morphogenesis during postnatal angiogenesis. *EMBO J.* **25**, 628–641 (2006).

77. Noren N, Lu M, Freeman A, Koolpe M and Pasquale EB. Interplay between EphB4 on tumor cells and vascular ephrin-B2 regulates tumor growth. *PNAS* **101**, 5583–5588 (2004).

78. Kertesz, N., Krasnoperov, V., Reddy, R., Leshanski, L., Kumar, S. R., Zozulya, S.

References

and Gil, P. S. The soluble extracellular domain of EphB4 (sEphB4) antagonizes EphB4-EphrinB2 interaction, modulates angiogenesis, and inhibits tumor growth. *Blood* **107**, 2330–2338 (2006).

79.   Williams, C. K., Li, J.-L., Murga, M., Harris, A. L. and Tosato, G. Up-regulation of the Notch ligand Delta-like 4 inhibits VEGF-induced endothelial cell function. *Blood* **107**, 931–9 (2006).

80.   Djokovic, D., Trindade, A., Gigante, J., Badenes, M., Silva, L., Liu, R., Li, X., Gong, M., Krasnoperov, V., Gill, P. S. and Duarte, A. Combination of Dll4/Notch and Ephrin-B2/EphB4 targeted therapy is highly effective in disrupting tumor angiogenesis. *BMC Cancer* **10**, (2010).

81.   Rutkowski, R., Mertens-Walker, I., Lisle, J. E., Herington, A. C. and Stephenson, S. A. Evidence for a dual function of EphB4 as tumor promoter and suppressor regulated by the absence or presence of the ephrin-B2 ligand. *Int. J. Cancer* **131**, 614–624 (2012).

82.   Kumar, S. R., Singh, J., Xia, G., Krasnoperov, V., Hassanieh, L., Ley, E. J., Scehnet, J., Kumar, N. G., Hawes, D., Press, M. F., Weaver, F. A. and Gill, P. S. Receptor tyrosine kinase EphB4 is a survival factor in breast cancer. *Am. J. Pathol.* **169**, 279–93 (2006).

83.   Noren, N. K. and Pasquale, E. B. Paradoxes of the EphB4 Receptor in Cancer. *Cancer Res* **67**, 3994–7 (2007).

84.   Munarini N, Jäger R, Abderhalden S, Zuercher G and Rohrbach V. Altered mammary epithelial development, pattern formation and involution in transgenic mice expressing the EphB4 receptor tyrosine kinase. *J. Cell Sci.* **115**, (2002).

85.   Noren, N. K., Foos, G., Hauser, C. A. and Pasquale, E. B. The EphB4 receptor suppresses breast cancer cell tumorigenicity through an Abl–Crk pathway. *Nat. Cell Biol.* **8**, (2006).

86.   Kaenel, P., Mosimann, M. and Andres, A.-C. The multifaceted roles of Eph/ephrin signaling in breast cancer. *Cell Adhes. Migr.* **6**, 138–147 (2012).

87.   Martiny-Baron, G., Korff, T., Schaffner, F., Esser, N., Eggstein, S., Marmé, D. and Augustin, H. G. Inhibition of tumor growth and angiogenesis by soluble EphB4. *Neoplasia* **6**, 248–57 (2004).

88.   Deininger, M., Buchdunger, E. and Druker, B. J. The development of imatinib as a therapeutic agent for chronic myeloid leukemia. *Blood* **105**, 2640–53 (2005).

References

89. Broggini, T. Effects of EphrinB2 - EphB4 signaling on spinal metastasis. (Universitätsmedizin Berlin, 2015).

90. Broggini, T., Czabanka, M., Piffko, A., Harms, C., Hoffmann, C., Mrowka, R., Wenke, F., Deutsch, U., Grötzinger, C. and Vajkoczy, P. ICAM1 depletion reduces spinal metastasis formation in vivo and improves neurological outcome. *Eur. Spine J.* **24**, 2173–2181 (2015).

91. Pitulescu, M. E., Schmidt, I., Benedito, R. and Adams, R. H. Inducible gene targeting in the neonatal vasculature and analysis of retinal angiogenesis in mice. *Nat. Protoc.* **5**, (2010).

92. Grunwald, I. C., Korte, M., Adelmann, G., Plueck, A., Kullander, K., Adams, R. H., Frotscher, M., Bonhoeffer, T. and Klein, R. Hippocampal plasticity requires postsynaptic ephrinBs. *Nat. Neurosci.* **7**, 33–40 (2004).

93. Feil, R., Wagner, J., Metzger, D. and Chambon, P. *Regulation of Cre Recombinase Activity by Mutated Estrogen Receptor Ligand-Binding Domains. Biochemical and physical research communications* **237**, (1997).

94. Virchow, R. *Die Cellularpathologie in ihrer Begründung auf physiologische und pathologische Gewebelehre*. (Verlag von August Hirschfeld, 1858).

95. James Ewing, A.M., M.D., Sc.D., Professor of Pathology at Cornell University Medical College, N. Y. P. to the M. H. Neoplastic Diseases: A Treatise on Tumours. *Br. J. Surg.* **16**, 174–175 (1928).

96. Fidler, I. and Kripke, M. Metastasis Results from Preexisting Variant Cells Within a Malignant Tumor. *Science (80-.).* **194**, 23–8 (1976).

97. Hart, I. R. and Fidler, I. J. Role of organ selectivity in the determination of metastatic patterns of B16 melanoma. *Cancer Res.* **40**, 2281–7 (1980).

98. Fidler, I. and Hart, I. Biological Diversity in Metastatic Neoplasms: Origins and Implications. *Science (80-.).* **217**, 361–363 (1982).

99. Yang, N.-Y., Lopez-Bergami, P., Goydos, J. S., Yip, D., Walker, A. M., Pasquale, E. B. and Ethell, I. The EphB4 receptor promotes the growth of melanoma cells expressing the ephrin-B2 ligand. *Pigment Cell Melanoma Res* **23**, 684–687 (2010).

100. Héroult, M., Schaffner, F., Pfaff, D., Prahst, C., Kirmse, R., Kutschera, S., Riedel, M., Ludwig, T., Vajkoczy, P., Graeser, R. and Augustin, H. G. EphB4 Promotes Site-Specific Metastatic Tumor Cell Dissemination by Interacting with Endothelial

References

Cell–Expressed EphrinB2. *Mol Canc Res* **8**, 1297-1309 (2010).

101. Watnick, R. S. The Role of the Tumor Microenvironment in Regulating Angiogenesis. *Cold Spring Harb Perspect Med* **2**, 1–20 (2012).

102. Kusumbe, A. P., Ramasamy, S. K. and Adams, R. H. Coupling of angiogenesis and osteogenesis by a specific vessel subtype in bone. *Nature* **507,** 323-329 (2014).

103. Broggini, T., Piffko, A., Hoffmann, C. J., Harms, C., Vajkoczy, P. and Czabanka, M. Passive entrapment of tumor cells determines metastatic dissemination to spinal bone and other osseous tissues. *PLoS One* **11**, 1–12 (2016).

104. Minna, J., Kurie, J. and Jacks, T. A big step in the study of small cell lung cancer. *Cancer Cell* **4**, (2003).

105. Khanna, C., Prehn, J., Yeung, C., Caylor, J., Tsokos, M. and Helman, L. An orthotopic model of murine osteosarcoma with clonally related variants differing in pulmonary metastatic potential. *Clin. Exp. Metastasis* **18**, 261–71 (2000).

106. Arguello, F., Baggs, R. B. and Frantz, C. N. A Murine Model of Experimental Metastasis to Bone and Bone Marrow. *Cancer Res.* **48**, 6876–6881 (1988).

107. Weiss, L. Transmural cellular passage in vascular sinuses of rat bone marrow. *Blood* **36**, 189–208 (1970).

108. Weiss, L., Orr, F. W. and Honn, K. V. Interactions of cancer cells with the microvasculature during metastasis. *FASEB J.* **2**, 12–21 (1988).

109. Hecht, N., Nieminen M., Vajkoczy P. and Woitzik J. Cerebral Hemodynamic Reserve and Vascular Remodeling in C57/Bl6 Mice Are Influenced by Age. *Stroke* 3052–3062 (2012).

110. Martiny-Baron, G., Holzer, P., Billy, E., Schnell, C., Brueggen, J., Ferretti, M., Schmiedeberg, N., Wood, J. M., Furet, P. and Imbach, P. The small molecule specific EphB4 kinase inhibitor NVP-BHG712 inhibits VEGF driven angiogenesis. *Angiogenesis* **13**, 259–267 (2010).

111. Cheng, N., Brantley, D. M., Chen, J., Zisch, A. H., Pasquale, E. B. and Ruoslahti, E. The ephrins and Eph receptors in angiogenesis. *Cytokine Growth Factor Rev.* **13**, 75–85 (2002).

112. Noberini, R., Lamberto, I. and Pasquale, E. B. Targeting Eph receptors with peptides and small molecules: Progress and challenges. *Semin. Cell Dev. Biol.* **23**, 51–57 (2011).

References

113. Binda, E., Visioli, A., Giani, F., Lamorte, G., Copetti, M., Pitter, K. L., Huse, J. T., Cajola, L., Zanetti, N., DiMeco, F., De Filippis, L., Mangiola, A., Maira, G., Anile, C., De Bonis, P., Reynolds, B. A., Pasquale, E. B. and Vescovi, A. L. The EphA2 receptor drives self-renewal and tumorigenicity in stem-like tumor-propagating cells from human glioblastomas. *Cancer Cell* **22**, 765–80 (2012).

114. Genander, M., Holmberg, J. and Frisén, J. Ephrins Negatively Regulate Cell Proliferation in the Epidermis and Hair Follicle. *Stem Cells* **28**, (2010).

115. Holmberg, J., Genander, M., Halford, M. M., Anneré, C., Sondell, M., Chumley, M. J., Silvany, R. E., Henkemeyer, M. and Frisé, J. EphB Receptors Coordinate Migration and Proliferation in the Intestinal Stem Cell Niche. *Cell* **125**, 1151–1163 (2006).

116. Dopeso, H., Mateo-Lozano, S., Mazzolini, R., Rodrigues, P., Lagares-Tena, L., Ceron, J., Romero, J., Esteves, M., Landolfi, S., Hernández-Losa, J., Castaño, J., Wilson, A. J., Ramon Cajal, S., Mariadason, J. M., Schwartz, S. and Arango, D. The Receptor Tyrosine Kinase EPHB4 Has Tumor Suppressor Activities in Intestinal Tumorigenesis. *Cancer Res* **69**, 7430–8 (2009).

117. Davalos, V., Dopeso, H., Castaño, J., Wilson, A. J., Vilardell, F., Romero-Gimenez, J., Espín, E., Armengol, M., Capella, G., Mariadason, J. M., Aaltonen, L. A., Schwartz, S. and Arango, D. EPHB4 and Survival of Colorectal Cancer Patients. *Cancer Res* **66**, 8943–8 (2006).

118. Zheng, L.-C., Wang, X.-Q., Lu, K., Deng, X.-L., Zhang, C.-W., Luo, H., Xu, X.-D., Chen, X.-M., Yan, L., Wang, Y.-Q. and Shi, S.-L. Ephrin-B2/Fc promotes proliferation and migration, and suppresses apoptosis in human umbilical vein endothelial cells. *Oncotarget* **8**, 41348–41363 (2017).

119. Noren, N. K., Yang, N.-Y., Silldorff, M., Mutyala, R., Pasquale, E. B. and Pasquale, E. B. Ephrin-independent regulation of cell substrate adhesion by the EphB4 receptor. *Biochem J* **422**, 433–442 (2010).

120. Foubert, P., Tobelem, G., Le Ricousse-Roussanne, S., Silvestre, J.-S., Souttou, B., Barateau, V., Martin, C., Ebrahimian, T. G., Leré-Déan, C., Contreres, J. O., Sulpice, E., Levy, B. I. and Plouët, J. PSGL-1-mediated activation of EphB4 increases the proangiogenic potential of endothelial progenitor cells. *J. Clin. Invest.* **117**, 1527–1537 (2007).

121. Brantley-Sieders, D., Zhuang, G., Hicks, D., Muraoka-Cook, R. and Chen, J. The

receptor tyrosine kinase EphA2 promotes mammary adenocarcinoma tumorigenesis and metastatic progression in mice by amplifying ErbB2 signaling. *J. Clin. Inverstigation* **118**, 64–78 (2008).

10 Abbreviations

Ang1 & 2 = Angiopoietin 1 & 2

bFGF = basic fibroblast growth factor

BMDC = bone marrow-derived cells

CRC = colorectal carcinoma

DAPI = 4′,6-diamidino-2-phenylindole

Dll4 = delta-like 4

DMEM = Dulbecco's Modified Eagle's Medium

DMSO = dimethyl sulfoxide

DPBS = Dulbecco's phosphate-buffered saline

DTC = disseminated tumor cells

EB2Fc = Ephrin-B2-Fc

EC = endothelial cell

ECD = extracellular domain

ECM = extracellular matrix

EDTA = Ethylenediaminetetraacetic acid

Eph = Erythropoietin-producing hepatoma

Ephrin = Eph receptor family interacting proteins

FBS = fetal bovine serum

FITC = Fluorescein isothiocyanate

FOV = field of view

GFP = green fluorescent protein

GPI = glycosylphosphatidylinositol

GTP = guanosine triphosphate

HCl = hydrochloric acid

IL-6 = interleukin 6

JAK = Janus kinase

MAPK = mitogen-activated protein kinase

MESCC = metastatic epidural spinal cord compression

MMTV = mouse mammary tumor virus

mRNA = messenger ribonucleic acid

NF-κB = nuclear factor-κB

OPG = osteoprotegerin

PDGF = platelet derived growth factor

PEG = polyethylene glycol

PFA = paraformaldehyde

PROK2 = prokineticin 2

PTHR-P = parathyroid hormone-related protein

PVP = polyvinylpyrrolidone

RANKL = receptor activator of nuclear factor-κB

RBD = receptor-binding domain

RLU = relative light units

RPMs = rounds per minute

RT = room temperature

RTK = receptor tyrosine kinase

SAM = sterile α motif

SDF = stromal-cell derived factor

SEM = standard error of the mean

siRNA = small interfering ribonucleic acid

SMC = supporting mural cellsm

TAF = tumor-associated fibroblasts

TAM = tumor-associated macrophages

TGFα = transforming growth factor α

TIE2 = Angiopoietin-1 receptor

TME = tumor microenvironment

TNFα = tumor necrosis factor alpha

Tris = 2-Amino-2-hydroxymethyl-propane-1,3-diol

VEGFA = vascular endothelial growth factor A

vSMCs =vascular smooth muscle cells

11 Affidavit

"I, András Piffkó certify under penalty of perjury by my own signature that I have submitted the thesis on the topic *Ephrin-B2 – EphB4 interaction as a therapeutic target in spinal metastasis formation*. I wrote this thesis independently and without assistance from third parties, I used no other aids than the listed sources and resources.

All points based literally or in spirit on publications or presentations of other authors are, as such, in proper citations (see "uniform requirements for manuscripts (URM)" the ICMJE www.icmje.org) indicated. The sections on methodology (in particular practical work, laboratory requirements, statistical processing) and results (in particular images, graphics and tables) correspond to the URM (s.o) and are answered by me. My interest in any publications to this dissertation correspond to those that are specified in the following joint declaration with the responsible person and supervisor. All publications resulting from this thesis in which I am author correspond to the URM (see above) and I am solely responsible.

The importance of this affidavit and the criminal consequences of a false affidavit (section 156,161 of the Criminal Code) are known to me and I understand the rights and responsibilities stated therein.

Date   Signature

12 Curriculum vitae

Mein Lebenslauf wird aus datenschutzrechtlichen Gründen in der elektronischen Version meiner Arbeit nicht veröffentlicht.

Curriculum vitae

13 Own publications

Thomas Broggini, Marcus Czabanka, **Andras Piffko**, Christoph Harms, Christian Hoffmann, Ralf Mrowka, Frank Wenke, Urban Deutsch, Carsten Grötzinger, Peter Vajkoczy. ICAM1 depletion reduces spinal metastasis formation in vivo and improves neurological outcome. *Eur. Spine J.* **24,** 2173–2181 (2015).

Thomas Broggini, **Andras Piffko**, Christian Hoffmann, Christoph Harms, Peter Vajkoczy, Marcus Czabanka. Passive entrapment of tumor cells determines metastatic dissemination to spinal bone and other osseous tissues. *PLoS One* **11,** 1–12 (2016).

Thomas Broggini, **Andras Piffko**, Christian Hoffmann, Adnan Ghori, Christoph Harms, Ralf Adams, Peter Vajkoczy, Marcus Czabanka. Ephrin-B2 – EphB4 signalling protects osseous tissues from metastatic disease – currently under review.

14 Acknowledgments